UNIVERSIDADE FEDERAL DE SANTA CATARINA
PROGRAMA DE PÓS-GRADUAÇÃO EM ENGENHARIA MECÂNICA

Henrique Raduenz

EXPERIMENTAL AND THEORETICAL ANALYSIS OF A HYDROSTATIC TRANSMISSION FOR WIND TURBINES

Dissertação submetida ao Programa de Pós-graduação em Engenharia Mecânica da Universidade Federal de Santa Catarina para a obtenção do Grau de Mestre em Engenharia Mecânica.
Orientador: Prof. Victor Juliano De Negri, Dr. Eng.

Florianópolis, 2018

Ficha de identificação da obra elaborada pelo autor,
através do Programa de Geração Automática da Biblioteca Universitária da UFSC.

Raduenz, Henrique
Experimental and theoretical analysis of a hydrostatic transmission for wind turbines / Henrique Raduenz ; orientador, Victor Juliano De Negri, 2018.
206 p.

Dissertação (mestrado) - Universidade Federal de Santa Catarina, Centro Tecnológico, Programa de Pós Graduação em Engenharia Mecânica, Florianópolis, 2018.

Inclui referências.

1. Engenharia Mecânica. 2. Wind Power. 3. Hydrostatic Transmission. 4. Wind Turbine Control. I. De Negri, Victor Juliano. II. Universidade Federal de Santa Catarina. Programa de Pós-Graduação em Engenharia Mecânica. III. Título.

Henrique Raduenz

EXPERIMENTAL AND THEORETICAL ANALYSIS OF A HYDROSTATIC TRANSMISSION FOR WIND TURBINES

Esta Dissertação foi julgada adequada para obtenção do Título de "Mestre em Engenharia Mecânica" e aprovada em sua forma final pelo Programa de Pós-Graduação em Engenharia Mecânica.

Florianópolis, 24th July, 2018.

_____
Prof. Jonny Carlos da Silva, Dr. Eng.
Coordenador do Curso

Banca examinadora:

_____
Prof. Victor Juliano De Negri, Dr. Eng.
Orientador
EMC / Universidade Federal de Santa Catarina

_____
Prof. Jonny Carlos da Silva, Dr. Eng.
EMC / Universidade Federal de Santa Catarina

_____
Prof. Júlio César Passos, Dr. Eng.
EMC / Universidade Federal de Santa Catarina

_____
Prof. Gierri Waltrich, Dr. Eng.
EMC / Universidade Federal de Santa Catarina

AKNOWLEDGMENTS

Along the development of this thesis I met so many persons that gave support, definitely they have played a major role in this thesis.

In first place I thank professor Victor Juliano De Negri for all the support and persistence dedicated to me and to the project.

I would like to thank my family for always backing me up and helping me to keep going forward. Shara… you came at end of it, but definitely in the right time, when things where rushing to finish.

The friends from LASHIP, Paulo, Job, Rafael, Lidiane, Henri, Thales, Tozzi, Marquito, Túlio, Giuliano, Adriano, Victor, Guilherme, Tiago, Vinícius, Andrei, Ivan, Nicodemos, Diego, João e Gabriel. They are the persons who pushed me forward and helped in the search for solutions and ideas to solve many of the problems found during the project.

The *Swedish Guys* Joel and Jonnatan for giving major contributions on the system analysis and also for the link they made with Parker Hanniffin in Brazil through Parker Hanniffin in Sweden, but most importantly for the friendship. Also professor Petter Krus from Linköping University played a major role into this.

Reivax Automation and Control S/A, specially João Marcos for all the support. Desyel, Fábio, Pedro, Rafael Geroldi, Rodrigo Gosmann, Ricardo Vituri, Elias, Valdinei, Gilmar, Matheus e Kleiton to their support in different moments of the system development.

Parker Hanniffin Brazil/Cachoeirinha did a fundamental contribution to the project by supplying components and technical support. Thank you Nelson and Gustavo for the support.

The CNPq for the financial support with the scholarship.

The Graduate Program in Mechanical Engineering of the Federal University of Santa Catarina.

Thank you God!

Problems never end,
when one is solved,
the next one is already lurking.
Be ready!

ANÁLISE EXPERIMENTAL E TEÓRICA DE UMA TRANSMISSÃO HIDROSTÁTICA PARA TURBINAS EÓLICAS

RESUMO

Visando o aumento da parcela de energia eólica na matriz energética mundial, a redução de custos com operação e manutenção são fatores chave a serem melhorados através de pesquisa e desenvolvimento. Existe uma tendência em pesquisar e desenvolver transmissões hidrostáticas para uso em turbinas eólicas. Essa tendência é fruto de pesquisas realizadas por instituições e companhias do setor eólico. Apesar de transmissões hidrostáticas, usando bomba e motor, serem uma tecnologia bastante desenvolvida, a aplicação em turbinas eólicas ainda possui desafios. Como a qualidade de controle, a eficiência energética e a viabilidade dos conceitos propostos. Essa dissertação trata da prova de conceito de uma transmissão hidrostática para turbinas eólicas. O conceito proposto tem a bomba na nacelle e o motor no nível do solo acionando o gerador síncrono. A transmissão hidrostática proposta é estudada analiticamente tendo seu comportamento e parâmetros descritos em função de propriedades do vento e da turbina. Uma análise da estabilidade em malha aberta é feita para a transmissão e gerador síncrono. Uma bancada de testes, usando componentes de prateleira, capaz de gerar e entregar energia elétrica para a rede foi construída para avaliar experimentalmente o conceito. Uma máquina de estados foi desenvolvida e implementada na bancada de testes. Dentro de cada estado existe um controlador atuando sobre o sistema para alcançar o objetivo da região de operação. É proposta uma nova estrutura para um destes controladores afim de aumentar a performance do sistema. Um modelo matemático prévio do sistema é melhorado com uso da nova estrutura de controle, dos parâmetros dos componentes e através da validação com as medições feitas na bancada. Como resultados desta dissertação tem-se a prova de conceito do sistema, onde sua viabilidade é mostrada. Outro resultado, é um modelo matemático validado que permite avaliações futuras do comportamento do sistema. Uma máquina de estados que pode ser usada numa turbina eólica real com transmissão hidrostática também é um resultado da dissertação. A solução de controle implementada se mostrou adequada e efetiva nas condições testadas. Entretanto, é necessário aprofundar a análise de estabilidade do sistema. Uma das conclusões é a de que a eficiência do sistema ainda é uma grande desvantagem. Entretanto, é mostrado que ela pode ser melhorada.

Palavras-chave: Energia eólica, transmissão hidrostática, controle de turbina eólica.

RESUMO EXPANDIDO

Introdução

As invenções e desenvolvimento de tecnologias para turbinas e parques eólicos nas últimas décadas levaram a uma redução dos custos de fabricação, instalação, operação e manutenção, tornando a eólica mais competitiva frente a outras fontes de energia. Mesmo assim, o aumento do uso da energia eólica continua impulsionando as pesquisas em novas tecnologias a serem aplicadas no setor.

Tendo em vista que sistemas hidráulicos têm uma grande capacidade de controle, densidade de potência e confiabilidade (RAMPEN (2006), SCHMITZ *et al.* (2012)), é direta a previsão de sua aplicação no setor eólico. Os requisitos de turbinas eólicas em termos de capacidade de potência, robustez e eficiência energética casam com aquilo que os sistemas hidráulicos podem prover.

O controle das rotações do rotor e do gerador são fatores chave para alcançar elevadas eficiências na extração de energia e geração respectivamente. Deste ponto é que surge a proposta de ter uma transmissão hidrostática, junto com um gerador síncrono conectado diretamente à rede, que seja capaz de controlar as velocidades do rotor e gerador ao mesmo tempo. (RAMPEN (2006), COSTA *et al.* (2015), SCHMITZ *et al.* (2012) THUL *et al.* (2011)).

Nesta dissertação uma bancada de testes é construída, onde o conceito de transmissão hidrostática proposto tem sua efetividade e funcionalidade provadas através de ensaios experimentais, fazendo assim a prova de viabilidade técnica. Ensaios experimentais são conduzidos para caracterizar a performance do sistema em termos de comportamento estático e dinâmico, bem como a sua eficiência global. A conexão direta do gerador com a rede também é detalhada e caracterizada.

Uma máquina de estados foi desenvolvida para o controle da turbina eólica com transmissão hidrostática. Ela realiza a troca de um estado para outro automaticamente para atingir um determinado objetivo de controle. É proposto um controlador para aumentar a performance do sistema em um dos estados de operação.

Com as informações coletadas experimentalmente um modelo matemático, já existente, é aprimorado e posteriormente validado .

Uma análise de estabilidade em malha aberta também é feita usando um modelo linear, na forma de espaço de estados, do sistema.

Objetivos

O objetivo principal é fazer a prova de um conceito da transmissão hidrostática para turbinas eólicas. É demonstrado experimentalmente, através de simulação e teoricamente, que o conceito proposto é capaz de lidar com três requisitos relacionados à geração de energia eólica. Eles são: a capacidade de controle da rotação do rotor, a capacidade de entregar energia diretamente para a rede sem o uso de conversores de frequência e fazendo isso com o uso de componentes de prateleira.

Outros dois objetivos da dissertação são a validação do modelo matemático para simulação do sistema e a identificação de limitações do sistema proposto para então, sugerir modificações de maneira a melhorar o sistema.

Os objetivos específicos envolvem e estão relacionados à construção da bancada, ao controlador do sistema, ao desenvolvimento do modelo matemático e à análise analítica do sistema.

Metodologia

São usados livros e material disponível em base de dados para coletar informações que fundamentam o assunto exposto e dissertado.

Para alcançar os objetivos é utilizada a análise de dados experimentais da bancada. Sendo estes dados medidos com um sistema de medição e aquisição de dados apropriado. O software para simulação multidomínio AMESIM é usado para a construção do modelo matemático de simulação do sistema. O software Matlab é usado para as demais funções que exigem programação e geração de figuras.

Resultados e Discussões

A caixa de engrenagens é um ponto negativo no projeto do conceito proposto pois um dos objetivos da transmissão hidrostática é não precisar dela. Entretanto, foi necessário usar ela por conta da limitação dos componentes hidráulicos disponibilizados pelo fabricante parceiro.

O desenvolvimento do modelo matemático do sistema uniu os campos de aerodinâmica do rotor, com a concepção proposta e o sistema hidráulico. Olhando da perspectiva de projeto do sistema, o equacionamento proposto serve como uma ferramenta de base para o projetista, permitindo que ele tire conclusões sobre aquilo que pode ser esperado do sistema em termos de tamanho de componentes, faixa de operação, frequências naturais e estabilidade em malha aberta.

A partir da análise teórica da frequência natural foi observado que o uso de uma transmissão hidrostática com um gerador no nível do solo não é prático acima de certa potência nominal de saída. Para altas potências nominais de saída a frequência de excitação do rotor no ponto de sincronização, por conta do efeito de sombreamento, se torna próxima à frequência natural do sistema, o que é considerado problemático. Portanto, turbinas eólicas menores (<400kW de potência nominal) com transmissão hidrostática não devem ter problemas de ressonância da transmissão no ponto de sincronização com a rede.

O objetivo principal do modelo matemático para simulação foi descrever o sistema com certa acuracidade para que seja possível extrair mais informação dos modelos do que é possível obter da bancada de ensaios. O modelo de simulação da bancada de ensaio mostrou ser representativo depois de ter sido validado e comparado com os dados experimentais. Observando os resultados, foi observado que tanto em regime permanente quanto em regime dinâmico o modelo pode representar com boa precisão o comportamento do sistema real. As principais fragilidades do modelo são os modelos de eficiência das bombas e motor hidráulicos. Apesar de a abordagem utilizada ter sido suficiente para validar o modelo do sistema e fazer a prova de conceito, existe uma incerteza significativa nestas eficiências. Se for possível ter essas informações, o uso de mapas reais de eficiência das bombas e motor hidráulico irá aumentar significativamente a acuracidade do modelo.

Quanto ao controle do sistema e seu controlador supervisório, foi possível observar através da comparação com a sequência de controle de uma turbina eólica real que o sistema desenvolvido é próximo ao que uma turbina real requere. Com pequenas modificações na estrutura de controle e com a adição do controle de passo das pás, o controlador supervisório desenvolvido pode ser aplicado em uma turbina eólica real com transmissão hidrostática para operar automaticamente de acordo com a velocidade do vento e os comandos do operador do parque eólico.

Referente à eficiência do sistema, foi notado que ela é menor para menores velocidades de vento e que ela é dominada pelo sistema hidráulico. Um fator importante que precisa ser contabilizado é o fato de o sistema não ter conversor de frequência entre o gerador e a rede elétrica. Em trabalhos futuros, a eficiência global do sistema obtida deve ser comparada com a eficiência de uma turbina eólica com conversor de frequência e caixa de transmissão.

Considerações Finais

A respeito do objetivo principal da dissertação, é concluído que o conceito do sistema cumpre os requisitos de funcionalidade. Com os resultados da bancada de ensaios é mostrado que é possível usar uma transmissão hidrostática para transferir a potência do topo da nacelle e acionar o gerador que está conectado diretamente à rede no nível do solo. Esse processo é realizado enquanto se está controlando o rotor segundo o objetivo da respectiva região de operação da turbina eólica. Também é concluído que é possível construir tal sistema usando componentes ditos de prateleira, evitando o desenvolvimento de componentes específicos para a aplicação.

Ainda a respeito do objetivo principal da dissertação, a máquina de estados desenvolvida se mostrou efetiva e pode ser vista como uma estrutura de base para a elaboração de uma máquina de estados para uma turbina eólica real com transmissão hidrostática.

A respeito do sistema de controle, a estratégia proposta inclui uma abordagem por ganhos variáveis e o uso de elementos de saturação para evitar o uso de outro controlador. É concluído que o controlador proposto é capaz de controlar o sistema. Entretanto, outras técnicas de controle mais avançadas devem trazer resultados mais promissores, aumentando significativamente a performance do controle do sistema.

Um modelo matemático do sistema foi aprimorado. Acredita-se que este modelo serve para futuras análises do sistema quando operando com outras estruturas de controle, diferentes potências nominais ou configurações de sistemas hidráulicos.

Sobre o modelo analítico, foi visto que com algumas equações fundamentais é possível prever o comportamento do sistema com certa acuracidade. Também é possível usar essas equações para determinar a estabilidade do sistema e explorar quais são os limites práticos dessa tecnologia.

Por fim, mas não menos importante, é concluído que a turbina eólica proposta com transmissão hidrostática com conexão direta com a rede tem limitações no que tange a potência máxima do sistema. Entretanto, existem vários campos a serem explorados, abrindo espaço para, e permitindo, melhorias consideráveis.

Palavras-chave: Energia eólica, transmissão hidrostática, controle de turbina eólica.

ABSTRACT

In the pursuit to increase the share of wind power in the global power matrix, the reduction of system, operability and maintenance costs are key factors to be improved through research and development. There is a trend to research and develop hydrostatic transmissions aiming to use them in wind turbines. This trend is set by research institutions and wind power companies around the world. Despite of fluid power transmissions with a pump and motor be a well developed technology, the application of them into wind turbines has a series of challenges. A few of them are: the system controllability, energetic efficiency and prove of concept feasibility. This thesis is about a prove of concept of a hydrostatic transmission for wind turbines. This concept has the pump at the top of the nacelle and the hydraulic motor driving a synchronous generator at the ground level. The hydrostatic transmission concept is theoretically studied, having its behaviour and parameters described in terms of wind and turbine properties. An analysis of the transmission and synchronous generator open-loop stability is performed. A test bench, using off-the-shelve components, capable of generating electricity and to deliver it to the grid, is built to evaluate experimentally the proposed concept. A state machine structure for system control in all the different turbine operation regions is developed and implemented at the test bench. Inside each turbine operation state there is a controller acting on the system to achieve the operation region task. It is proposed a new structure to one of these controllers to increase the system performance. A mathematical model of the whole system, that was previously developed by other authors, is improved by introducing the new control structure, components parameters and also by validating it with the measurements from the test bench. The performance of the system is assessed and demonstrated using two different wind profiles. As outcomes of this thesis there is the prove of the system concept, where it is shown its feasibility. Another output is a validated mathematical model that allows for further and deeper analysis of the system behaviour. A state machine structure that can be used in a real turbine with this transmission concept, is also delivered. In terms of control quality, the proposed control solution showed to be suitable and effective on the tested conditions. However, it is necessary to continue with the system stability analysis. One of the conclusions is that the system efficiency is still the major disadvantage. However, it is shown that it can be improved.

Keywords: Wind power, hydrostatic transmission, wind turbine control.

LIST OF FIGURES

LIST OF TABLES

LIST OF ABBREVIATIONS

CAD	Computer-Aided Design
CVT	Continuous Variable Transmission
LASHIP	Laboratory of Hydraulic and Pneumatic Systems
LIDAR	Laser Doppler Anemometry
LVDT	Linear Variable Differential Transformer
MPT	Maximum Power Tracking
PCD	Proportional relief valve electronic module
PWM	Pulse Width Modulation
RNS	Rotor Nominal Speed
SYNC	Synchronization
TSR	Tip Speed Ratio
UFSC	Federal University of Santa Catarina

LIST OF SYMBOLS

GREEK ALPHABET

α_M	Hydrau. motor vol. displacement setting	[%]
$\alpha_{M,ref}$	Hydrau. motor vol. disp. reference	[%]
β	Blade pitch angle	[°]
β_e	Fluid effective bulk modulus	[Pa]
δ	Generator torque angle	[rad]
λ	Tip speed ratio	[1]
λ_i	Auxiliary rotor specific speed	[1]
λ_{ideal}	Ideal tip speed ratio	[1]
$\lambda_{\omega_{R,n}}$	Tip speed ratio at maximum rotor speed	[1]
Δp_{loss}	Pump to motor pressure loss	[bar]
Δp_n	Nominal pressure diff. between lines	[bar]
$\Delta p_{P,max}$	Pump maximum pressure difference	[Pa]
Δp_P	Pump pressure difference	[Pa]
Δp_{static}	Pump – Motor Static pressure difference	[Pa]
Δp_{1V2}	1V2 valve cracking pressure	[bar]
$\Delta\overline{T_{GSe}}$	Generator normalised electrical torque deviation	[1]
$\Delta\overline{T_{MGSm}}$	Normalised hydraulic motor and generator mechanical torque deviation	[1]
$\Delta\overline{\omega_{GS}}$	Normalised generator speed deviation	[1]
η_{CC}	Charging circuit motor efficiency	[1]

η_{0ME1m}	0ME1 mechanical efficiency	[1]
η_{0P2}	0P2 pump overall efficiency	[1]
η_{0P3}	0P3 pump overall efficiency	[1]
η_G	System overall efficiency	[1]
η_{GBm}	Gearbox mechanical efficiency	[1]
η_{GD}	Power deliver system efficiency	[1]
η_{GS}	Generator Efficiency	[1]
η_{HT}	Hydrostatic transmission efficiency	[1]
η_i	Power input efficiency	[1]
η_M	0M1 Motor overall efficiency	[1]
η_{Mm}	0M1 Motor mechanical efficiency	[1]
η_{Mv}	0M1 Motor volumetric efficiency	[1]
η_P	0P1 Pump overall efficiency	[1]
η_{Pm}	0P1 Pump mechanical efficiency	[1]
η_{Pv}	0P1 Pump volumetric efficiency	[1]
η_{Rm}	Rotor mechanical efficiency	[1]
ρ_f	Hydraulic fluid density	[kg/m^3]
ρ	Air density	[kg/m^3]
ζ_{1V11}	1V11 damping ratio	[1]
θ	Generator rotor rotational angle	[rad]
τ_{0ME1}	0ME1 dynamics time constant	[s]
$\tau_{0ME1,d}$	0ME1 time delay	[s]
τ_{1V11}	1V11 time delay	[s]
$\omega_{EM,max}$	Electric motor maximum speed	[rpm]
ω_{GS}	Generator rotational speed	[rpm]
$\omega_{GS,n}$	Generator nominal rotational speed	[rpm]
ω_{HE}	Heat exchanger motor rotational	[rpm]
ω_{CC}	Charge circuit motor speed	[rpm]
ω_P	Pump rotational speed	[rads/s]
ω_M	Hydraulic motor rotational speed	[rads/s]
ω_{nf}	System natural frequency	[rad/s]
$\omega_{n,1V11}$	1V11 natural frequency	[Hz]
ω_R	Rotor rotational speed	[rads/s]
$\omega_{R,ideal}$	Rotor ideal rotational speed	[rad/s]
$\omega_{R,n}$	Rotor nominal speed	[rpm]
$\omega_{R,sync}$	Rotor speed at synchronization point	[rpm]
Ω	Blade azimuthal angle	[°]

LATIN ALPHABET

A_R	Rotor swept area	[m²]
$A_{Pv,loss}$	Pump flow rate losses area	[m²]
$A_{Pv,loss,max}$	Maximum pump flow rate losses area	[m²]
c_{GS}	Generator viscous friction coefficient	[Nms/rad]
c_R	Rotor shaft friction coefficient	[Nms/rad]
c_p	Power coefficient	[1]
$c_{p,ideal}$	Maximum power coefficient	[1]
c_q	Torque coefficient	[1]
d	Hydraulic line diameter	[m]
d_L	Low pressure hydraulic line diameter	[m]
d_H	High pressure hydraulic line diameter	[m]
D	Turbine tower diameter	[m]
D_M	Motor volumetric displacement	[m³/rad]
$D_{M,max}$	Max. motor volumetric displacement	[m³/rad]
D_P	Pump volumetric displacement	[m³/rad]
$D_{P,max}$	Max. pump volumetric displacement	[m³/rad]
D_{0P2}	0P2 Pump volumetric displacement	[m³/rad]
D_{0P3}	0P3 Pump outlet vol. displacement	[m³/rad]
E_n	Nominal Output Voltage	[V]
f_{exc}	Rotor excitation frequency	[Hz]
f_{GS}	Generated power frequency	[Hz]
f_{Gr}	Grid power reference frequency	[Hz]
$f_{\omega_R,comp}$	Rotor speed compensation signal	[1]
g	Gravity acceleration	[m/s²]
h	Wind turbine tower height	[m]
H	Generator inertia constant	[1]
h_{PM}	Pump to hyd. motor height difference	[m]
i_{GB}	Gearbox transmission ratio	[1]
i_{HT}	Hydrostatic transmission ratio	[1]
$J_{0ME1,P}$	Electric motor and pump mass moment of inertia	[kgm²]
J_{MGS}	Generator and Hydraulic motor combined mass moment of inertia	[kg.m²]
J_R	Rotor mass moment of inertia	[kg.m²]
k_A	Generator to grid connection damping torque coefficient	[1]
$k_{i,1V11,MPT}$	1V11 MPT controller integral gain	[1]

$k_{i,1V11,SYNC}$	1V11 SYNC controller integral gain	[1]
$k_{i,MPT}$	MPT controller integral gain	[1]
$k_{i,Speed}$	Speed compensation integral gain	[1]
$k_{i,SYNC}$	SYNC controller integral gain	[1]
$k_{p,1V11,MPT}$	1V11 MPT controller prop. gain	[1]
$k_{p,1V11,SYNC}$	1V11 SYNC controller prop. gain	[1]
$k_{p,MPT}$	MPT controller proportional gain	[1]
$k_{p,Speed}$	Speed compensation proportional gain	[1]
$k_{p,SYNC}$	SYNC controller proportional gain	[1]
k_s	Gen. synchronization torque coef.	[1]
k_V	Ratio of hydraulic lines volumes	[1]
l	Hydraulic lines length	[m]
m	Rotor swept area average wind speed	[1]
m_R	Rotor mass	[kg]
n_{GS}	Generator number of pair of poles	[1]
p_{1V11}	1V11 pressure	[bar]
$p_{1V11,ref}$	1V11 pressure reference	[bar]
p_H	High pressure line pressure	[Pa]
p_L	Low pressure line pressure	[Pa]
p_{Pi}	Pump inlet pressure	[Pa]
p_{Po}	Pump outlet pressure	[Pa]
p_{Mp}	Hydraulic motor disp. pilot pressure	[bar]
$p_{Mp,ref}$	Hydraulic motor disp. pilot pressure reference	[bar]
p_{Mi}	Hydraulic motor inlet pressure	[m]
p_{Mo}	Hydraulic motor outlet pressure	[Pa]
$p_{Po,ideal}$	Ideal pump outlet pressure	[Pa]
$p_{Po,max}$	Max pump outlet pressure	[Pa]
p_{0P2o}	0P2 Pump outlet pressure	[Pa]
p_{0P3o}	0P3 pump outlet pressure	[Pa]
p_{1S4}	Low pressure line bottom pressure	[Pa]
P_{CCi}	Charging circuit system input power	[W]
P_i	System input power	[W]
P_{HEi}	Heat exchanger motor input power	[W]
P_{GSi}	Generator power input	[W]
P_{GSo}	Generator power output	[W]
$P_{GSo,n}$	Generator nominal power output	[W]
$P_{GS,sync}$	Generator power at synchronization	[W]
P_P	Pump hydraulic power	[W]

P_{Pi}	Pump power input	[W]
P_w	Wind Power	[W]
P_{Rw}	Extracted wind power	[W]
$P_{Rw,n}$	Nominal extracted wind power	[W]
$P_{Rw,sync}$	Extrac. power at synchronization point	[W]
$q_{p,loss}$	Pump flow losses	[m³/s]
$q_{p,loss,calc}$	Calculated pump flow losses	[m³/s]
q_{Pi}	Pump inlet flow rate	[m³/s]
q_{Po}	Pump effective flow rate	[m³/s]
$q_{Po,ideal}$	Pump flow rate at ideal rotor operation	[m³/s]
q_{Pt}	Pump theoretical flow rate	[m³/s]
q_{Mi}	Hydraulic motor inlet flow rate	[m³/s]
q_{Mo}	Hydraulic motor outlet flow rate	[m³/s]
q_n	System nominal flow rate	[L/min]
r	Rotor radius	[m]
t	Time	[s]
T_{0ME1}	Electric motor torque	[Nm]
$T_{0ME1,ref}$	Electric motor reference torque	[Nm]
T_{CCi}	Charging circuit motor input torque	[Nm]
T_{GSe}	Generator electric torque	[Nm]
T_{GSm}	Generator mechanical torque	[Nm]
T_{GSo}	Generator output torque	[Nm]
T_{HEi}	Heat exchanger motor input torque	[Nm]
T_{max}	Fluid maximum temperature	[°C]
T_{Mo}	Hydraulic motor output torque	[Nm]
T_{Pi}	Pump input torque	[Nm]
$T_{Pi,t}$	Pump theoretical input torque	[Nm]
T_{Rf}	Rotor shaft friction torque	[Nm]
$T_{Rf,Coulomb}$	Rotor Coulomb friction torque	[Nm]
T_{Rloss}	Rotor input shaft torque losses	[Nm]
T_{Ro}	Output/opposing rotor torque	[Nm]
T_{Rw}	Extracted wind torque	[Nm]
$T_{Rw,n}$	Nominal extracted wind torque	[Nm]
$\overline{T_{Rw}}$	Normalized extracted wind torque	[1]
U1	Hydraulic motor inlet pressure signal	[V]
U2	1S15 pump speed signal	[1]
U3	Pump inlet pressure signal	[mV]
U4	Prop. pressure relief valve command	[mA]
U5	1V14 safety valve power supply	[V]

$U6$	Electric motor torque reference signal	[mA]
$U7$	Electric motor torque signal	[mA]
$U8$	Generator speed signal	[rpm]
$U9$	Open 52 safety signal	[V]
$U10$	52 circuit breaker state	[v]
$U11$	Hydrau. motor control pressure signal	[mA]
$U12$	1S6 Pump outlet pressure signal	[mV]
v	Wind speed	[m/s]
v_{eqts}	Tower shadow eff. equi. wind speed	[m/s]
v_{eqws}	Wind shear eff. Equivalent wind peed	[m/s]
$v_{fluid,H}$	High pressure line average fluid speed	[m/s]
$v_{fluid,L}$	Low pressure line average fluid speed	[m/s]
v_h	Wind speed at hub height	[m/s]
v_n	Nominal wind speed	[m/s]
$v_{tip,max}$	Maximum blade tip speed	[m/s]
$v_{\omega_{R,n}}$	rotor nominal speed wind speed	[m/s]
$V_{1V11,ref}$	1V11 solenoid voltage reference	[V]
V	Hydraulic line volume	[m^3]
V_H	High pressure line volume	[m^3]
V_L	Low pressure line volume	[m^3]
x	Distance from turbine tower	[m]
y	Distance from ground level	[m]

SUMMARY

1. INTRODUCTION

"Why people are so afraid of running out of fossil fuels? There are many other forms of energy in nature, we only have to find a way to harvest them." (Harari, 2014)

"... how natural and easy it is to make the power of wind do the work now done by coal." (*Lord Kelvin – Windmills must be the future source of power, 1902)*

"But windmills as hitherto made are very costly machines; and it does not seem probable that, without inventions not yet made, wind can be economically used to give light in any considerable class of cases, or to put energy into store for work of other kinds." (Lord Kelvin – On the sources of energy in nature available to man for the production of mechanical effect, 1881)

1.1 CONTEXTUALIZATION

Wind, now, is already a well settled power source for electric power generation. The inventions and development of technologies for wind turbines and wind farms along the last decades, led to the reduction of manufacturing, installation, operation and maintenance costs, making it become economically competitive with other power sources. Nevertheless, the increasing use of wind power continues to drive researches on new technologies to be applied to this sector.

Knowing that hydraulic systems have a high control capability, power density and reliability (RAMPEN (2006), SCHMITZ *et al.* (2012)), it is straight forward to foresee their application in the wind power sector. Wind turbines are required to attend a broad range of power capacities, be robust, have high energetic efficiency, have low downtime and have a long operation lifetime. These wind turbine requirements match with what hydraulic systems can provide.

Following the trend of continuous technological innovation to attend the wind turbine requisites, a considerable amount of effort is being placed on the systems that transfer the power between the turbine rotor and the electric generator. Usually such task is performed with the use of direct shafts or planetary gearboxes (BURTON et al (2011), HAU (2006)). However, a solution being studied that could be capable of performing the task and at the same time keep up with the turbine requisites is the hydrostatic transmission.

It can be stated that, the control of rotor and generator speed are key factors to achieve high efficiencies in the power extraction and generation, respectively. From there emerges the idea of having just one system in between, that is able to control both variables, rotor and generator speed. A hydrostatic transmission together with a synchronous generator connected directly to the grid is a solution that is capable to control the rotor and generator speed at the same time, enabling high efficiencies to be achieved. (RAMPEN (2006), COSTA *et al.* (2015), SCHMITZ *et al.* (2012) THUL *et al.* (2011)).

In the application of hydrostatic transmission to wind turbines, aside from other institutes and companies around the world, previous theoretical works were done at LASHIP (Laboratory of Hydraulic and Pneumatic Systems at the Federal University of Santa Catarina – UFSC) by Flesch (2012), Rapp and Turesson (2015) and Raduenz (2015) and it was proved, through mathematical models, that the use of a hydrostatic transmission is a possible solution. With these early results at hand, it was gathered the support of two companies, REIVAX S/A Automation and Control and Parker Hannifin Ltd, to build a test bench where this system concept could have its effectiveness and functionality proven through experimental tests. Therefore, making a prove of concept feasibility.

This thesis describes the technical solutions chosen for the test bench that allows the realization of experiments. Experimental tests are carried to assess the system performance. It is demonstrated in terms of static and dynamic behaviour and overall efficiency. The direct connection of the generator with the grid is detailed.

During the development of this thesis it was necessary to build the test bench. This task started by searching for the physical space. Most of the structures to support generator, electric motor and hydraulic components were in house made and mounted at LASHIP. Afterwards, the hydraulic system was installed. The electric circuit, data acquisition and sensors were installed with the support from REIVAX staff. After the system was assembled, the process of commissioning it was carried on to enable the tests to begin.

Contributing to the previous analytical studies, a steady state analysis is performed where the hydrostatic transmission and generator behaviour and parameters are related to the wind and turbine parameters.

In terms of control of the turbine with hydrostatic transmission, a state machine was developed. It is responsible for supervising and controlling it throughout all the wind turbine operation range. Depending on measurements and user inputs it switches from one state to another to

achieve a certain control task. Inside the variable speed operation region, a controller is proposed to increase the system performance.

With the information collected experimentally and understanding of system behaviour, the previous mathematical models developed by Flesch (2012), Rapp and Turesson (2015) and Raduenz (2015) were improved and compared with the measured data. The outcome of such procedure is the validation of the system model that can be used for future development of the system.

A system open-loop stability analysis is also done using a linearized model, in the state space form, of the system. It is shown that, the system is stable when delivering power to the grid.

After this brief introduction the thesis goals are set.

1.2 GOALS

1.2.1 Main goal

This thesis has as objective to make a prove of concept of the proposed concept of hydrostatic transmission for wind turbines. It is demonstrated experimentally, through simulation and theoretically that the concept can overcome three issues related to the wind power generation with a hydrostatic transmission. They are the capacity to control the rotor speed, capacity to deliver the generated power directly to the grid without the use of frequency converters and use of off-the-shelve components to fulfil the first two issues.

Another two goals of this thesis are to validate a mathematical model for simulation of the system and to identify the limitations of the proposed system to suggest suitable modifications in order to improve it.

1.2.2 Specific goals

As a support to achieve the main goal, a set of specific goals are defined. They are related to the test bench construction, the system controller, the development of a mathematical model and the approach to the analytical analysis.

1.2.2.1 Test bench goals

The test bench will be used to evaluate experimentally the hydrostatic transmission and prove its concept. The obtained results serve to improve and validate the mathematical model for simulation.

The bench should allow for a correct evaluation of the system, representing the operation of the real wind turbine.

It is necessary to have the capability to implement different control strategies to evaluate and improve the system control quality.

To have the bench ready to be operated it is necessary to:

- select hydraulic components;
- select electric/electronic devices to deal with the input power, with the delivery of the generated power to the grid, data acquisition and control actions;
- determine the layout of the system in order to fit it to the available physical space at LASHIP;
- develop the supervisory system (state machine) that takes care of controllers selection and safety actions at the test bench;
- establish safety procedures.

The transmission concept was developed by Flesch (2012), improved by Raduenz (2015) and by Rapp and Turesson (2015).

It is noteworthy that the selection of the hydraulic components and sensors and data acquisition systems where done together with Rapp and Turesson (2015).

Until the end of this thesis there were no notice of a similar system being developed in Brazil by other research groups or industry.

1.2.2.2 Mathematical model goals

As part of this project, Flesch (2012) developed the first mathematical model of a hydrostatic transmission. It was developed for a wind turbine of 150kW rated power. In order to build a physical prototype of the system and prove the concept, Raduenz (2015) downsized the system model to 20kW and added features that were necessary for it to become a test bench. The model of a wind turbine hydrostatic transmission system became the model of a hydrostatic transmission for wind turbine test bench.

Rapp and Turesson (2015) implemented in the model the parameters of the real hydraulic components that were selected and developed different control strategies for the transmission.

To continue the improvement of this model, in order to use it for future development, there are some targets to be achieved, they are:

- improve the parameters of the model to better represent the real behaviour of the system;

- to validate the model based on experimental measurements from the test bench.

The use of a reliable mathematical model allows the deeper comprehension of system operation and also the behaviour of it when sized for higher rated powers.

1.2.2.3 Theoretical analysis

In order to size the system correctly and assess its stability, static and dynamic performance, an analytical analysis must be carried out. This allows the understanding of the transmission properties related to wind and grid properties.

This analysis is made in the following steps:

- definition of wind, rotor and grid properties and requirements;
- definition of static equations that describe wind power extraction, hydraulic system power transmission and power delivery to the grid;
- establish static equations to related hydraulic system parameters and properties to the wind, rotor and grid properties;
- develop a suitable set of equations to evaluate system efficiency;
- develop a linear model to assess the system stability.

1.3 JUSTIFICATION AND CONTRIBUTIONS

Throughout the study, it is confirmed the capacity of a hydraulic systems to fulfil the application requirements.

It allowed a study related to electric power generation and connection with the grid using hydraulic systems. This characterised it as a multidisciplinary work. It serves as a background to future studies.

The bench can be used for teaching and demonstration inside the Mechanical Engineering Department and for further development of such systems.

1.4 THESIS STRUCTURE

The thesis structure follows, as much as possible, the flow of power through a wind turbine. Which means, from the wind to the hydraulic system and to the electric power generation. All the sections have a similar structure, where first what is related to wind is explained, then

the related to the hydraulic system and, at the end, what is related to the electric power generation.

It starts with a literature review where variable speed horizontal axis wind turbines are briefly introduced to the reader in Chapter 2.

Chapter 3 is used to describe the details and reasons for the technical solutions adopted in the test bench. Information about the layout, hydraulic and electrical circuits, sensors, data acquisition and control are presented in the inside sections. A great attention is given to the description of the control and supervisory system.

Chapter 4 presents the system analytical model and analysis. Starting from the steady state equations that describe the system, the hydrostatic transmission parameters are related to the wind turbine and grid parameters. An analysis of the power throughout the system is made. In addition, an estimation of system efficiency is done. At the end, in Section 4.7, a linear model of the system is used to evaluate its open-loop stability.

Chapter 5 deals with the development and improvement of the test bench mathematical model. Only the main model features are presented. The model validation process is also described.

Chapter 6 presents a resume of results obtained with the test bench and with the simulation of the mathematical model. The observed hysteresis in the proportional pressure relief control valve and the electric motor time response is also shown in Chapter 6.

Chapter 7 brings discussions regarding the results added to comments and further development of such system.

Chapter 8 presents the thesis conclusions and comments regarding the future possibilities.

2. LITERATURE REVIEW

"If I have seen further is because I was standing in the shoulders of giants!" (Newton)

In this chapter, a review of previous and ongoing studies related to hydraulic wind turbines is made. By referencing other authors and describing the very basic theory behind wind turbines and hydrostatic transmissions, a background is made to support the development of this thesis.

Firstly, the theory behind power extraction from the wind with horizontal axis variable speed wind turbines is presented. In Section 2.1.3 the objectives and structures of such turbine controllers are addressed. Afterwards, in Section 2.2 the basics regarding hydrostatic transmissions are shown where in Section 2.2.1 the application of these drivetrains in wind turbines is presented. In order to be able to control them, it is necessary not only to look into wind/rotor interaction, but also to understand the process of delivering power to the grid, that is presented in Section 2.3.

2.1 HORIZONTAL AXIS VARIABLE SPEED WIND TURBINES

2.1.1 General considerations for horizontal axis variable speed wind turbines

In hydro or thermal power plants, the power that arrives at the turbine can be controlled by regulating the water or the steam flow rate. In wind turbines there is no control of the power that arrives in the turbine since that is dependent on the wind speed. Therefore, the system is constantly facing varying wind power input conditions.

This thesis deals with horizontal axis variable speed wind turbines. Unless specified differently, when the term wind turbine is used it refers to a horizontal axis variable speed wind turbine.

In variable speed wind turbines, for a given wind speed, the blades achieve maximum aerodynamic performance for a specific rotor speed. Therefore, the turbine must constantly adapt to the wind conditions in order to operate with maximum performance and maximum power extraction.

Horizontal axis variable speed wind turbines are responsible for most of wind power generation (BURTON *et al.*, 2011). The authors demonstrate that the wind power extracted (P_{Rw}) by this kind of turbine

can be described by Equation (2.1), that is a function of wind speed (v), air density (ρ), power coefficient (c_p) and rotor swept area (A_R),

$$P_{Rw} = \frac{1}{2}\rho A_R v^3 c_p. \tag{2.1}$$

The power coefficient is the ratio of the extracted wind power and the available power in the wind. It has a maximum, called Lanchester-Betz limit, of 0.59 that is derived from the disk actuator theory demonstrated by Hau (2006) and Burton *et al.* (2011). Due to non-optimal aerodynamic blade design and drag losses, this limit is never achieved.

As described by Burton *et al.* (2011), the performance of a wind turbine can be characterized by the manner in which power, torque and thrust vary with wind speed. In this thesis the first two are considered.

The power coefficient is a function of the blade aerodynamic design and can be described as a function of wind speed, rotor speed (ω_R) and blade pitch angle (β). The aerodynamic performance is commonly described by the dimensionless parameter called Tip Speed Ratio (λ - TSR), which is the ratio of the rotor tip linear speed and wind speed,

$$\lambda = \frac{\omega_R r}{v}, \tag{2.2}$$

where r is the rotor radius.

Figure 2.1 presents a power coefficient distribution, as a function of the tip speed ratio and blade pitch angle for a specific blade design.

For zero blade pitch angle the power coefficient reaches a maximum value, called $c_{p,ideal}$, for a certain tip speed ratio value that is called ideal tip speed ratio (λ_{ideal}). Since the wind speed cannot be controlled and the rotor radius is constant, it is necessary to control the rotor speed in order to achieve, in the steady state, λ_{ideal} and consequently $c_{p,ideal}$, leading to a maximum wind power extraction.

The aerodynamic torque, or rotor extracted wind torque (T_{Rw}), that acts upon the rotor shaft, is calculate by,

$$T_{Rw} = \frac{P_{Rw}}{\omega_R} = \frac{1}{2}\rho A v^3 c_p \left(\frac{1}{\omega_R}\right). \tag{2.3}$$

This is called dynamic torque by Dolan *et al.* (2006). It is simply the power extracted from the wind divided by the current rotor speed.

Figure 2.1 - Power coefficient distribution for a specific blade design.

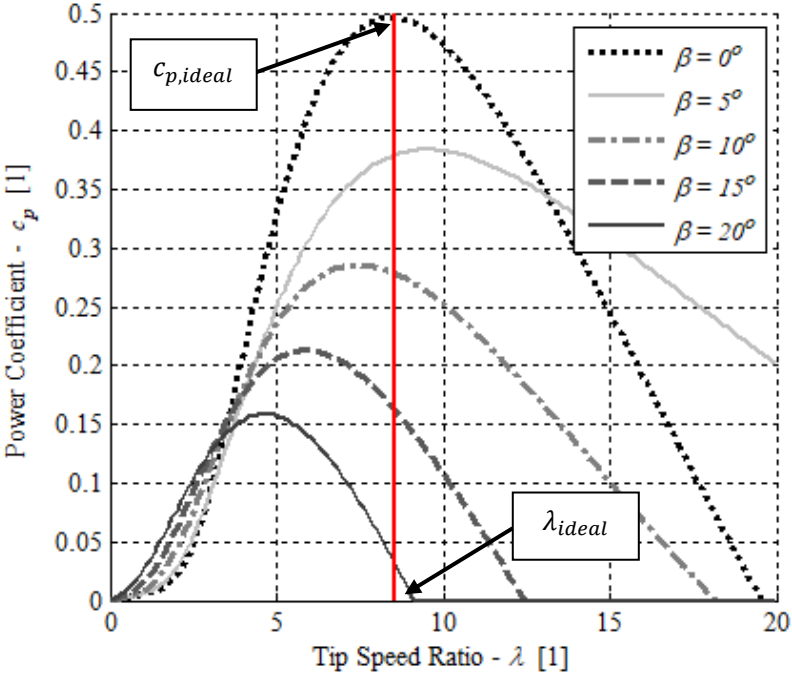

Source: Author.

As demonstrated by Burton *et al.* (2011), if the power coefficient is divided by the tip speed ratio the torque coefficient ($c_q(\lambda, \beta)$) is obtained, that is,

$$c_q(\lambda, \beta) = \frac{c_p(\lambda, \beta)}{\lambda}. \tag{2.4}$$

The author also explains that it does not give any additional information about the turbine performance, but it is used for torque assessment purposes when the rotor is connected to a gearbox and generator. It can be seen as a capacity to accelerate or decelerate the rotor. Figure 2.2 presents the torque coefficient distribution as a function of λ.

Figure 2.2 - Torque coefficient distribution as a function of the tip speed ratio.

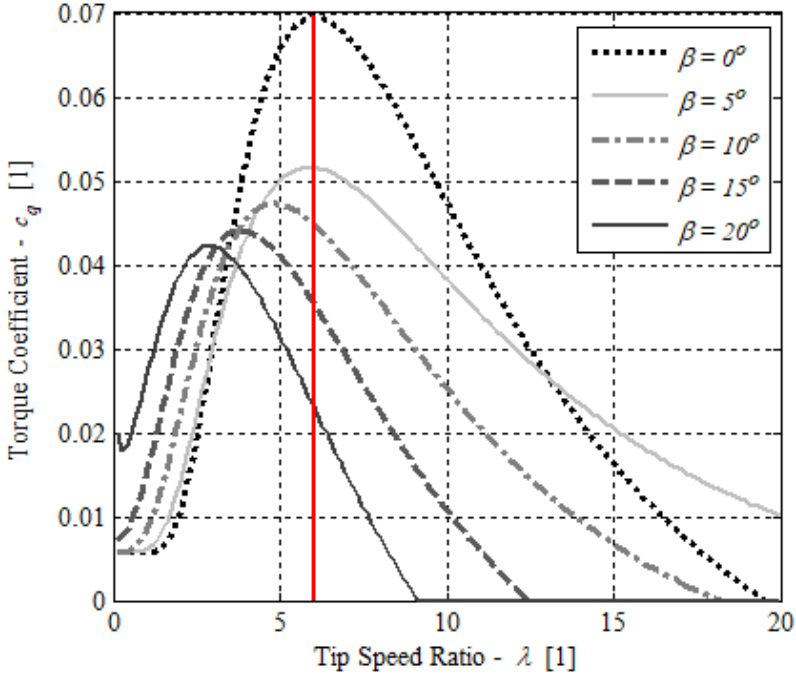

Source: Author.

By comparing Figure 2.2 and Figure 2.1, it is seen that for the same pitch angle, the maximum torque coefficient and maximum power coefficient occur at different λ. From that, it is possible to conclude that the turbine can be controlled to obtain a desired extracted wind torque or extracted wind power. This feature is not explored in this thesis however, it is worthy of looking at it with more attention in future works.

The variation of torque over the turbine systems result in fatigue, which translates into system lifetime reduction. The variation of torque is a result of changes in wind speed, controller actions and tower shadow effect. These torque variations are to be reduced as much as possible to increase system lifetime.

The blocking of the air flow by the tower results in a region of reduced wind speed, immediately in front of the tower (BURTON *et al.*, 2011). This is called tower shadow effect. As presented in Figure 2.3, it

is possible to see the effect of the tower shadow on the wind speed profile (The wind profile in front of the tower is at the bottom part of Figure 2.3).

Figure 2.3 - Wind speed profile deficit due to tower shadow.

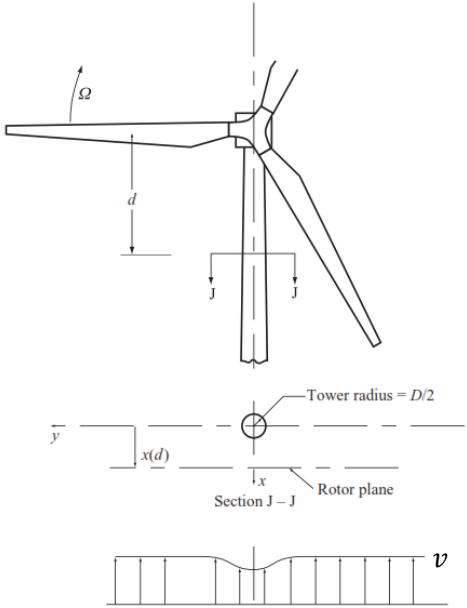

Source: Adapted from Burton *et al.*, (2011).

In Figure 2.3, D is the tower diameter (considered constant along the whole tower), $x(d)$ is the distance between the rotor rotation plane and the tower centre, Ω is the blade azimuthal angle.

When the blade is in the region immediately in front of the tower, it experiences a smaller wind speed and so it extracts a smaller power from the wind, resulting in a smaller wind torque. In other regions the torque is not affected by the tower shadow.

The turbine rotor is also affected by the wind shear effect. Which is a reduction of the wind speed close to the ground due to the friction of the wind with the ground surface. Figure 2.4 shows the representation of the wind shear effect.

The wind shear makes the wind speed to not be uniform along the rotor swept area. This effect should be accounted specially for small wind turbines (up to and around 150 kW) that have the hub close to the ground. Looking from the ground perspective, there is an increase in wind speed from the ground surface to a point far from it.

Dolan *et al.* (2006) defines an equation between torque and wind speed that allows the direct calculation of the aerodynamic torque accounting wind shear and tower shadow effects.

Figure 2.4 - Wind shear effect.

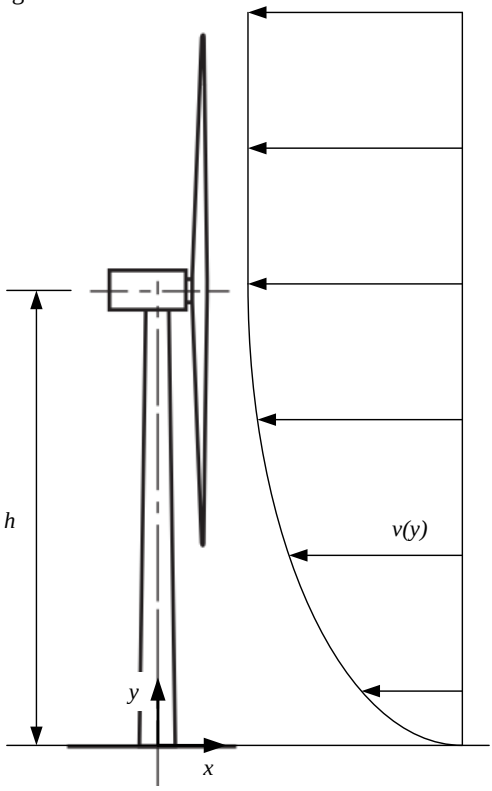

Source: Adapted from Burton *et al.* (2011).

The author defines a normalized extracted wind torque $\overline{T_{Rw}}$ as,

$$\overline{T_{Rw}}(t,\Omega) = 1 + \frac{2}{mv_h}\left(v_{eqws} + v_{eqts} + (1-m)v_h\right), \qquad (2.5)$$

where v_h is the wind speed at hub height, m is the constant that defines the average wind speed on the rotor swept area (A), v_{eqws} is the equivalent wind speed due to wind shear and v_{eqts} is the equivalent wind speed due to tower shadow effect. All the variables vary with time (t). The terms v_{eqts} and v_{eqws} are functions of the wind shear, tower diameter, distance

between the blades and tower, and other empirical factors. The formulation of these terms are beyond the scope of this thesis, but they can be found in Dolan *et al.* (2006). Equation (2.5) is plotted in Figure 2.5 as a function of the blade azimuth angle.

Figure 2.5 - Normalized extracted wind torque as a function of blade azimuth angle.

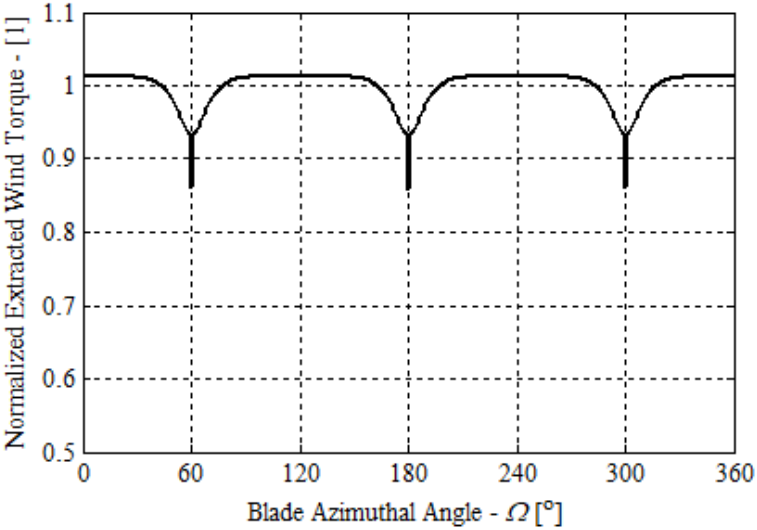

Source: Author.

The main parameters used for generating the normalized extracted wind torque are shown in Table 2.1. The other required parameters were defined based on Dolan *et al.* (2006) study and on information from small turbines datasheets.

Table 2.1 - Normalized extracted wind torque parameters.

Parameter	Value
D	0.8 m
$x(d)$	1.2 m
h	10.0 m
v_h	10.0 m/s

Source: Author.

Vatheuer *et al.* (2011) observed in their studies a torque reduction as high as 15.0 % due to the tower shadow. This confirms that the torque reduction shown in Figure 2.5 is reasonable.

By multiplying equations (2.3) and (2.5), the torque extracted from the wind with the effects of wind shear and tower shadow is obtained.

It is important to account for these two effects once the torque oscillations are transmitted, in the current wind turbines, through the axis and gearbox to the generator. The generator input torque oscillation can be transmitted to the generated electricity. Due to the fluid compressibility and use of accumulators, the hydrostatic transmission can damp these oscillations resulting in smaller structural stresses and improved power quality. Diepeveen *et al.* (2014) use as a requirement for the design of a wind turbine with hydrostatic transmission, that peaks detected in the aerodynamic torque due to tower shadow or turbulence should not be visible from readings at the end of its transmission system.

In terms of connection between rotor and generator, most of the wind turbines either have a direct coupling or a gearbox connecting them. Where direct coupling usually requires a multipole generator due to its low speed, and gearboxes can make use of generators with fewer poles since they are able to increase the speed at its output shaft.

If the rotor speed is to vary according to the wind speed, consequently the generator speed, on variable speed wind turbines, will vary, since direct couplings and gearboxes have fixed transmission ratios. If the generator shaft speed varies, the generated electric power frequency also vary. Which then requires the use of frequency converters to convert the power for the desired grid frequency and voltage before delivering it to the grid. The facts presented in this paragraph were concluded from the resume and comparison of different wind turbines topologies made by Gonzalez (2012).

According to Burton *et al.* (2011) and Gonzalez (2012), there are several means of achieving variable speed operation with the use of frequency converters. Figure 2.6 shows a diagram of a turbine with a frequency converter that must convert all the generated power.

A more extensive analysis of wind turbines with different generators and frequency converters configurations can be found in Gonzalez (2012), a masters thesis developed at LASHIP.

The concept presented in this thesis, that uses a hydrostatic transmission between rotor and generator and a synchronous generator directly connected to the grid, eliminates the need for frequency converters. A more detailed description of this concept will be presented in Section 2.2.1.

Figure 2.6 – Example of a wind turbine with frequency converter.

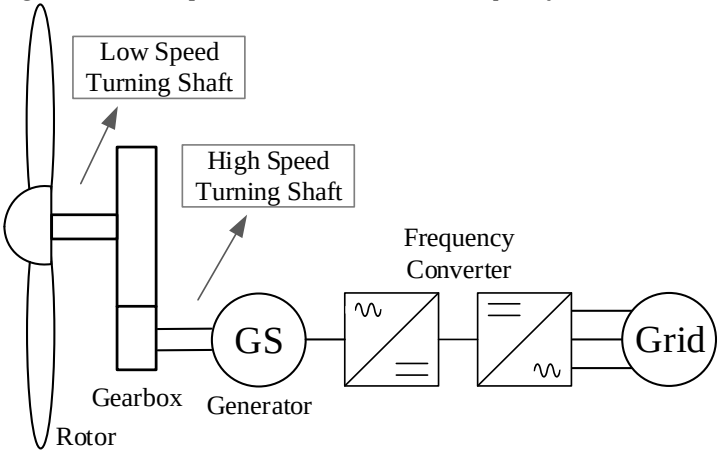

Source: Adapted from Gonzalez (2012).

2.1.2 Wind turbine operation regions

The operation regions of a variable rotor speed wind turbine with a synchronous generator with direct grid connection, are described in this section.

Figure 2.7 presents a set of curves that represent the wind turbine operation regions according to wind speed. The steady state behaviour of the extracted wind power, rotor rotational speed, generator rotational speed and generated power are shown in the figure. They are all normalized with respect to their nominal values in order to be able to plot them in the same figure and observe their behaviours in each region.

Region *I* is from zero wind speed up to wind speed *a*, where the wind power overcomes the system static losses and so providing enough power for the rotor to rotate and extract power from the wind. Point *a* is called the cut-in speed.

Region *II* range is from wind speed *a* up to *b*. *a* is when the power extracted from the wind is the amount necessary to overcome the losses and bring the system to the point, *b*, where it is able to start the synchronization to the grid. The power extracted is dissipated by shaft friction, gearbox/hydrostatic transmission inefficiencies and generator losses. The generator losses are characterised by core, winding and friction losses. There are no electric power generation up to this point.

Figure 2.7 - Operation regions of variable speed wind turbines with synchronous generator with direct connection to the grid.

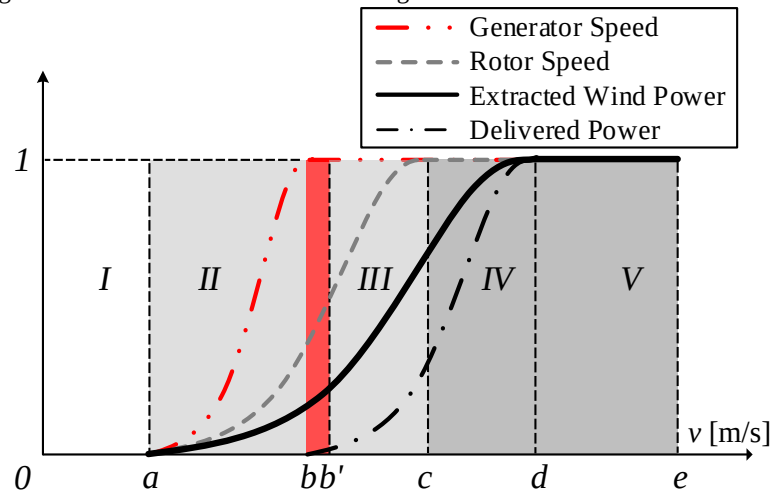

Source: Author.

Wind speed *b* is where the synchronous generator reach its synchronous speed. However, the generator must be excited to achieve the correct voltage, in this case, the grid voltage. The power extracted at wind speed *b* is not enough to overcome the increased load produced by the generator excitation. Such that a higher wind speed (*b'*) is required to allow the synchronization between generator and grid. When synchronized, the principle of infinite busbar can be assumed to describe the interaction of the generator and the grid (COSTA and SILVA, 2000, *apud* FLESCH, 2012). The principle of infinite busbar for a synchronous generator connected to it is presented in Section 2.3.1. The generator speed is kept approximately constant regardless the wind speed. Only small transients occur when the wind speed changes or a control action is performed. Any increase in wind speed will result in increase of power delivery to the grid such that all generated power, except the generator losses, is delivered.

With the system synchronized and delivering power to the grid, from point *b'* up to wind speed *c* is region *III*. This is the region where variable wind speed turbines have their advantage over fixed speed turbines. Through this region the rotor speed is controlled according to the measured wind speed in order to achieve the maximum power coefficient ($c_{p,ideal}$) resulting in maximum wind power extraction. This region is often called the Maximum Power Tracking (MPT) region. Wind speed *c* results in the maximum rotor speed. Thul *et al.* (2011) mention that a

general guideline is to limit the blade tip speed to 60 m/s in noise sensitive environments, but it is common for wind turbines to have tip speeds of 80 m/s or higher.

From wind speed *c* to *d* (region *IV*), the rotor speed must be limited in order to avoid structural damage due to excessive loads and the generation of noise above permitted limits. Since the rotor speed is kept constant, the increase of wind speed will reduce the power coefficient. The tip speed ratio will decrease (Equation (2.2)). The extracted power still increases because it is a cubic function of wind speed and that overcomes the power coefficient decrease (Equations (2.1)). Regions *III* and *IV* are often called as partial load operation regions since the generated power is below-rated.

Region *V* is where the system reaches its rated power, which is a limitation imposed by the turbine components design. To limit the extracted wind power, blade pitching control is used. By pitching the blades, the angle of attack is increased resulting in lower lift forces acting on the blades. Therefore, reducing the extracted power. At *e*, cut-off speed, the pitching system is no longer able to limit the power extraction, so the system must be turned off. This is done by turning the hub away from the wind stream direction or by using shaft breaks.

The proposed hydrostatic transmission is developed to handle the turbine control in regions *II*, *III* and *IV*. Section 2.2.2 brings the explanation of how it is able to perform the turbine control through these regions.

2.1.3 Control of wind turbines

In variable speed wind turbines the principle of controlling the rotor speed in regions *II*, *III* and *IV* is through the equilibrium of torques acting over the rotor. For turbines with gearbox or direct coupling the generator electrical torque is controlled to oppose the wind extracted torque in order to, at steady state, achieve the desired rotor speed. Equation (2.6) is derived from equations (2.2) and (2.3) and represents the opposing torque that must be applied over the rotor to achieve $c_{p,ideal}$.

$$T_{Ro} = \frac{1}{2}\rho A_R {\omega_R}^2 r^3 c_{p,ideal}\left(\frac{1}{\lambda_{ideal}^3}\right). \tag{2.6}$$

Burton *et al.* (2011) states that for below nominal power (*d* in Figure 2.7) the turbine should simply be trying to produce as much power as possible, there is generally no need to vary the pitch angle in regions *II* and *III* since the optimum pitch angle does not change much with wind

speed. This is the reason why the analysis carried in the thesis use a constant and equal to zero pitch angle. Therefore, the control in these regions resumes to control the opposing torque over the rotor without pitching the blades.

Different strategies are applied to control the opposing electrical torque. This is performed, for a variable speed wind turbine, for example, via the frequency converter. The detailed description of opposing torque generation and control in terms of electrical properties is out of the scope of this thesis.

Burton *et al.* (2011) states that for tracking the ideal power coefficient ($c_{p,ideal}$) below-rated wind speed, the quadratic algorithm (Equation (2.6)) works well and gives smooth and stable control. However, in turbulent winds, the large rotor inertia prevents it from changing speed fast enough to follow the wind, so it will operate in a lower mean c_p. It is possible to manipulate the generator torque to cause the rotor speed to change faster when required, so staying closer to the peak of the c_p curve. One possible method to find a suitable generator torque reference is to use available measurements to make an estimate of the wind speed, calculate the rotor speed required for $c_{p,ideal}$, and then modify the generator torque to rapidly achieve that speed (BURTON *et al.*, 2011).

Burton *et al.* (2011), says that a simple PI controller can be used, acting on the speed error, to calculate a generator torque demand which will track the desired rotor speed.

2.2 HYDROSTATIC TRANSMISSIONS

The basic elements in a hydraulic transmission are the hydraulic pump, fluid, hydraulic lines and hydraulic motor. The pump converts mechanical power into hydraulic power. The fluid transports the energy, in terms of pressure and flow rate, from the pump to the motor. The motor converts hydraulic power back to mechanical power at the output shaft (COSTA *et al.*, 2015).

A simple hydrostatic transmission with variable displacement motor scheme if shown in Figure 2.8.

Figure 2.8 - Basic hydrostatic transmission scheme.

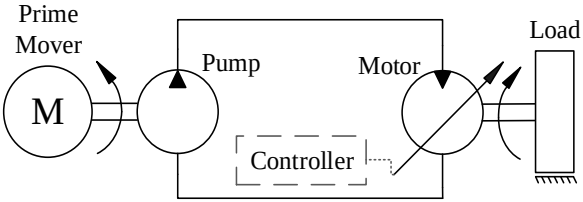

Source: Author.

Considering a hydrostatic transmission without volumetric losses, the flow rate that outputs the pump (q_{Po}) is, in steady state, the flow rate that enters/drives the motor (q_{Mi}) (Equation (2.7)). The flow rate of a hydraulic pump or motor can be described as the product of its rotational speed and its volumetric displacement. Equations (2.7) to (2.9) describe the relation between pump and motor speed or the relation between volumetric displacements which are the transmission ratio (i_{HT}).

$$q_{Po} = q_{Mi}. \tag{2.7}$$

$$\omega_P D_P = \omega_M D_M. \tag{2.8}$$

$$i_{HT} = \frac{\omega_M}{\omega_P} = \frac{D_P}{D_M}. \tag{2.9}$$

Figure 2.9 presents the two-quadrant operation, in terms of displacement, that is possible to achieve with a hydrostatic transmission with a variable displacement pump, and variable displacement, bi-directional motor.

In Figure 2.9, the hydrostatic transmission, due to its constructive characteristics, operates as a continuously variable transmission having infinite transmission ratios between pump and motor maximum displacements.

The capacity to operate in any of the two quadrants gives the transmission a significant amount of functionalities that it can perform, such as, deliver power continuously, change direction of rotation and recover power.

Considering a positive rotational direction of the pump prime mover ($\omega_P > 0$), Table 2.2 describe the two-quadrant hydrostatic transmission operation in terms of transmission ratio and motor rotational direction.

Figure 2.9 - Two quadrant operation of a hydrostatic transmission with bidirectional displacement motor and unidirectional variable displacement pump.

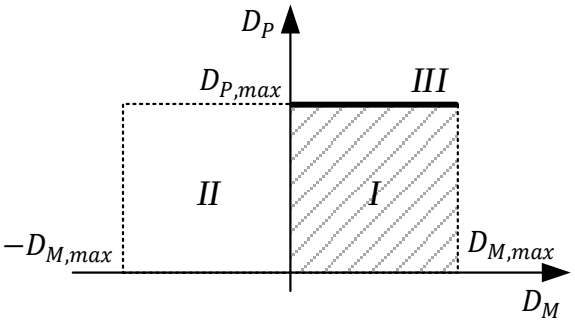

Source: Author.

It must be noticed that a too small motor displacement would result in a too high transmission ratio, which means a high motor speed. The critical point would be zero motor displacement that would result in infinite motor speed. In practice this situation result in the pressure build-up (COSTA *et al.*, 2015).

Table 2.2 - Hydrostatic transmission ratio and motor rotation direction.

Quadrant	Transmission ratio $(sign(i_{HT}))$	Motor Rotation Direction $(sign(\omega_M))$
I	>0	>0
II	<0	<0
III	>0	>0

Source: Author.

2.2.1 Hydrostatic transmissions in wind turbines

Horizontal axis wind turbines are developed to have only one direction of rotation. On the other side, the generator is also developed to operate in only one direction of rotation. That limits the operation region to be only in quadrant *I* in Figure 2.9. This operation is possible to be achieved with pump with motor with positive volumetric displacements.

As seen in Section 2.1, most of horizontal axis wind turbine operate with variable rotor speed in order to maintain high efficiency in wind power extraction. From the generator side it is required for it to generate power with the same grid frequency and voltage amplitude.

Hydrostatic transmissions are capable, by changing pump and/or motor displacement, to decouple the input and output speeds. That allows

the system to maintain the rotor at the best speed for maximum power extraction while keeping the generator at the synchronous speed.

Diepeveen *et al.* (2014) says that state of the art offshore wind energy power conversion and transmission technology is complex, heavy, expensive and requires frequent maintenance. The author also states that in any industry where robust machinery is required to handle large torques, hydraulic drive systems are a common choice, therefore a feasible solution for wind turbines.

Wind turbines have rated power that ranges from a few kilowatts to megawatts. That makes hydrostatic transmissions attractive by the capacity to be scalable to different power levels, for example by using separate hydrostatic transmission modules, switching pumps and/or motors. The application of different concepts of hydrostatic drivetrains to wind turbines is being studied and developed by different research groups and companies around the world. Each claim a few benefits when adopting their particular solution.

Regarding system power scalability, the Dutch company Hydrautrans BV together with the fluid power company INNAS BV are developing a 12MW hydro-mechanic transmission for off-shore wind turbines. Their system consists of four 3MW independent power generation modules allowing to be turned on and off according to the available wind power.

Masashi *et al.* (2014) presents the development of a large capacity hydrostatic transmission for wind turbines. The authors confirmed that it is possible to manufacture and provide hydrostatic transmissions with capacity larger than 7MW. This project is under development and tests will be carried on the offshore of Fukushima, Japan. It is a joint venture between Mitsubishi Heavy Industries, Ltd. and Vestas Wind Systems A/S. The hydrostatic transmission uses digital pump and motor technology, designed by Artemis Intelligent Power, Ltd. According to the authors the advantages of hydrostatic transmissions in wind turbines are:

- the easy maintenance or replacement of main components because of the modular design concept that can be applied to the hydraulic system;
- the rotational frequency of the generator is kept constant against the wind condition change;
- the complete drivetrain configuration can be simplified because the hydrostatic transmission does not need a power converter.

The main advantage of a hydrostatic transmission over geared and direct drive systems is the possibility to continuously change the

transmission ratio. Therefore, it is possible to operate with variable rotor speed whilst using a synchronous generator directly coupled to the grid, thereby reducing or even eliminating the need of power electronics (DIEPEVEEN *at al.*, 2011). Other authors also support and show this capacity (SCHMITZ *et al.*, 2010; VARPE, 2008; DOLAN *et al.*, 2012).

The transmission of power is made by means of pressurized fluid instead of a mechanical contact between gears. Diepeveen *et al.* (2011) states that there is a reduction of torsional vibrations due to the damping characteristics of the fluid power transmission, reducing wear and increasing power quality. That is an advantage over gearboxes or direct shafts since it increase system lifetime and reliability.

Schmitz *et al.* (2010) used a morphological matrix to generate concepts of hydrostatic transmissions for wind turbines in the very beginning of the project design process. The authors concluded that the concept that showed to be more promising was the one with both variable displacement pump and motor.

Lin *et al.* (2014) used a concept of hydrostatic transmission with fixed pump and variable motor, and showed few simulation results for it, however the model did not accounted a direct coupling of the generator to the grid, so the results did not seemed to be representative.

In terms of efficiency, the hydrostatic transmission solution is less efficiency then the direct coupling or gearboxes. The transmission of power mechanically is usually more efficient than by a hydraulic system.

This thesis study is about a variable speed wind turbine with a hydrostatic transmission that drives a synchronous generator with a direct connection to the grid.

The hydrostatic transmission concept explored in this study is presented in Figure 2.10. As it can be seen, the fixed displacement hydraulic pump is driven by the rotor. The pressurized fluid flow drives the variable displacement hydraulic motor that is connected to the synchronous generator, which, when synchronized, is directly connected to the grid. As will be explained further in the document, the controller sets the motor displacement to control the whole system.

Figure 2.10 - Wind turbine with hydrostatic transmission concept.

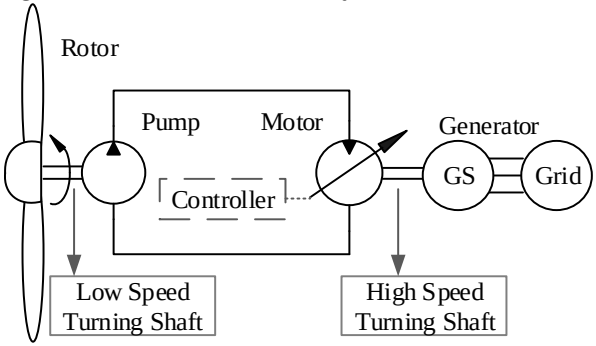

Source: Author.

Vatheuer *et al.* (2011) says that the big advantage of the concept presented in Figure 2.10 is the low number of components and an easy way to control the transmission. As a drawback, the author mentions the limited opportunities to adapt the system when operating at low power. At the test bench developed in this project, it was implemented variable gains in the controllers in order to adapt the system behaviour for the low power operation region.

According to Figure 2.9, the fixed displacement pump makes the operation region to be reduced from quadrant *I* to only the line *III*. The use of a fixed displacement pump and not a variable displacement pump in this project is due to the financing constraints set by the project supporters. Variable displacement pumps are, usually, more expensive then fixed displacement pumps. Another reason is the less availability of variable displacement pumps for low speeds.

Since the of use a direct connection to grid fixes the generator speed, both the hydraulic motor and generator can be designed to operate at maximum efficiency at such speed, and therefore increase system overall efficiency.

Another advantage of hydrostatic transmission is the ability to overcome problems regarding the positioning of components in complex structures. The use of pipes and hoses to link pump and motor allows to place them along different parts of the physical system, giving it a characteristic of modularity and flexibility. This provides the possibility to reduce the nacelle mass (DIEPEVEEN *et al.*, 2011).

In the Delft Offshore Wind Turbine Concept (DOT), a hydrostatic transmission to drive a seawater pump is intended to be used. The pressurized water flow of many turbines are added to drive a Pelton hydraulic turbine that is coupled to an electric generator to centralize the

electric power generation. Inside this project, Diepeveen *et al*. (2014) presents the preliminary design of a wind turbine hydraulic drivetrain used to drive the seawater pump.

By applying this feature to wind turbines it is possible to place the hydraulic motor and generator at ground level reducing the weight on the top of the tower (DIEPEVEEN *et al.*, 2014; FLESCH, 2013; RAJABHANDHARAKS, 2008; VARPE, 2008; DOLAN, 2012). That, inherently, makes most off maintenance procedures to be performed at ground level.

2.2.2 Control of hydrostatic transmissions in wind turbines

In wind turbines the equilibrium of torques acting over the rotor, makes it run with the desired speed. Whereas in turbines with direct coupling or gearbox the rotor opposing torque is controlled electrically, in turbines with hydrostatic transmission it is controlled hydraulically.

Equation (2.10) describes the equilibrium of the torques acting on the rotor of the wind turbine with hydrostatic transmission, assuming no losses at the rotor and no gearbox. A similar formulation is adopted by Pedersen *et al.* (2016),

$$T_{Rw} - T_{Pi} = J_R \left(\frac{d\omega_R}{dt}\right), \tag{2.10}$$

where, T_{Pi} it the pump input shaft torque and J_R is the rotor mass moment of inertia.

The wind torque over the rotor T_{Rw} is given in Equation (2.3). The input torque at the pump shaft is related to the difference between the inlet (p_{Pi}) and outlet (p_{Po}) pressures by,

$$T_{Pi} = \frac{(p_{Po} - p_{Pi})D_P}{\eta_{Pm}}, \tag{2.11}$$

where, D_P is the pump volumetric displacement and η_{Pm} the pump mechanical efficiency.

Replacing equations (2.3) and (2.11) into (2.10) and rewriting it in terms of the outlet pump pressure (p_{Po}), Equation (2.12) is obtained when the steady state condition is achieved.

$$p_{Po} = \frac{\rho A v^3 c_p}{2\omega_R}\frac{\eta_{Pm}}{D_P} + p_{Pi}. \tag{2.12}$$

Applying Equation (2.2) in Equation (2.12) and solving for the ideal pump outlet pressure ($p_{Po,ideal}$) results in,

$$p_{Po,ideal} = \frac{\rho A\, r^3 c_{p,ideal} {\omega_R}^2}{2\lambda_{ideal}^3}\frac{\eta_{Pm}}{D_P} + p_{Pi}. \tag{2.13}$$

The ideal pump outlet pressure produces the correct opposing torque to the rotor, leading it to rotate at the ideal speed which makes it extract the maximum amount of power from the wind.

Looking to the hydraulic motor, its output shaft mechanical torque is given by,

$$T_{Mo} = \frac{(p_{Mi} - p_{Mo}) D_M \alpha_M}{\eta_{Mm}}, \tag{2.14}$$

where, $(p_{Mi} - p_{Mo})$ is the pressure drop across the motor, D_M is the motor maximum displacement, α_M is the motor displacement setting and η_{Mm} the mechanical efficiency. The motor output torque is a consequence of the power being supplied to the grid. In this way the motor inlet pressure can be written as,

$$p_{Mi} = \frac{T_{Mo}\eta_{M,m}}{D_M \alpha_M} + p_{Mo}. \tag{2.15}$$

Knowing that the pump outlet is connected to the motor inlet, by controlling the hydraulic motor displacement the pump outlet pressure can be controlled. This way of controlling the rotor is valid for the first four turbine operation regions (Figure 2.7).

Equation (2.13) is the pump outlet reference pressure. There are many techniques and ways of controlling this pump outlet pressure. Several authors proposed those techniques according to their systems trying to improve their control quality.

For operation region *I*, Dolan *et al.* (2012) shows a strategy where a smaller reaction torque is applied in order for λ to be higher than the ideal, allowing the rotor and generator to accelerate, and therefore approach the point for synchronization with the grid.

Diepeveen *et al.* (2014) describes a passive torque control that is provided by the architecture and dimensioning of the fluid power transmission system.

Since such large torque variations are required to achieve only a modest increase in power output, it is usual to use the simple quadratic law (Equation (2.13)), possibly augmented by some inertia compensation (BURTON *et al.*, 2011).

After the variable speed operation region, (region *III* in Figure (2.6)) it is usual to limit the rotational speed to some level, usually determined by aerodynamic noise constraints, which is reached still some way below-rated wind speed. It is then cost-effective to increase to torque demand further, at essentially constant speed, until rated power is reached. Turbines designed for noise-insensitive sites may operate along the optimum power coefficient trajectory all the way until rated power is reached (BURTON et al., 2011).

Burton *et al.* (2011) mention that the development of *LIDAR* (Laser Doppler Anemometry) systems has reached the point where these devices can be used effectively for wind speed measurement at a distance. The possibility to use them to scan the approaching wind field in front of the turbine, for the purposes of improving the control, has been suggested and is perhaps now becoming a possibility. Such devices might be used to reduce loads and/or increase power capture. Measuring the upstream wind speed gives the control system time to take action in anticipation.

Wang *et al.* (2013) presents a more advanced control strategy where a model predictive control is applied together with the $K\omega^2$ law, Equation (2.13). The model prediction is used to track the desired rotor speed. A system model, linearized for a specific operation point, is used to predict the control output. The authors observed a bad control stability for large wind speed steps.

Pedersen *et al.* (2016) presented a variable speed control strategy for a turbine with fixed displacement pump and a digital motor displacement that is varied to control the pressure. Consequently, the turbine rotor speed is controlled through the motor displacement. A model based feedback control together with the $K\omega^2$ law is used to set the opposing torque reference. When calculating this reference, the authors take into account a varying rotor mechanical efficiency by using the rotor viscous friction coefficient.

Dolan e*t al.* (2012) present the turbine and hydrostatic transmission steady state operation points, which are used as desired values for feedforward control. The system model is in extended linearized form, and it is used to design a gain scheduled linear quadratic regulator with wind speed and pressure difference as scheduling parameters. When determining the torque reference with the $K\omega^2$ law, the authors mention that the rotor shaft bearings and pump efficiency change with the operation

point, however, in their analysis they considered it constant. The optimal TSR is used to obtain the rotor speed reference.

Laguna *et al.* (2014) also use the $K\omega^2$ law to control the pump opposing torque by means of pressure regulation through the motor displacement setting. The pressure reference values are taken from the corresponding steady state values for different rotational speeds of the rotor.

Rajabhandharaks (2014) shows a method for controlling a hydrostatic transmission with both pump and motor with variable displacement. For the pump control it uses the strategy to maximize the power coefficient taking the reference from the $K\omega^2$ law. A transmission losses minimization strategy is used to control the motor. Therefore, the author aims to achieve the system maximum overall efficiency.

Schulte *et al.* (2014) also explore the use of both pump and motor with variable displacement. The authors proposed a nonlinear control based on a Takagi-Sugeno model. Still, the desired pressure difference over the pump, is calculated with the $K\omega^2$ law.

The controller used in this thesis is based on the commonly used $K\omega^2$ law, Equation (2.13). However, it is added to it a compensation signal and saturation elements. These two added features allows the same controller for maximum power extraction to have an enhanced performance and at the same time to operates in two turbine control regions. The proposed controller is presented in Section 3.4.

2.3 POWER DELIVERY TO THE GRID

When it comes to electric power deliver to the grid, a set of requirements must be attended in order to ensure a stable and safe transfer of the power. These requirements standardize the power generation in terms of voltage amplitude, frequency and phase shift so that they match the electric grid standards and set power quality levels.

Ali (2012) describes that power quality is the quality of electrical service. The author says that, power quality problem may be defined as any power problems manifested in voltage, current or frequency deviations, which results in failure or miss operation of customer equipment. Hau (2006) also states that frequency oscillations and harmonics might interfere in the functioning of other interconnected equipment.

Ali (2012) also writes that the power quality can be evaluated through impulsive and oscillatory transients that occur either when generating or when connecting generators to the grid. The sudden connection of a large turbine can result in brownout (voltage drop incurred when instantaneous load exceeds generated power) due to the current required to

magnetize the generator, often followed by a power peak when active power from the generator is fed to the network (MUYEEN *et al.*, 2013). Since wind turbines are subjected to intermittent wind speeds, the problems of oscillatory transients and frequent connection and disconnection from the grid are present.

Hau (2006) states a few disadvantages of coupling a synchronous generator to the grid. One of them is that only very small load angles (The load angle is equivalent to the time lead or lag of the grid voltage compared to the generator rotor voltage (HAU, 2006)), are possible for compensating the dynamic loads imposed upon the generator by the wind rotor. Large wind load surges, for example due to strong wind gusts, can cause a loss of synchronization. The synchronous generator, in response to even small load peaks (for example tower shadow in the case of a downwind rotor) tends to produce oscillations which are only poorly damped (HAU, 2006). This is confirmed by Muyeen *et al.* (2013) mentioning that short-term wind power variations cause voltage fluctuations in the grid, known as flicker.

The wind turbine concept evaluated in this thesis has to deal with the issues described above. The generator in this wind turbine concept is a synchronous generator with a direct connection to the grid. The electrical grid where the system is connected to is close to end consumers. Thereby, it is important to have a minimum level of power quality in order to not compromise the local grid and the transitions when bringing the generator online and offline should be smooth.

The problem of voltage and frequency oscillations, mentioned by Hau (2006) and Muyeen *et al.* (2013) shouldn't be the case for the hydrostatic transmission, where most of fluctuations can be damped by the hydraulic coupling between rotor and generator. Supporting this affirmation, Hau (2006), states that turbines retrofitted with fluid couplings in the mechanical drivetrain in order to achieve better damping and smoother power output, also proved to be inadequate to attain complete mastery over the dynamic problems. These fluid couplings are not hydrostatic transmissions, they are a hydraulic clutch placed between the rotor and generator shafts.

Since the test bench is a prototype where the understanding of system behaviour will be built, it is very likely that faults will occur and that control actions will result in oscillations in the power delivered to the grid. These are directly related to the robustness and stability of the hydrostatic transmission and electric and electronic systems controllers. A virtual state machine was developed to supervise and control the test bench.

Individual components controllers were used in order to attain to minimal power quality. They are all described in Section 3.4.

Ali (2012) describes the necessary conditions to synchronize a generator to the grid. The voltage, amplitude, frequency and phase sequence of the generator must be equal to that of the busbar.

Hau (2006) states that difficulties arise with synchronization to the grid, requiring complex automatic synchronization equipment. The stiffness of the direct grid coupling results in a highly uneven power output of the wind turbine. The author says that every wind fluctuation captured by the rotor is passed on to the grid without any smoothing. In addition to difficult operating characteristics, the direct coupling of a synchronous generator to the grid results in high dynamic loads being imposed on the mechanical drivetrain.

At the test bench, the procedure for coupling the generator to the grid is to first match the frequency and the voltage to the grid standards, then the phase shift is brought to zero by leading or legging the generated voltage in comparison with the grid voltage. Once these three factors are within a minimum range around the reference values, the generator to grid circuit breaker is closed. The generator can start to deliver power to the grid. As it will be mentioned in Section 3.4.2.3, the connection with the grid is controlled in such a way that it occurs when the net generated power is around zero. This means that the grid should have approximately zero phase shift and deviation from the nominal frequency and voltage values when the connection occurs.

2.3.1 Synchronous generator connected to an infinite busbar

The direct connection of the generator to grid is a key feature of the concept studied in this thesis. This section is used to describe the physical principles and theory around a synchronous generator with direct connection to an infinite busbar.

The generated power frequency (f_{GS}) on a synchronous machine is a function of the generator rotational speed (ω_{GS}) and number of pair of poles (n_{GS}), that is,

$$f_{GS} = \frac{n_{GS}\omega_{GS}}{60}. \tag{2.16}$$

If the generator is operating at the synchronous speed ($\omega_{GS,n}$) the generated power frequency is the grid frequency. Connecting the generator directly to the fixed-frequency grid forces the generator to run at constant speed (HAU, 2006). When the generator is connected to an infinite

busbar, the terminal voltage is also constant (SHEPHERD and ZHANG, 2011).

According to Kundur (1994), when two or more synchronous machines are interconnected, the stator voltages and currents of all machines must have the same frequency and the rotor mechanical speed of each is synchronized to this frequency. Therefore, the rotors of all interconnected synchronous machines must be in synchronism.

Ali (2012) mentions that a large number of synchronous machines are usually connected in parallel to supply the loads, forming a large power system known as a grid. The author continues his description saying that the voltage and frequency on the grid remain substantially constant (Kundur (1994) develops his work and calls it power system stability). Ali (2012) continue saying that when a synchronous generator is connected to the grid, its terminal (stator) voltage and frequency are fixed by the grid and it is said to be operating on infinite busbars. A change in the operating in the generator mechanical power input will cause a corresponding change in the electrical power output.

According to Shepherd *et al.* (2011) for a generator connected to a large power system, the generator speed must be governed to remain constant at the value consistent with the system frequency.

Shepherd *et al.* (2011) also mention that the load angle δ (also called power or torque angle) is the angle between phasors of the rotor voltage and the voltage at the generator terminal(stator). The transient effects are often considered in terms of variations of the load angle δ.

Having explained the principle of an infinite busbar, it can be concluded that the generator used in this thesis will operate with the synchronous speed when synchronized. Another conclusion is that, when synchronized the mechanical power provided by the hydrostatic transmission to the generator will be transferred to the grid.

Flesch (2012) presented in his thesis a more extensive description of the physical principle of power delivery to the grid by a synchronous generator. Since his thesis can be seen as a base for the development of this one, only a brief review of the physical principle of power deliver to the grid is shown here.

Kundur (1994 *apud* Flesch (2012)) states that the relevant equations to analyse the stability of power systems are the ones that describe the imbalance between the mechanical torque (T_{GSm}) at the generator input shaft and the electric torque (T_{GSe}). The difference produces an accelerating torque described as,

$$T_{GS,m} - T_{GSe} = J_{MGS}\left(\frac{d^2\theta}{dt^2}\right), \tag{2.17}$$

where J_{MGS}, for this thesis, is the combined generator and hydraulic motor mass moment of inertia and θ the rotor rotation angle with respect to a fixed reference. The following reference system is used to describe the effects of the mechanical torque variation on the electrical torque.

Figure 2.11 - Reference coordinates system for synchronous machines.

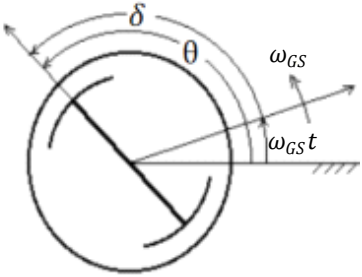

Source: Adapted from Costa *et al.* (2000 *apud* Flesch (2012)).

Flesch (2012) continues his analysis saying that, when a mechanical torque exists it will produce a relative angular displacement (δ) on the rotor with respect to the rotating reference ($\omega_{GS}t$), given by,

$$\theta = \omega_{GS,n}t + \delta. \tag{2.18}$$

Deriving Equation (2.18) twice with respect to time results in,

$$\frac{d\theta}{dt} = \omega_{GS,n} + \frac{d\delta}{dt}, \tag{2.19}$$

$$\frac{d^2\theta}{dt^2} = \frac{d^2\delta}{dt^2} = \frac{d\omega_{GS}}{dt}. \tag{2.20}$$

In steady state (equilibrium of torques), the rotor speed will be the synchronous speed ($\omega_{GS,n}$) and δ will be constant meaning that a certain constant power is being delivered to the grid.

The power stability analysis for a given disturbance in the mechanical torque and its respective influence over the electric torque can be described in terms of the load angle δ. This analysis is made by Flesch (2012).

3. TEST BENCH DESCRIPTION

"Experience never errs; it is only your judgments that err by promising themselves effects such as are not caused by your experiments."
(Da Vinci)

The main goal with the test bench is to perform the experimental evaluation of the wind turbine concept described in Section 2.2.1. With the experiments it is intended to have the confirmation of the expected system behaviour and to observe other unknown behaviours.

The hydrostatic transmission in the test bench is considered to be the hardware-in-the-loop. The rotor interaction with the wind, and calculation of the aerodynamic performance is the online simulation.

Different test bench concepts were studied by Raduenz (2015) during previous work done in the project. A suitable concept was chosen and developed having practical issues as a guidance. The laboratory facility physical available space and the components supplied by the project sponsors were the key constraints.

The bench need to be fitted inside the physical space available at LASHIP, where height difference between the pump and motor/generator was the strongest constraint. The height between the pump and motor/generator is height between the floor and the building roof.

Since the focus is the transmission itself the tests couldn't rely on local wind availability to be performed. Therefore, an electric motor controlled by a frequency converter is used to emulate the rotor action over the transmission input pump shaft.

The bench was sized according to the electric components provided by REIVAX and the hydraulic components provided by PARKER. The processes of sizing hydraulic components and selecting them from PARKER portfolio is described by Rapp and Turesson (2015).

The rotor rotational speed of wind turbines is low so the pump should have high volumetric displacement and high global efficiency at low speeds. Off-the-shelve PARKER pumps are not developed for such low speeds, under 150 rpm, and high displacements. Therefore, with small displacement and low efficiency the pump wouldn't be able to deliver the hydraulic power needed for the system. For those two reasons a gearbox is placed in between rotor output shaft and pump input shaft. The gearbox amplifies the speed which allows for the use of a pump with smaller displacement operating at higher speed, therefore also increasing global efficiency.

The electric motor used to drive the pump would also struggle to provide a high output electric torque at low speeds. So the gearbox operation is also emulated by the electric motor as explained in the sequence.

The electric motor that drives the pump is controlled by the frequency converter with a virtually calculated torque reference. This torque reference is the torque that the gearbox would deliver at its output shaft. The output shaft torque and the input shaft torque at the gearbox are coupled through the gearbox transmission ratio. The gearbox input torque is the rotor torque due to wind. Therefore, there is no need for the physical gearbox at the test bench. It is implemented in the supervisory and control system as a virtual gearbox having its behaviour being calculated based on wind torque and gearbox transmission ratio. The implantation in the virtual controller is detailed in Section 3.4.1. The effectiveness and suitability of the inclusion of such device is discussed in Chapter 7.

The test bench also has a fluid temperature control unit. The long transmission lines from the top to the bottom of the building provides a considerable heat exchange area to cool the fluid naturally. The detailed description of this heat transfer mechanism is not part of the scope of this thesis.

Table 3.1 presents a synthesis of the test bench main parameters.

Table 3.1 - Synthesis of the test bench main parameters.

Description	Symbol	Value
Nominal Output power	$P_{GSo,n}$	28.50 kW
Motor to Pump height difference	h	8.00 m
System Nominal flow rate	q_n	110.00 L/min
Nominal pressure difference between lines	Δp_n	210.00 bar
Maximum electric motor speed	$\omega_{EM,max}$	1550.00 rpm
Generator nominal speed	$\omega_{GS,n}$	1800.00 rpm
Maximum fluid temperature	T_{max}	42.50 °C
Nominal Output voltage	E_n	380.00 V

Source: Author.

A detailed description of layout, hydraulic circuit, electrical circuit, sensors, data acquisition and control and supervisory systems is done in the following sections.

A CAD drawing scheme of the bench placed at LASHIP facilities is presented in Figure 3.1.

Figure 3.1 - Test bench layout.

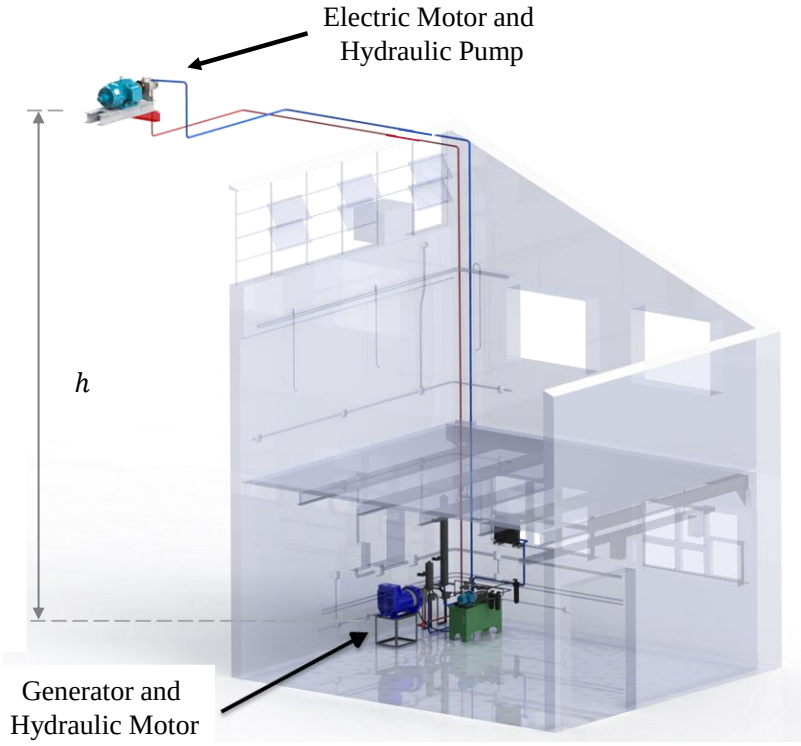

Source: adapted from Rapp and Turesson (2015).

The system layout was developed together with Adriano Martins, Joel Rapp and Jonatan Turesson previously on the project.

To deal with the height difference proposed with the concept, the hydraulic pump and electric motor were placed on the roof while the hydraulic motor and generator inside the lab at ground level. This height is not exactly the one found on commercial wind turbines with this range of output power. Even being different, it allows the evaluation of dynamic effects due to long pressure lines and assembly issues due to the height.

Hydraulic lines followed the building shape and available space, this added more curves and length to them in comparison with what a real wind turbine would have. This extra length and curves result in more pressure drop on the system. In the same way, a change in the dynamic

behaviour is expected since the increase in fluid volume reduces the system stiffness.

Reservoir, hydraulic charging system and motor displacement control hydraulic system are placed beside the generator. This layout ensures a weight reduction in the turbine nacelle consequently, a smaller weight that the turbine tower would have to sustain. As mentioned before, by having most components at ground level the maintenance/service of such system should become easier.

On the electric/electronic components side, the frequency converter, soft starter, data acquisition and control system are placed on ground level as well. Those devices and the connections between them are better detailed in Section 3.2.

3.1 HYDRAULIC CIRCUIT

It is a closed-loop hydrostatic transmission with a fixed displacement pump and variable displacement motor, as shown in Figure 2.10 . A charging circuit is added to refill to the main circuit the fluid that flows out of it through external leakage in the hydraulic motor and pump. Since the motor displacement is hydraulic piloted a separate hydraulic circuit is needed to control it.

As a starting point for the bench development, the work done by Flesch (2012) was taken. The components where downsized by Raduenz (2015) and selected by Rapp and Turesson (2015). Only those major components that were added during this work have their function described in this thesis. For better whole system explanation please refer to the mentioned authors.

As Rapp and Turesson (2015) described, the hydraulic components used in the bench were selected from PARKER portfolio. Not all the components were available for the project since their cost was a determinant to supply or not the project with them. Most part of the used components are for mobile application and not for industrial purpose, and specially not for wind turbine systems. It is noteworthy that these components are suitable to prove the functionality of the concept but, obviously it is not expected to achieve high efficiencies with them since they are not working exactly in the conditions that they were designed for.

Two pictures showing the hydraulic system assembly are shown in Figure 3.2 and Figure 3.3.

Figure 3.2 - Motor and pump assembly in the test bench.

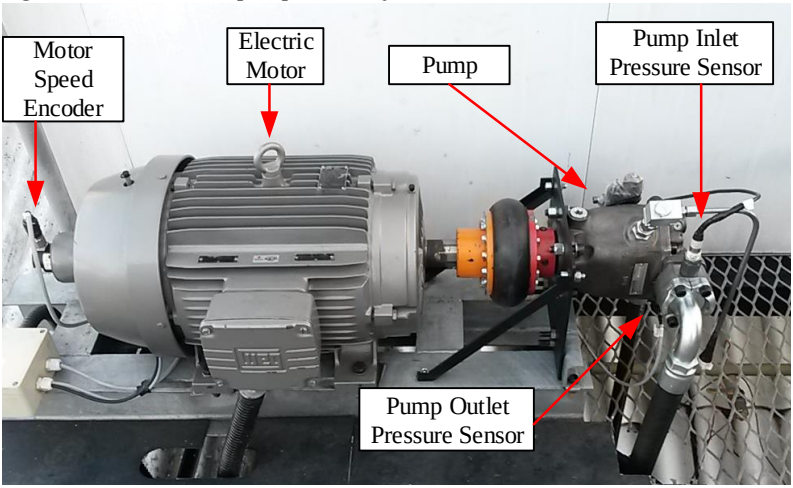

Source: Author.

As said, the hydraulic pump and electric motor are assembled on the roof. The rest of the hydraulic components are placed inside the building as depicted in Figure 3.3. Only the hydraulic lines, power and signals cables are used to connect the bottom part with the upper part.

Figure 3.3 - Test bench hydraulic circuit assembly.

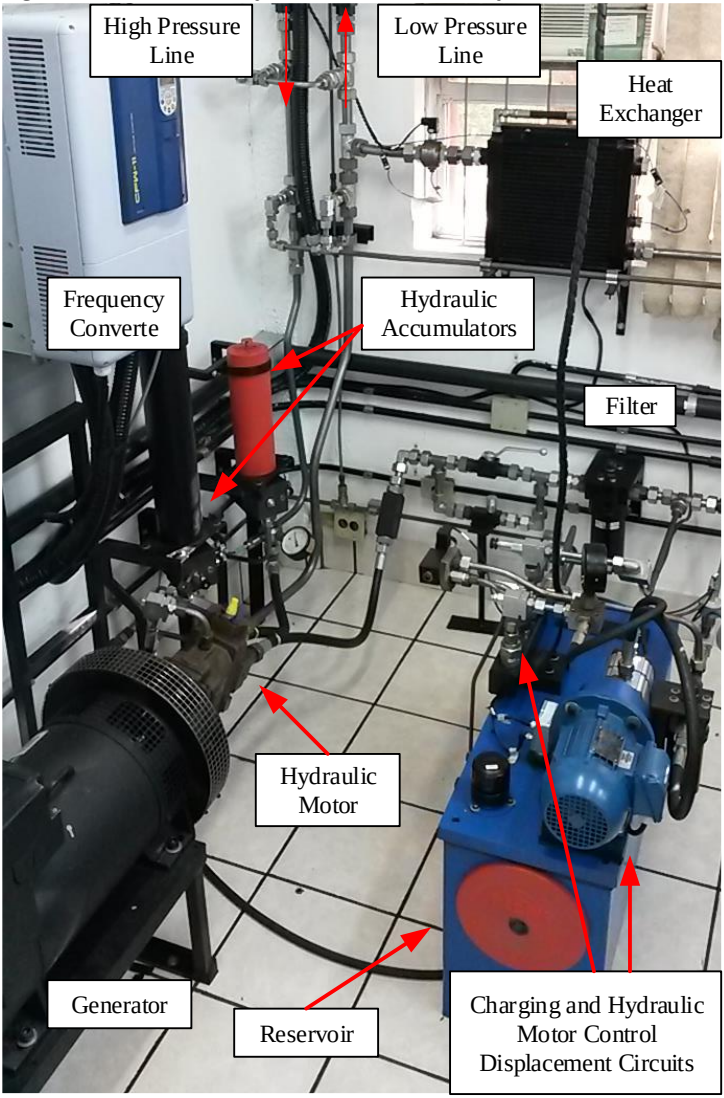

Source: Author.

A full detailed list with all the hydraulic components main parameters is place at Appendix D. Figure 3.4 presents the main hydraulic circuit diagram together with sensors, electric motors and generator.

Figure 3.4 - Test Bench Main Hydraulic Circuit.

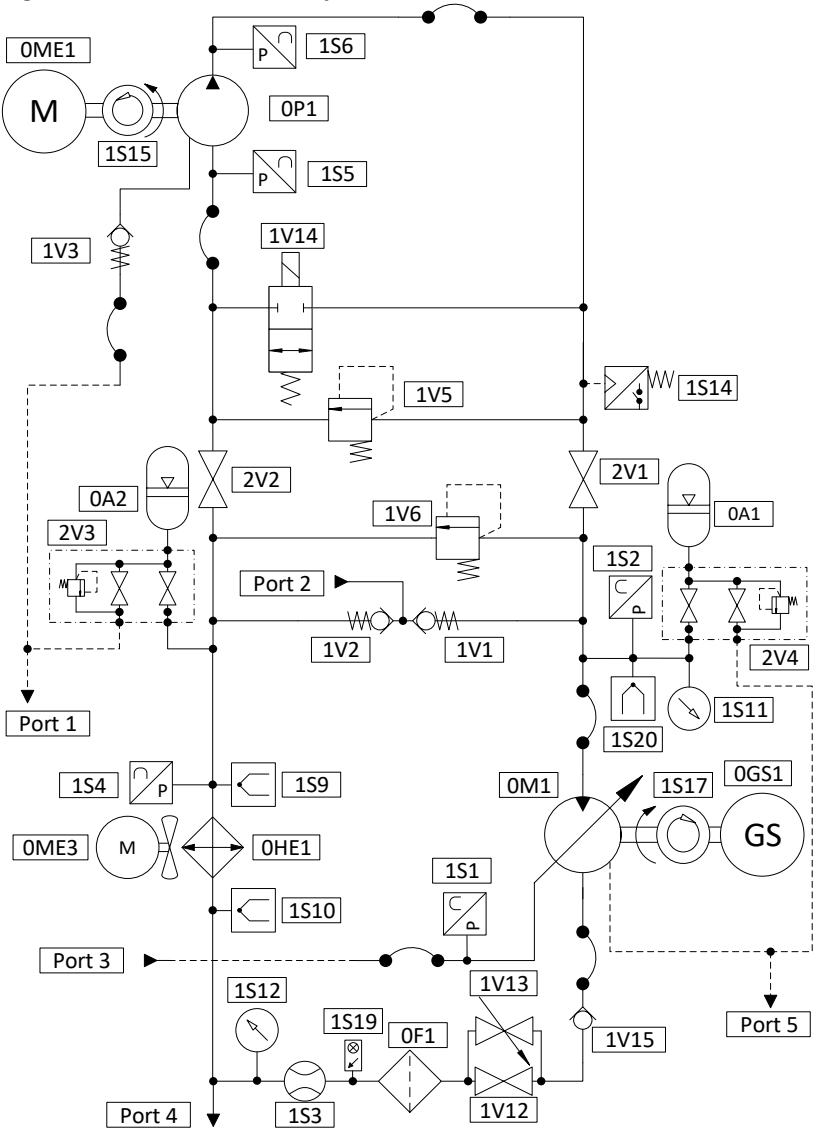

Source: Author.

Figure 3.5 presents the charging, motor control hydraulic circuits and the reservoir.

Figure 3.5 - Charging and Motor Control Hydraulic Circuit.

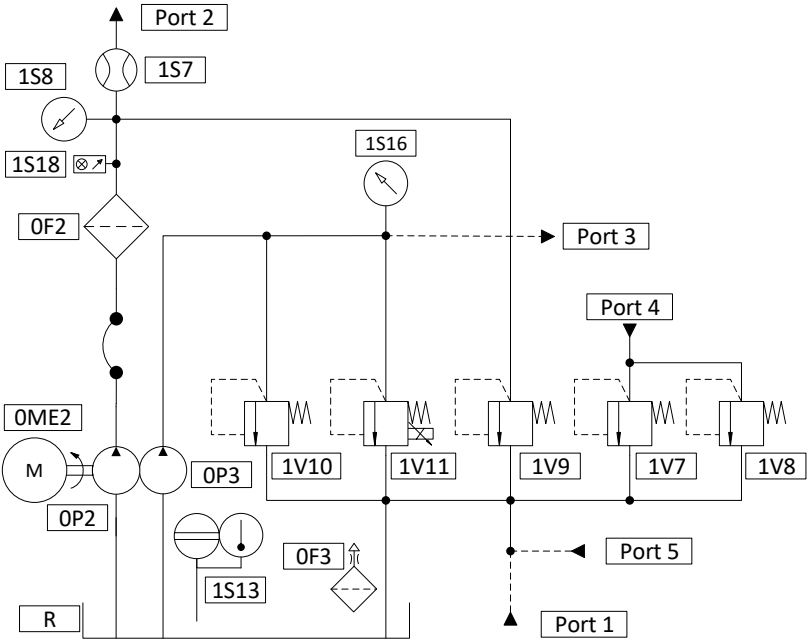

Source: Author.

3.1.1 Main circuit

This section contains a brief description of the components present in the hydrostatic transmission main circuit.

To ensure a safety action in case of system failure, an on/off normally open valve (1V14) is included between high and low pressure lines. When it is energized its solenoid closes the fluid path, in case of a safety action, the power supply to it is shut down and it opens the fluid path. This action brings the pressure in both lines to an equilibrium at a maximum of 4.0 to 5.0 bar which is the 1V7 valve cracking pressure. With that happening, it is avoided to have a generator over speed or to keep the high pressure line pressurized when the system is turned off. 1V8 is a redundant valve for safety. It's cracking pressure is slightly above 1V7.

Another different system feature are the valves 1V12 and 1V13. They are used to control the fluid flow, preventing the generator to over speed while running tests with the generator disconnected from the grid.

Pressure relief valves 1V5 and 1V6 work as safety valves in order to limit the power generated by the system. When the pressure reaches the cracking pressure it will divert part of the flow to the low pressure line. At this point the system loses part of its controllability since there is no way to increase the pressure in order to control the rotor speed. System nominal pressure difference (Δp_n) was set to be 210 bar between lines, in order to not lose control at this point, 1V5 and 1V6 cracking pressure is set to 225 bar.

Another safety device included on the high pressure line is a pressure switch 1S14. It is regulated to 230.0 bar. If this pressure is reached it activates the emergency state, where the system is shut down.

The presence of accumulators affects the response time of the transmission. Accumulators reduce the stiffness of the hydraulic medium, causing the motor to take longer time to sense an input at the pump (COSTA *et al.*, 2015). From the other side, looking from the perspective of controlling the turbine rotor through the change in the hydraulic motor displacement, the motor control action is perceived by the pump with an increased time delay. The accumulators are present in the circuit to damp peaks of torques created by the interaction of the rotor with the wind. The low pressure side accumulator (0A2) also helps to prevent cavitation in the pump (0P1) inlet, for example in case of fast rotor accelerations during wind gusts.

With the selected pump and motor, the hydrostatic ratio (i_{HT}) can vary infinitely between 6.25 and 1.25 since the pump displacement is 75.00 cm^3/rev and the motor range is from 12.00 to 60.00 cm^3/rev.

3.1.2 Charging circuit

Pump and motor volumetric losses induce a pressure reduction on the main hydraulic lines that contributes to cavitation occurrence in closed-loop hydrostatic transmissions. The charging circuit is used to replace the fluid that flows out of the main circuit. It can also be called replenishment or boost circuit/system.

The charging circuit is connect to the high and low pressure lines via check valves, 1V1 and 1V2, in order to provide the fluid back to the main circuit.

The fluid column on the pump inlet might be too high to suction it without cavitation occurrence. Another charging circuit function, that it fulfils together with the accumulator 0A2, is to assure an above zero pressure on the pump inlet to avoid cavitation. The whole system is prevented to start up or is shut down if the pump pressure is/or drops below 1.0 bar.

The pressure difference between the lines is related to the wind speed, as explained in Section 2. Higher wind speeds results in higher pressure and flow rate and consequently in higher volumetric losses in the pump and motor. The charging circuit must handle the worst case, which is when the system operates with rated power, when the highest leakage is expected. As demonstrated by Rapp and Turesson (2015), in this operation point the low pressure line pressure must be at around 5.0 bar. To set such pressure, the 1V9 relief valve is adjusted to above 5.0 bar.

3.1.3 Motor displacement control circuit

The hydraulic motor has a hydraulic proportional volumetric displacement control. The swash plate position is set through the equilibrium of forces from springs, system pressure (ports A and B) and the pilot pressure (port X5) acting on an internal proportional directional valve as shown in Figure 3.6.

Figure 3.6 - Hydraulic motor displacement internal control circuit.

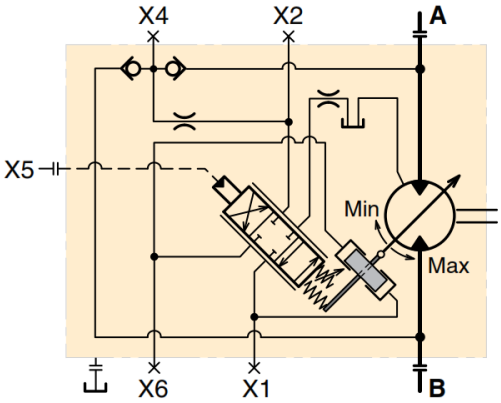

Source: Parker catalogue, V12 motor, hydraulic proportional control.

By setting a determined pressure at pilot port X5, the swash plate reach an equilibrium position and so setting a proportional motor displacement. The relation of pilot pressure to displacement is given by the manufacturer and is shown in Figure 3.7.

Figure 3.7 - Motor displacement setting as a function of pilot pressure.

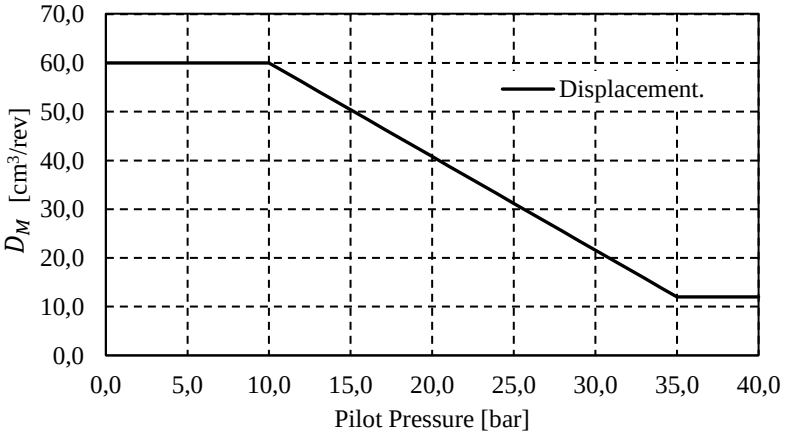

Source: Adapted from Parker V12 Hydraulic motor HP control - catalogue.

Equation (3.1) describes the linear displacement setting relation with pilot pressure between the threshold pressure (10 bar) and the pressure for minimal displacement (35 bar),

$$\alpha_M = (-0.8p_{Mp} + 33)/25, \tag{3.1}$$

where, α_M is the hydraulic motor displacement setting and p_{Mp} the pilot pressure.

Equation (3.1) can be rewritten in terms of pressure, resulting in Equation (3.2),

$$p_{Mp} = -(25\alpha_M - 33)/0.8. \tag{3.2}$$

A pump (0P3), two pressure relief valves (1V10 and 1V11) and a pressure sensor (1S1) compose the motor displacement control circuit. The pump 0P3 is tandem with pump 0P2 and they are driven by the electric motor 0EM2. 0P3 only function is to provide hydraulic power for the motor displacement control circuit. The hydraulic circuit is show in Figure 3.8.

The pressure measured with 1S1 is used to close the feedback loop by transforming it into the real displacement with Equation (3.1) and comparing it with the displacement reference $\alpha_{M,ref}$, thus controlling the displacement.

Figure 3.8 – Hydraulic motor displacement control circuit.

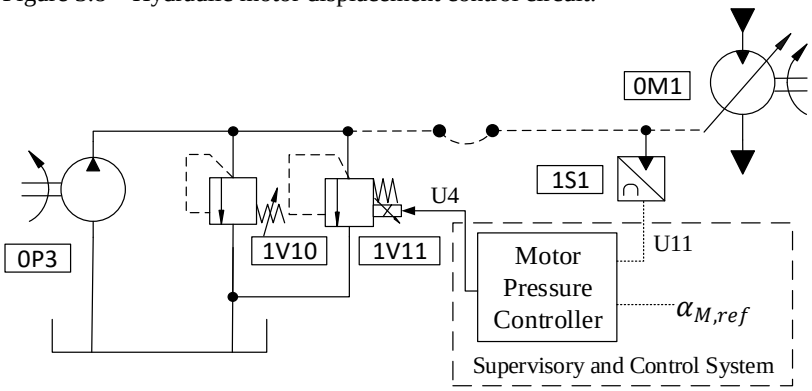

Source: Author.

The pilot pressure is controlled with a direct operated hydraulic proportional pressure relief valve (1V11). The valve hydraulic diagram is presented in Figure 3.9. Port P is connected to the flow source, in this case pump 0P3, and port A is the pilot port connected to the motor pilot port X5. The chosen valve works with a PWM signal that have its duty cycle varying between 0.0 and 100.0 %. The relation between control signal and controlled pressure at the valve is show in Figure 3.10, 5.0 L/min curve.

Figure 3.9 - Proportional relief valve hydraulic circuit.

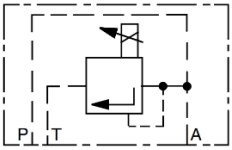

Source: PARKER catalogue.

The valve works together with a digital amplifier modulus that generates and controls the PWM signal sent to the valve, U4 in Figure 3.8. The command input signal to this module is a 0.0 to 10.0 VDC signal. 0.0 VDC means a 0.0 % duty cycle signal resulting in total opening of it and consequently a near zero bar regulated pressure, only the valve pressure drop (from ports A and P to T) is present. A 10.0 VDC command signal represents a 100.0 % duty cycle resulting in the total closing of the valve and consequently the maximum valve controlled pressure, 105.0 bar for this valve.

Figure 3.10 – Proportional pressure relive valve controlled pressure as a function of the PWM command signal.

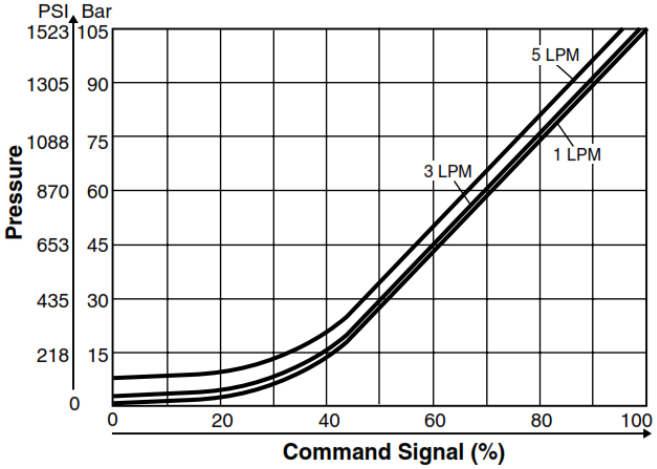

Source: PARKER catalogue.

Since a pressure acts against the proportional solenoid, if the valve power supply is turned off, the valve will open and the pressure at port A becomes the valve pressure drop. If a 10.0 VDC command signal is mistakenly provided to the valve it will close and pressure at port A will rise to 105.0 bar. This is not allowed since it can cause damage to the hydraulic motor displacement control system. Therefore, a pressure relief valve (1V10) with cracking pressure set to 45.0 bar is connected in parallel to avoid such pressure build up.

3.2 ELECTRIC CIRCUIT

This section objective is to present the main electric circuit and its components characteristics. The three phase connection is 380 VAC and 60 Hz. These are the grid characteristics that the generated electric power must have. A detailed list with all the electric components parameters is place at Appendix E. Figure 3.11 and Figure 3.12 are pictures from the test bench. They show the assembly layout of the main electrical components at the test bench.

The nominal output power is relatively small, 28.5 kW, if compared to most of electrical power generation systems and to the systems connected to the grid. Thereby, the influence of delivering such power to the grid is considered to be insignificant. At the same time, the point

where the power that supplies the system is taken from is the same point where the generated power is delivered.

Figure 3.11 - Test bench electrical components layout.

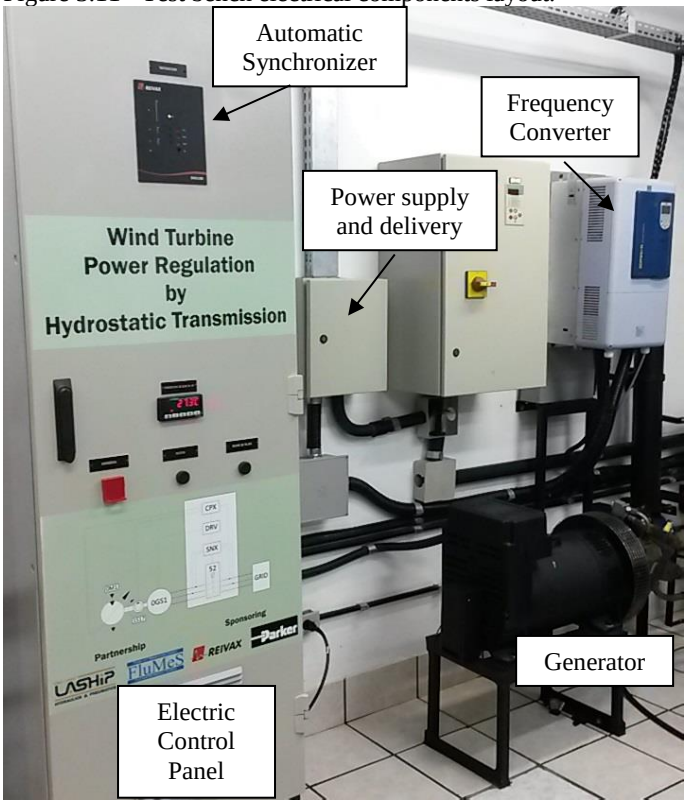

Source: Author.

Regarding the power input in the circuit, as will be further detailed in Section 3.4, the wind turbine rotor operation is virtually simulated. The action of it over the pump input shaft is carried by an electric motor controlled by the frequency converter.

This frequency converter receives a torque reference from the supervisory and control system and controls the electric motor in a way to ensure it is applying this torque over the pump. The applied torque is the simulated torque extracted from the wind. The electric motor speed is controlled by the hydrostatic transmission.

Another power input to the system is the power provided by the electric motor 0EM2. It drives the charging circuit and motor displacement

control pumps, 0P2 and 0P3. This motor is driven by a soft starter to control its start-up, after that it runs at constant speed, 1130.0 rpm.

Figure 3.12 - Electric control panel - inside components layout.

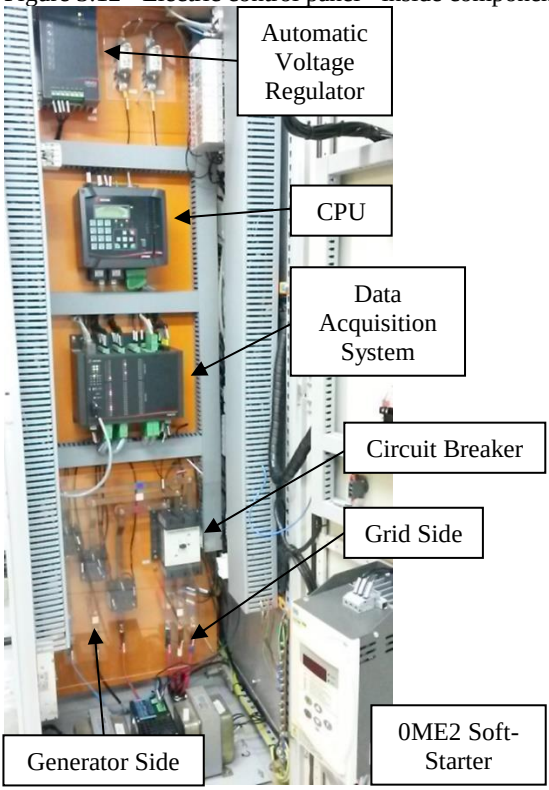

Source: Author.

Regarding the power generation and delivery, nominal voltage and nominal frequency are the two main parameters pursued when synchronizing the system with the grid and when delivering the power to it.

Before the synchronization the generator frequency is brought to its nominal value. When it reaches it, the automatic voltage regulator is enabled and it ramps up the generators voltage until the nominal/grid value. This is called generator excitation. When it reaches the nominal value the synchronization action is enabled.

The synchronization action is performed by an automatic synchronizer. It compares the generator frequency, voltage and phase shift with the respective grid values. Based on the errors it controls each generator

values to match the grid values. When all of them lie in closed range around the grid values it closes the circuit breaker that connects the generator to the grid. When the circuit breaker is closed the system is said to be synchronized.

When synchronized, the system relies on the principle of infinite busbar, than, voltage and frequency are kept constant by the grid. This is true because the grid stiffness is very high due to the number of synchronous machines connected to it and because the test bench generator power is very small, and therefore not capable to interfere in the grid.

While exciting, synchronizing or delivering power the voltage is regulated by the REIVAX components.

3.3 SENSORS AND DATA ACQUISITION

A set of sensors was used in the bench in order to control it, ensure a safe operation and to collect information of the system state. The sensors present at the bench are pressure, flow rate, temperature, voltage and current sensors. Their signal outputs are either in mV, V or mA.

For data acquisition and control a REIVAX device is used. It is responsible for all the reading of the system as for the dispatch of control commands. It operates only with mA ports, such that the input and output signals that arrive in V or must be sent in V are converted using isolators/converters, also from REIVAX.

A detailed list with all sensors and data acquisition components parameters is place at APPENDIX C.

3.4 CONTROL AND SUPERVISORY SYSTEM

The control and supervisory system is a set of virtual and hardware components and signals that deals with safety, control and operation of the system. There is a difference between the control and supervisory system for the test bench and for the mathematical model for simulation.

For the test bench, the control and supervisory system handles the automation of the system in order for it to run in all operation envelope presented in Section 2.1.2. Inside each operation region they control the system in order to obtain the desired system behaviour and performance.

For the mathematical model for simulation, the control structure aims to control the system to obtain the desired performance during the simulations. As will be explained in Section 5, the model for simulation represents the system only when operating in regions *III* and *IV*. Therefore, there is no supervisory system implemented in the simulations.

Along this section, the control and supervisory system for the test bench is detailed and, when necessary, the control structure for the simulation model is referred to.

This section is divided in a few topics. It starts by describing the system control structure and the main control signals and components. Then the control loops are described, followed by how these control loops are switched along the system operation. Each control loop has a set of gains that also must be switched. At the end of the section the state machine developed for the test bench is described.

Raduenz (2015) presents a simplified block diagram of the whole test bench. It is used in this work as base to present details and explanation of each part of the control and supervisory system. This diagram was adapted to the present test bench status and it is presented in Figure 3.13.

Figure 3.13 - Test bench block diagram.

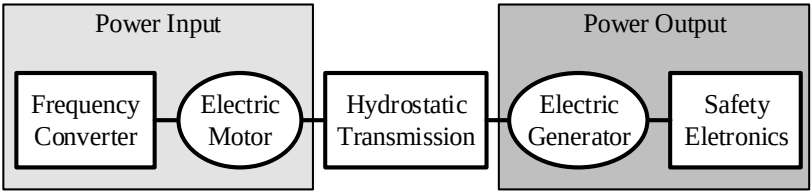

Source: Adapted from Raduenz (2015).

The system is divided in three main groups that are: Power Input, Hydrostatic Transmission and Power output. This division is herein used to explain how the supervisory and control system works for each group.

Figure 3.14 is a block diagram of the bench containing the major control signals and components of the control and supervisory system.

Table 3.2 contains the descriptions of all signals and components of Figure 3.14. These signals and components nomenclature are used in this section. To begin with, the power input control is described.

Figure 3.14 - Detailed control and supervisory system diagram.

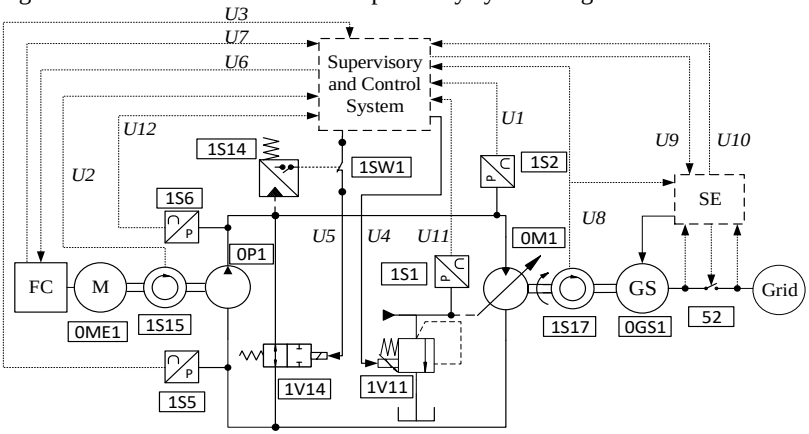

Source: Author.

Table 3.2 - Description of Figure 3.14 components and signals

Component / Signal	Description
FC	Frequency Converter
SE	Safety Electronics
0ME1	Power input electric motor
0P1	Hydraulic pump
0M1	Hydraulic motor
0GS1	Synchronous generator
1V11	Proportional pressure relief valve
52	Generator to grid circuit breaker
1SW1	Electric switch
1S1, 1S2, 1S5, 1S6	Pressure sensors
1S15	Pump rotational speed sensor
1S17	Generator rotational speed sensor
1V14	On/off safety valve
1S14	Pressure switch
U1	High pressure line pressure signal
U2	Pump rotational speed
U3	Pump inlet pressure signal
U4	Proportional relief valve PWM signal
U5	On/off safety valve power supply
U6	Motor torque reference signal
U7	Measured motor torque signal
U8	Generator Speed
U9	Open 52 (Safety)

U10	52 State
U11	Motor control pressure signal
U12	Pump outlet pressure signal

Source: Author.

3.4.1 Power input control

To evaluate the hydrostatic transmission performance as a power transmission system for wind turbines it is necessary to reproduce, as much as possible, the real wind turbine behaviour on the test bench.

As explained at the beginning of Section 3, the test bench does not have a physical rotor to extract power from the wind neither a physical gearbox. Therefore, to have the same input power behaviour as the turbine would have the electric motor must be controlled in a way to reproduce the dynamic behaviour of the rotor and gearbox. This dynamic behaviour is virtually and on-line simulated to be applied to the physical system power input. This is also called real-time simulation or hardware-in-the-loop. Therefore, the physical system is the hardware-in-the-loop. Figure 3.15 presents a scheme showing the real wind turbine power input system (using a commercially available pump) and the test bench power input system, where it is possible to understand the real and virtual parts.

Similar test bench solutions, where the rotor inertia is accounted via real-time simulation, are adopted by IFAS Aachen (SCHMITZ *et al.*, 2012) and the CCEFP in Minnesota (THUL *et al.*, 2011), at their test benches for wind turbine hydrostatic transmission.

The whole test bench is operated according to a wind speed input. By using equations (2.1), (2.2), (3.3) and (3.4), the wind speed is converted into the power extracted from the wind. A detailed explanation of such equations can be found in Rapp and Turesson (2015) and Raduenz (2015).

The equation that describes the performance of the blade aerodynamic profile used in the present work is the same as used by Freitas (2008 *apud* Flesch (2012)). This aerodynamic performance is presented in equations (3.3) and (3.4) and it is a function of the rotor tip speed ratio and blade pitch angle.

Figure 3.15 - a) Representation of the wind turbine power input system; b) Real and virtual parts of the test bench power input system.

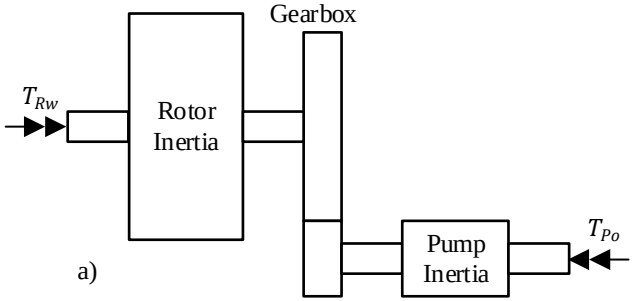

a)

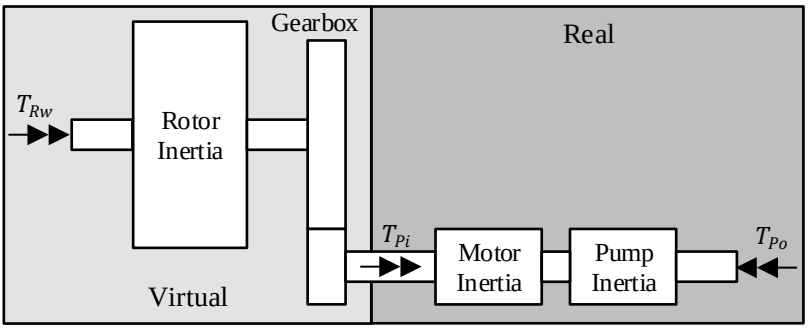

b)

Source: Author.

$$c_p = 0.258\left(\frac{100}{\lambda_i} - 0.4\beta - 2.164\right) exp\left(\frac{-15.21}{\lambda_i}\right) + 0.00571\lambda \tag{3.3}$$

$$\lambda_i = \left(\frac{1}{\lambda + 0.08\beta} - \frac{0.035}{\beta^3 + 1}\right)^{-1}. \tag{3.4}$$

The pitch angle β is part of the equations, however in the operation regions herein studied it is considered to be zero, which results in maximum power coefficient curve, Figure 2.1. The system is not evaluated when it enters the pitch regulated operation region *V* in Figure 2.7. If the reader is interested in understanding how the turbine is controlled through blade pitching, the author invites to read the masters thesis of Gonzalez (2012).

The power extracted from the wind (Equation (2.1)) is divided by the measured rotor speed to obtain the extracted wind torque over the rotor (T_{Rw}), Equation (2.3). The rotor speed is coupled to the electric motor speed through the gearbox transmission ratio, as described in Equation (4.1). The pump speed is equal to the electric motor speed

The test bench electric motor and hydraulic pump does not have the same mass moment of inertia as the real wind turbine rotor. With different mass moments of inertia the dynamic response of the test bench differ from the real system. To achieve a similar dynamic response the rotor dynamic behaviour is implemented via real-time simulation. Equation (3.5) represents the torque balance on the rotor inertia, which is a single-degree rotational system.

$$T_{Rw} - T_{Ro} - T_{Rf} = J_R\left(\frac{d\omega_R}{dt}\right), \tag{3.5}$$

where, T_{Ro} is the output shaft rotor torque and T_{Rf} is the rotor shaft friction torque.

The rotor shaft friction torque is modelled as a viscous friction dependent on its speed and the viscous friction coefficient (c_R), and a Coulomb constant friction ($T_{Rf,Coulomb}$),

$$T_{Rf} = c_R\omega_R + T_{Rf,Coulomb}. \tag{3.6}$$

Considering Equation (3.7), that is derived from the equation of power transmission through a gearbox, it is possible to obtain the gearbox output torque that is equal to the pump input torque (T_{Pi}).

$$T_{Pi} = \frac{T_{Ro}\eta_{GBm}}{i_{GB}}, \tag{3.7}$$

where η_{GBm} is the gearbox mechanical efficiency.

The gearbox is here considered to have a small mass moment of inertia compared to the rotor inertia and to be rigid, such that its dynamic behaviour is neglected.

Through real-time simulation, the pump input torque is calculated with equations (3.3) to (3.7). This pump input torque is sent to the frequency converter as a reference signal (*U6* in Figure 3.16). The frequency converter then controls the motor for it to apply this torque over the pump. In this way, the rotational speed of the rotor/pump is free to be controlled by the hydrostatic transmission. The frequency converter controls the torque and not the rotational speed. The rotor speed is controlled according to the description made in Section 2.2.2.

Figure 3.16 is the power input system block diagram that presents how the dynamic behaviour is calculated and the torque reference delivered to the frequency converter to be applied over the pump.

Figure 3.16 - Block diagram of the power input system.

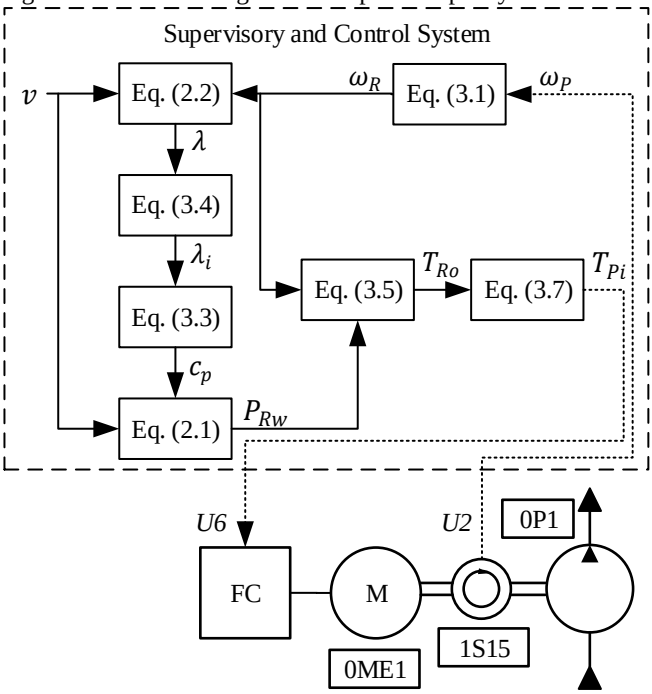

Source: Author.

The torque that the motor applies on its shaft is proportional to a torque current supplied to it, as described by its manufacturer. The frequency converter controls this torque current delivered to the motor. The torque reference sent to the frequency converter, *U6*, is actually a percentage of the motor nominal torque current. At the same time a reference speed must be provided.

Internally the frequency converter has a torque saturation element as the dominant controller. That means that it will reach the speed reference if it is below the torque limit. So, in order for it to always apply the desired reference torque to the motor the speed reference is always set to 15.0 % higher than the measured speed, *U2*. In resume, it will always try to reach the reference speed, but it is prevented by the torque limit, which

is the reference provided by the test bench controller, which, in its turn, is the calculated pump inlet torque (T_{Pi}).

After a change in wind speed, part of the power is converted in rotor acceleration such that not all the torque is transmitted to the output shaft. The output torque is temporarily decreased, while the rotor is accelerating. After the acceleration process ends the output torque is stabilized according to the input.

Vatheuer *et al.* (2011) demonstrates how the rotor acts like a buffer by storing and delivering kinetic energy. At the same time it shows that most of the input torque fluctuations are damped by the rotor huge mass moment of inertia.

In the test bench, there is a concern related to the frequency converter time response. It has a certain time delay and rate of application of the reference torque over the motor. The wind turbine has naturally a slow time response due to its big mass moment of inertia. However, if the response time of the frequency converter is around the same magnitude the dynamic behaviour at bench might not represent the wind turbine dynamic behaviour. The influence of the frequency converter time response is tested, the results are presented in Section 6.1.

3.4.2 Hydrostatic transmission control

The next sections describes how the hydrostatic transmission is controlled in each operation region according to Figure 2.7.

Burton *et al.* (2011) mention that the design of the wind turbine controller must take into account the effect of loads and, at least ensure that excessive loads are not a result from the control action. These loads can be generated by rotor or generator torque variations or even pitch control actions. They can propagate throughout the turbine, from rotor to tower, causing structural stresses. However, the authors mention that the control of such loads in detriment to a loss in power generation is only justified if it causes very little or no loss of power production.

There are several control objectives in a wind turbine, two are explored in this thesis. One of them is the maximization of power production in below-rated wind speed operation. Another one is to limit the rotor speed to avoid a higher than maximum rotor speed. Added to these two control objectives there is the control to synchronize and interconnect the generator to the grid.

In the following sections it is presented a controller named Maximum Power Tracking controller (MPT), responsible for the maximization of power extraction in below-rated wind speeds. The Rotor Nominal

Speed controller (RNS) is implemented as a limitation in the MPT controller. The SYNC controller is responsible for the system control while in the synchronization phase.

3.4.2.1 Maximum Power Tracking control (MPT Controller)

This section describes a control method that is used when a maximum wind power capture is desired, which resumes to operate the rotor in its ideal point resulting in maximum aerodynamic performance. It is a control mode used for the operation regions *II* and *III*. Equation (2.13) is rewritten again since it is the MPT controller basis, it is considered the gearbox (η_{GBm}) and rotor mechanical efficiencies (η_{GBm}),

$$p_{Po,ideal} = \frac{\rho A\, r^3 c_{p,ideal} \omega_R^2}{2\lambda_{ideal}} \frac{\eta_{Pm}\eta_{GBm}\eta_{Rm}}{i_{GB} D_P} + p_{pi}. \tag{3.8}$$

Equation (3.8) is the steady state pressure reference that results in the ideal rotor speed ($\omega_{R,ideal}$). A PI controller is used to control the pressure. The comparison between $p_{Po,ideal}$ to the system measured pressure (p_{Po}) is the error input to the PI controller.

There are a few considerations that must be done regarding the correct determination of the pressure reference.

Looking to Equation (3.8), it is seen that the pump inlet pressure (p_{Pi}) could possibly be neglected as it usually is done. That assumption is valid when the output pressure is significantly higher than the input pressure. When operating with rated power the pressure difference on the pump is high (210.00 bar) such that neglecting it would be a valid assumption. However when operating with low wind speeds the pressure difference is much smaller such that the assumption turns to be less correct. That is the reason to not neglect it in the implemented controller. As explained in Section 3.1, there is a charging circuit in the system to guarantee a minimum pressure in the low pressure line to avoid cavitation.

There is also the effect of the static pressure due to the fluid column along the tower height. Equation (3.9) is used to calculate the static pressure (Δp_{static}),

$$\Delta p_{static} = \rho_f g h, \tag{3.9}$$

where, ρ_f is the hydraulic fluid density and g is the gravity acceleration.

With 9.81 m/s^2 gravitational constant, the static pressure difference is 0.67 bar for the system being evaluated.

Because of the flow inside the pipe there is a resultant pressure drop occurring from the top of the tower to the bottom. This pressure drop is higher than the static pressure gain due to the gravitational acceleration effect for most of the operation. Therefore, the pump outlet pressure can be higher than the motor inlet pressure, for most of the operation envelope. The pressure drop is higher for higher flow rates, which occurs for higher wind speeds.

The pressure reference ($p_{Po,ideal}$) is set in the pump outlet at the top of the tower. The control action is performed at the bottom of the tower through the motor displacement control. This means that the controller should overcome the pressure drop if the pressure control loop is closed with the pressure measurement at the pump outlet.

Since there are pressure sensors on both the pump outlet and motor inlet, the pressure loss (Δp_{loss}) is determined as the difference between them as described in Equation (3.10),

$$\Delta p_{loss} = p_{Po} - p_{Mi} - \Delta p_{static}. \tag{3.10}$$

It must be discounted the static pressure difference due to the fluid column. Despite the effect of pressure drop and static pressure gain occur in the system they are not included in Equation (3.8) to determine the correct reference pressure.

It is known that the exact pressure drop is hardly measured or calculated since it suffers a considerable variation along the system operation. From another perspective, there are pressure waves propagating in the lines, such that if the pressure drop based on the measurement of pressures were to be included in Equation (3.8) it would add this dynamics to the pressure reference, which can cause the controller to be unstable.

There are other important issues with the parameters used to determine the correct pressure reference. Some of them are the mechanical efficiencies.

On previous studies carried at LASHIP (FLESCH, 2012; and RADUENZ, 2015) the pump mechanical efficiency was considered to be constant. However, the mechanical efficiency is variable, depending on pressure difference and shaft rotational speed as described by Rap and Turesson (2015). Two examples are given to demonstrate what the incorrect estimation of such efficiencies can lead to.

When the pump is operating with a lower efficiency (η_{Pm}) than the used in Equation (3.8), the estimated pressure reference is higher, which leads to a higher regulated pump outlet pressure. The higher pump outlet pressure results in a higher pump opposing torque (T_{Po}), which for that

given wind speed will make the rotor speed be lower than the ideal speed due to the torque balance.

The opposite is truth as well. If the pump is operating at a higher efficiency (η_{Pm}) than the used in Equation (3.8), the estimated pressure reference is smaller, which leads to a lower pump outlet pressure. The lower pump outlet pressure results in a lower pump opposing torque (T_{Po}), which for that given wind speed will make the rotor speed to be higher than the ideal speed due the torque balance. The rotor operation with a wrong speed decreases the aerodynamic performance.

This problem with the pump efficiency estimation is also truth for the gearbox and rotor mechanical efficiencies since they also vary along the operation and their estimation is not exact.

To have the correct pressure it is necessary to account the variable efficiencies. However, components efficiency maps are usually not available an if available, they still remain an approximation and don't predict exactly the efficiency.

The varying condition of the pump, gearbox, rotor mechanical efficiencies and the pressure drop add uncertainties to the pressure reference. Therefore, if an uncertainty compensation technique isn't used, the turbine will hardly operate with maximum power coefficient ($c_{p,ideal}$).

If the rotor is not operating with maximum power coefficient it means that it is not operating at the ideal rotor speed ($\omega_{R,ideal}$). Therefore, a compensation technique could be used having the rotor speed error ($\omega_{R,ideal} - \omega_R$) as input. The ideal rotor speed ($\omega_{R,ideal}$) is determined by rewriting Equation (2.2) in terms of the rotor speed and applying the ideal TSR to it. The rotor speed error is used as an input for a PI controller.

The output of the PI controller ($f_{\omega_R,comp}$), called rotor speed compensation signal, multiplies the measured rotor speed and the result of this multiplication substitutes the rotor speed in Equation (3.8), that becomes,

$$p_{Po,ideal} = \frac{\rho A r^3 c_{p,ideal} (\omega_R f_{\omega_R,comp})^2}{2\lambda_{ideal}^3} \frac{\eta_{Pm}\eta_{GBm}\eta_{Rm}}{D_P} + p_{P,i}. \tag{3.11}$$

When a deviation from the ideal rotor speed occurs, the compensated speed ($\omega_R f_{\omega_R,comp}$) will act on the pressure reference to eliminate the rotor speed error, therefore making it to operate with maximum aerodynamic efficiency. Figure 3.17 shows the block diagram of the MPT controller with the speed compensation.

Figure 3.17 – Maximum power tracking controller block diagram.

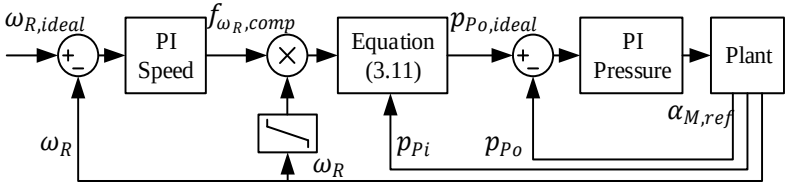

Source: Author.

The advantages and effectiveness of the speed compensation in the pressure controller is shown in the results, Section 6.3. The output of the PI Pressure controller is the hydraulic motor displacement setting control reference.

The error signals that enter the PI Speed and Pressure controllers are multiplied by -1. The reason for that naturally arises from the analysis of the error signal and the desired control action that must be taken in terms of pump outlet pressure and hydraulic motor displacement.

If the error $(p_{Po,ideal} - p_{po})$ is higher than zero, the pump outlet pressure (p_{po}) should increase. Multiplying this error by -1 makes $(p_{Po,ideal} - p_{po})$ to become lower than zero, which makes the multiplication and integration in the PI Pressure to decrease the hydraulic motor displacement reference $(\alpha_{M,ref})$. Considering the same hydraulic power arriving at the hydraulic motor, a smaller displacement setting makes the system pressure to increase (Equation (2.14)). For the opposite case, when $(p_{Po,ideal} - p_{po})$ is lower than zero, the multiplication by -1 also works.

For the speed compensation controller the multiplication by -1 also works. If the error $(\omega_{R,ideal} - \omega_R)$ is higher than zero, the rotor speed (ω_R) should increase. Multiplying the error by -1 makes $(\omega_{R,ideal} - \omega_R)$ to become smaller than zero, which makes the multiplication and integration in the PI Speed to decrease the speed compensation signal $(f_{\omega_R,comp})$. A smaller speed compensation signal makes the reference pressure from Equation (3.11) to become smaller. For the same wind speed, a smaller pressure results in the acceleration of the rotor, increasing the rotor speed. For the opposite case, when $(\omega_{R,ideal} - \omega_R)$ is smaller than zero, the multiplication by -1 also works.

The errors in pressure and speed are divided by their respective values before the PIs actions such that the controllers operate in a per-unit signal (pu).

3.4.2.2 Rotor Nominal Speed control (RNS Controller)

As explained in Section 2.1.2, variable speed wind turbines have a maximum speed that they are able to operate. The rotor will reach such rotational speed for the rotor nominal speed wind speed $v_{\omega_{R,n}}$, which is, in steady state, wind speed *d* in Figure 2.7.

The limitation in the rotor speed is made via two saturation elements in the structure of the MPT controller. One saturation is placed after the calculation of the ideal rotor speed that is used at the rotor speed compensation controller. In this way the maximum ideal rotor speed is the maximum allowed rotor speed. The other saturation is placed on the rotor speed signal that is used in for the pressure reference determination (Equation (3.11)).

When the wind speed increases above this limit the reference speed for the speed compensation and pressure reference saturates. As a result the calculated pressure reference will in steady state be the one that results in the maximum rotor speed. Figure 3.18 shows the block diagram of the structure that limits the rotor speed.

Figure 3.18 – Rotor nominal speed controller block diagram.

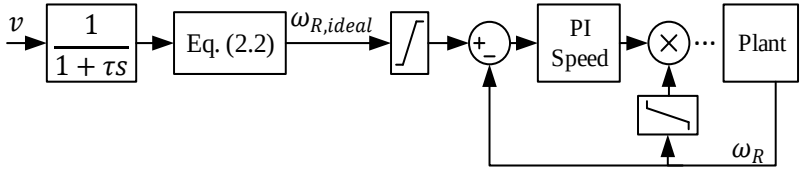

Source: Author.

It wasn't mentioned previously, but there is a low-pass first-order filter on the wind speed measurement. The wind speed tends to vary considerably due to turbulence and also due to the inherent signal noise from the sensor. Since the controller is based on wind speed, a noisy and turbulent measurement would result in a noisy input to the controller, which is not desirable. For this reason a filter is used for the wind speed measurement.

One thing that must be noticed is that the maximum rotor speed might be surpassed in transient moments, for example after a fast rotor acceleration due to a wind gust. The important thing is that the controller is able to bring it back to the maximum speed afterwards.

With the use of a saturation element a switching between controllers is avoided, which reduces a potential discontinuity at the controller output. However, there is still the switching between MPT and SYNC

controllers. They occur in a point where the system is about to be connected to the electric grid.

3.4.2.3 Synchronization Control (SYNC controller)

When synchronizing the system with the grid it is necessary to have the generated power parameters, as explained in Section 2.3, in a certain range around the grid power reference.

When executing the synchronization process, the frequency is the first controlled parameter. When wind speed is equal or higher than b (Figure 2.7), the generator is able to operate with the reference frequency. The system controls the generator speed in order for it to achieve its nominal speed ($\omega_{GS,n}$). For the selected generator, this speed results in 60.00 Hz generated power frequency, which is calculated by Equation (2.16).

The generator speed, that is measured by the pick-up sensor (1S17 in Figure 3.19), is compared to its nominal speed and the error signal is divided by the nominal speed value in order to have a per-unit signal to be sent to a PI controller. The control signal from the PI is sent to the motor displacement pressure control system. In this way it is ensured that the generator speed is controlled to its nominal value during the synchronization. Figure 3.19 presents a diagram of such controller.

For both controllers MPT and SYNC, the output of their respective PI controllers is the hydraulic motor displacement reference ($\alpha_{M,ref}$).

Figure 3.19 - Generator speed controller block diagram.

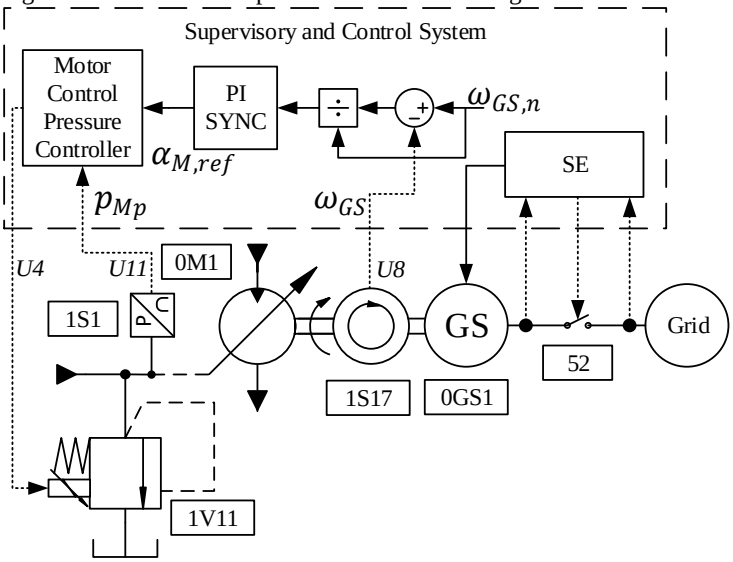

Source: Author.

3.4.2.4 Hydraulic motor displacement pressure control

As mentioned in Section 3.1.3, the hydraulic motor displacement is proportionally pressure controlled. Therefore, the displacement reference that is outputted from the MPT and SYNC controllers is converted into the hydraulic motor displacement pressure reference ($p_{Mp,ref}$) using Equation (3.2).

This displacement pressure reference is compared with the measured pressure at the pump displacement control unit port (p_{Mp}) and divided by the respective nominal value to have a per-unit signal.

This signal is multiplied and integrated in a PI controller which outputs a controlled pressure reference ($p_{1V11,ref}$). This pressure signal is converted into a voltage reference signal ($V_{1V11,ref}$) that is sent to the module that controls the proportional pressure relief valve (1V11). This process is also explained in Section 3.1.3.

Figure 3.20 presents the block diagram of the motor displacement pressure control.

The motor displacement pressure measurement also passes through a filter before being used at the controller.

Figure 3.20 - Motor displacement pressure control block diagram.

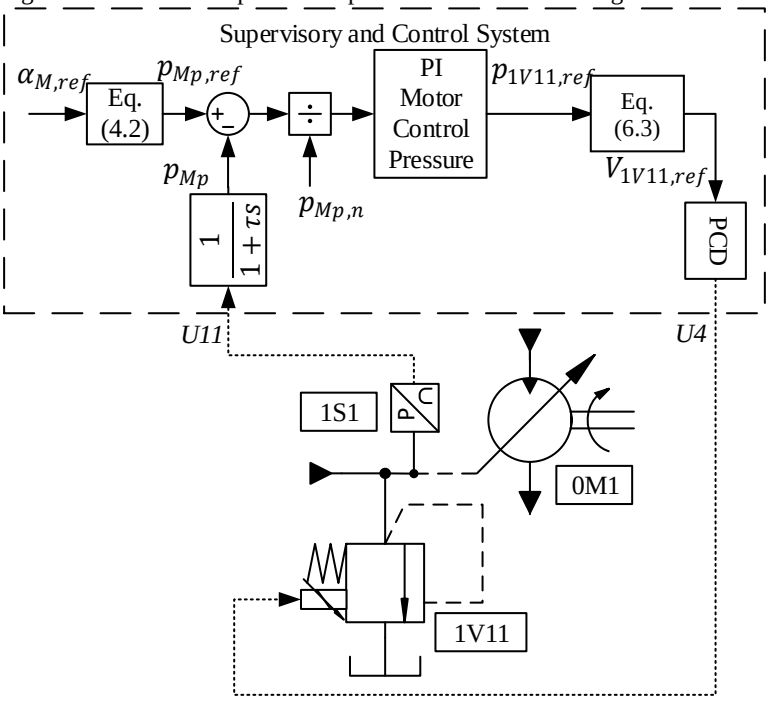

Source: Author.

3.4.3 Power output control

Wind turbines produce a so called green energy. Therefore, when looking from the environmental perspective, the more green energy being fed to the grid the better it is. That is because the power production with other non-sustainable energy sources can be reduced.

Despite being possible to control the amount of power being supplied to the grid, this is not studied in this thesis. Therefore, the maximum amount of power extracted from the wind is supplied to the grid.

The reactive power can be controlled via the direct current excitation of the generator rotor (HAU, 2006). REIVAX voltage regulator is capable of controlling the reactive power. However, these are the very first experimental analysis of the system, in this way, there is no control of generated reactive electric power, only the active power is analysed.

While delivering power to the grid, the only control being used at the power output is the voltage control which is carried by the REIVAX voltage regulator.

3.4.4 Switching controls between operation regions

On previous sections it was shown that the wind turbine with hydrostatic transmission has two controllers in order to cover its operation through the wind speed range. This is the case when not considering the pitch regulated region, where an extra controller is necessary.

It is necessary to change controllers in order to achieve the desired system action and behaviour. Figure 3.21 is a representation of the wind turbine operation regions and also an indication of where each controller operates.

Figure 3.21 - Controllers operation regions.

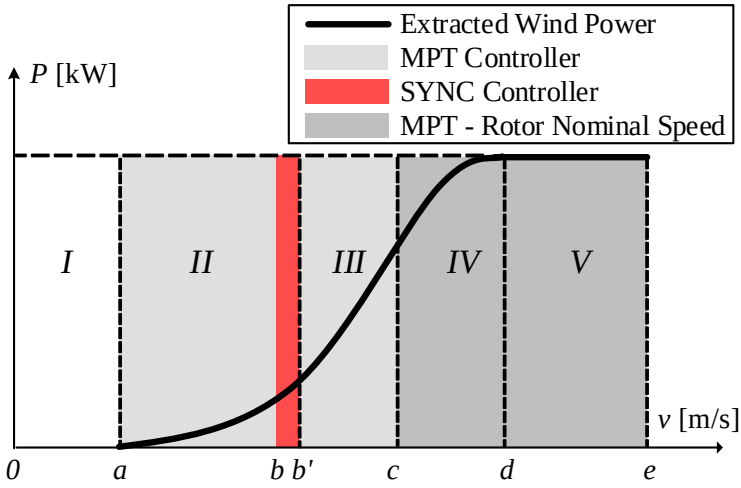

Source: Author.

As it can be seen in Figure 3.21, the MPT and SYNC controllers might get in conflict because the SYNC controller is in the middle of the wind speed range of the MPT, the variable speed operation range. The rotor nominal speed is a part of the MPT controller. There is no conflict between them since it is just made with the saturation elements.

The switching between controllers impose a few possible discontinuities in the controller operation. To make this switching, few rules

where defined based on user inputs, system parameters and real-time measurements.

The switching process and rules are explained from the turbine start-up up to maximum rotor speed, an increasing wind speed. The reverse process is also explained, which is from the maximum rotor speed, down to zero wind speed. The description of the switching process and rules are placed at Appendix B.

Despite the existence of the switching between controllers, a single PI structure is implemented. The reasons for this implementation are detailed in the following section.

3.4.5 Single PI structure and switching between controller gains

There are two control modes in the system, MPT and SYNC. They are switched between different operation regions. Since they are based in different references, when the switching between them happens the output would most likely suffer a discontinuity. This discontinuity would be transmitted to the motor displacement control, resulting in an abrupt pressure change in the system. This is not desirable at all.

In order to avoid such behaviour, a single PI control structure is used for both the MPT and SYNC control modes. The switching between the control modes will act on the references, measured values and gains that are inputs to the PI controller. To simplify the explanation of the control, up to this point in the thesis the MPT and SYNC controllers were told to each one have its own PI structure. From now on, it must be considered that they have only one PI structure.

The use of a single controller having only the inputs switched between the control modes makes the integrative part to always be continuous, however it does not entirely prevent the discontinuities from the proportional part. For that reason a first-order filter is used at the output of the controller to filter the discontinuity caused by the proportional part.

Figure 3.22 shows the whole control structure with the indication of the switching between control modes.

Another point that must be remarked and described is the controller gain setting. The system state varies considerably along the whole operation envelope. For example, the system pressure ranges from 0.0 to 210.0 bar, the flow rate from 0.0 to 110.0 L/min, the rotor speed from 0.0 to 120.0 rpm, the generated power from 0.0 to 28.5 kW, and so on. The different system states makes the it to behave differently along the operation. Therefore, to tune controller gains for a specific operation point

would not result in the same expected behaviour at other point. Therefore the gains of the controllers must vary along the operation.

Figure 3.22 - Control structure, switching between control modes.

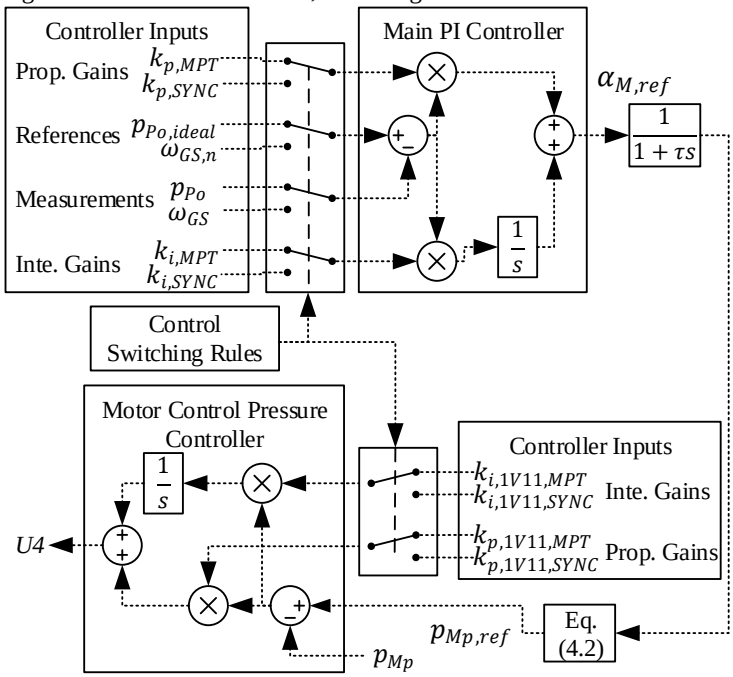

Source: Author.

A gain scheduling approach was used to determine the gains for the pressure MPT controller, for the speed compensation controller and for the 1V11 valve controller. The scheduling parameter is the wind speed and the gains were selected taking in consideration the observed through simulation and experimental tests. Figure 3.23 shows the gains used as a function of wind speed.

As it is observed in Figure 3.23 that the controllers gains tend to decrease as wind speed increase. Until 4.0 m/s wind speed they are kept constant. This is the operation in regions *I* and *II* (Figure 3.21) which is part of the test bench and the real system, but are not part of the system performance analysis carried in this thesis.

The system changes from operation region *III* to *IV* at around 9.2 m/s wind speed. That is why it is observed an increase in the gains around

that region. As will be seen in Section 6.4 the increase in gains is necessary to obtain a faster control action of the rotor nominal speed.

Figure 3.23 - Controllers gain scheduling. a) MPT controller; b) Speed compensation controller; c) 1V11 valve pressure controller.

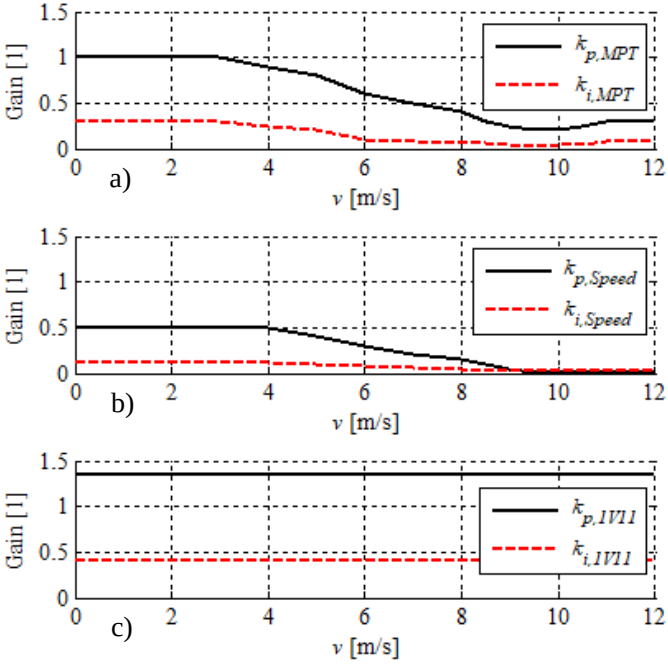

Source: Author.

It was observed that gains of the motor displacement pressure controller ($k_{p,1V11}$ and $k_{i,1V11}$, Figure 3.23c) could be kept constant. The variation of them did not caused a significant change in the overall system control quality.

3.4.6 State machine

In this section, it is shown the supervisory control built for the system as a finite state machine model. The supervisory control can be considered as the means whereby the turbine is brought from one operational state to another (BURTON *et al.*, 2011). It is responsible to manage the change of operation estates, the actions of one inner controller or another and actions that are required to operate the test bench safely. The inputs provided by the user, the measurement signals from sensors and

predefined parameters, define the current machine state and provide the required conditions for the automatic transitions from a state of control to another.

When it comes to electric power generation the major states are the system stand-by, synchronization to the grid, power production, stop and safety/emergency states.

The supervisory control developed and build for the test bench is based on a state machine of a hydroelectric power station. This state machine was provided by REIVAX. It was adapted to include the wind turbine/hydrostatic transmission/teste bench states, controls and functionalities. In terms of operation states, the operation of a hydroelectric turbine and of a wind turbine are very similar, that is why it was possible to adapt the supervisory control.

The whole system control structure and user/machine interfaces where implemented at the REIVAX SEC software, which is similar to the Matlab Simulink. However, it is for industrial application and therefore very robust. The sketch of the test bench state machine is presented in Figure 3.24.

Figure 3.24 -State machine structure.

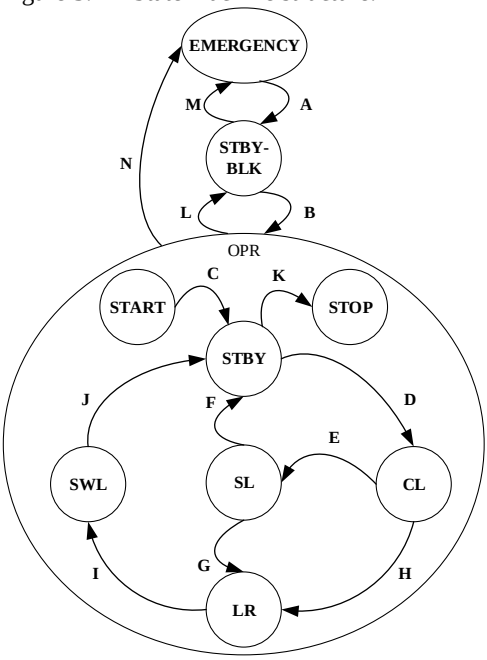

Source: Author.

The states of operation are described in Table 3.3.

Table 3.3 - Description of states of the state machine.

State	Description
EMERGENCY	When a situation that occurs at the bench characterise an emergency. The system is turned off.
STBY-BLK	When turned off and not in EMERGENY, wait for the user start command.
OPR	Outer state when the system is operating.
START	Brings the system from a stand-by-block state to a stand-by state where it waits for the user to command it to enter in operation according or not to the wind.
STBY	Waits for user inputs – running with minimum speed
CL	Control with load - For operation as the wind turbine. With the MPT and SYNC controllers.
SL	Stop with load - The system performs the stop operation procedure.
LR	Load Rejection - State for a lost of connection with the grid. The control prevents the generator runaway.
SWL	Stop to stand-by procedure after a Load Rejection.
STOP	To stop the test bench operation.

Source: Author.

The supervisory controller must check that each state is successfully completed before moving on to the next (BURTON *et al.*, 2011). That ensures that there are never two active states at the same time, which could cause a wrong combination of control actions.

Burton *et al.* (2011) says that the safety system must be capable of overriding the normal controller in order to bring the turbine to a safe state if a serious problem occurs. Therefore, in this project, all the emergency and safety actions are at the end of the control chain, which allows it to bypass all other control actions and ensure system safety.

Table 3.4 describes the paths between the control states.

Table 3.4 - Paths of the state machine.

Paths	Description
A	System check performed to leave emergency state.

B	The hydraulic charge system and frequency converter are turned on and enter operation is commanded.
C	User commands to start-up the bench.
D	Control with load (CL) was selected by the user, the system will operate as the wind turbine.
E	Can be commanded by the user or automatically occurs if a safety condition is reached. Stop with load procedure is carried.
F	Minimum conditions to entry in STBY mode.
G	Load rejection occurs during SL.
H	Load rejection occurs when system is in control with load (CL)
I	The system reaches a safe stop condition.
J	Minimum conditions to entry in STBY mode.
K	User commands the system to stop.
L	The system leaves OPR, turns off automatically to the STBY-BLK
M	An emergency situation occurs while in the STB-BLK state
N	An emergency situation occurs while in OPR.

Source: Author.

Hau (2006), presents the control sequence of a wind turbine. They are: System check, stand still, start-up, running-up to speed, power production, shutdown and stopping. This control sequence can be seen as the supervisory control actions or machine control states.

A comparison between Hau (2006) wind turbine control states description and the state machine developed for the turbine with hydrostatic transmission can be made. This comparison is presented in Table 3.5.

Table 3.5 - Comparison of machine control states.

Hau (2006) Turbine Control Sequence	HT Test Bench Supervisory
Stand Still	STBY-BLK
System Check	STBY-BLK
Start-up	START – STBY – CL
Running-up to Speed	CL
Power Production	CL
Shutdown	SL – SWL – LR
Stopping	STOP

Source: Author.

The implemented states are similar. The main differences are the Stand Still and System Check that are performed at the STBY-BLK state at the bench. The Start-up and Running-up to Speed and Power Production are performed by the START, STBY and CL states, where inside of it the MPT and SYNC controllers operate. The Shutdown is compared to

the SL, SWL and LR where, due to low wind speed or grid disconnection, the system must be brought to the Stand Still state. Another difference is that at the bench these actions lead to STBY and not the STBY-BLK. The Stopping procedure brings the system to complete stop, it is performed by the STOP state in the test bench.

With such comparison, one can see that the development of a state machine for a wind turbine test bench based on a hydroelectric power station state machine is a possible procedure, since both are similar.

4. ANALYTICAL MODEL AND ANALYSIS

"Theory – A formal statement of the rules on which a subject of study is based or of ideas that are suggested to explain a fact or event …"
(Cambridge Dictionary)

In the previous chapters a brief analysis of the wind turbine was carried where the power and torque coefficients were related to wind speed, rotor speed and tip speed ratio. Also a brief introduction on how to control the wind turbine with a hydrostatic transmission was made.

This chapter focuses on the study, using mostly steady state equations, of the hydrostatic transmission and generator. The objective is to define how their parameters and states vary along the wind turbine operation range. The parameters under analysis are correlated to the wind and rotor characteristics. The equations and model presented here are similar to what was presented by Flesh (2012), Raduenz (2015) and Rapp and Turesson (2015). The main differences lay on the extension of parameters range in order to see what behaviour to expect, the inclusion of the system natural frequency analysis and the analysis of the system open-loop stability. This chapter can be used for an early phase in the design of a wind turbine with hydrostatic transmission.

Unless specified differently, the values for the parameters used in this analysis are the ones shown in Table 4.1.

Table 4.1 - Main parameters values used for the analytical model.

Parameter	Value
r – rotor radius	6.16 m
ρ – air density	1.225 kg/m^3
$c_{p,ideal}$ – ideal power coefficient	0.4964
D_P – Pump volumetric displacement	75.00 cm^3/rev
$D_{M,max}$ – Motor max. volumetric disp.	60.00 cm^3/rev
$D_{M,min}$ – Motor min. volumetric disp.	12.00 cm^3/rev
$\omega_{GS,n}$ – Generator nominal speed	1800 rpm

Source: Author.

Figure 4.1 shows the system diagram with the variables used in the analytical model and analysis that are described from now on.

Figure 4.1 - System diagram for the analytical model and analysis.

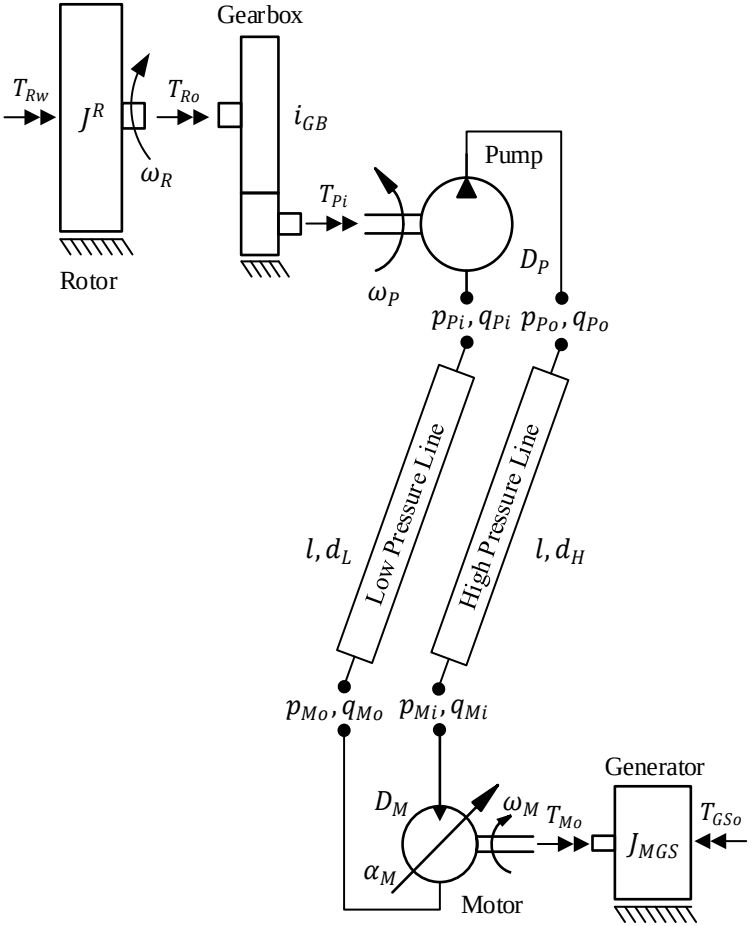

Source: Author.

Table 4.2 presents the description of Figure 4.1 variables. Variables already presented in previous sections are not described again.

Table 4.2 - System variables description for the analytical analysis.

Parameter	Description
J_R	Rotor mass moment of inertia.
J_{MGS}	Motor and generator mass moment of inertia.
T_{Mo}	Hydraulic motor output torque.
T_{GSo}	Generator output torque.

l	Hydraulic line length
d_H, d_L	Hydraulic lines diameter
q_{Mi}, q_{Mo}	Hydraulic motor inlet and outlet flow rates
p_{Mi}, p_{Mo}	Hydraulic motor inlet and outlet pressures
q_{Pi}, q_{Po}	Hydraulic pump inlet and outlet flow rates
p_{Pi}, p_{Po}	Hydraulic pump inlet and outlet pressures
i_{GB}	Gearbox transmission ratio

Source: Author.

4.1 PUMP SPEED

The pump speed (ω_P) is directly related to the rotor speed. As it was mentioned in Chapter 3, there might be the inclusion of a gearbox between the rotor and pump. Therefore, their speeds are coupled through the gearbox transmission ratio (i_{GB}),

$$\omega_P = \omega_R i_{GB}. \tag{4.1}$$

In the case where there is no gearbox in the system, the continuing analysis is still valid by using i_{GB} equal to 1 and not accounting its inefficiency.

One can describe the pump speed as a function of tip speed ratio and wind speed by applying the rotor speed from Equation (2.2) into Equation (4.1),

$$\omega_P = \frac{\lambda i_{GB} v}{r}. \tag{4.2}$$

As described in Section 2.1, the power coefficient (c_p) achieves its maximum for zero pitch angle ($\beta = 0$) and at the ideal tip speed ratio (λ_{ideal}). As it is known, one of the wind turbine control strategies is to seek the maximum power coefficient, which resumes to operate the system as close to the ideal tip speed ratio as possible.

For a given rotor/blade design, the λ_{ideal} and rotor radius r are known. Thereby, it is possible to define the pump speed when operating at the ideal rotor condition as function of gearbox transmission ratio and wind speed. Figure 4.2 shows the pump speed range, when operating at the ideal rotor speed, as function of wind speed for different gearbox transmission ratios.

Figure 4.2 - Ideal pump speed versus wind speed for different gearbox transmission ratios.

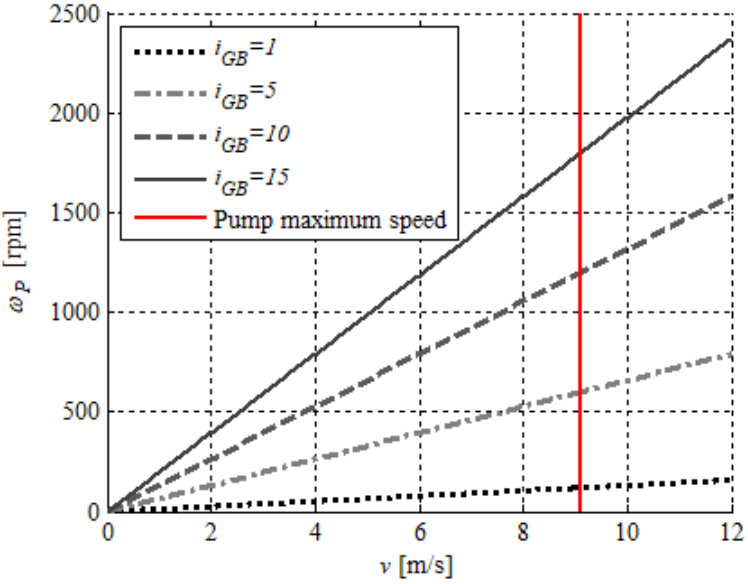

Source: Author

Since the rotor has its maximum operating speed, the pump consequently has one. It is defined by the rotor maximum speed ($\omega_{R,max}$) and gear ratio. Figure 4.2 shows the pump speed limits when the rotor speed achieves its maximum speed, resulting from the maximum linear speed at the blade tip. The rotor maximum speed is achieved in steady state, for the same blade design, for a certain wind speed. This speed can be calculated using Equation (2.2) using the rotor ideal tip speed ratio, the radius and the maximum speed.

With such analysis the design engineer can have at hand, for a given wind speed range, the possibility to choose a suitable gearbox if necessary and already know what pump speed to expect. That allows to choose a suitable pump with high efficiency at the expected wind speed range.

4.2 SYSTEM PRESSURE AND FLOW RATE

The determination of wind power is directly related to the rotor and tower characteristics. However, all components on the wind turbine must be able to handle that power.

For the hydrostatic transmission, as defined in literature, hydraulic power is the product of pressure difference and flow rate. Equation (4.3) represents the pump hydraulic power output (P_P),

$$P_P = q_{Po}(p_{Po} - p_{Pi}) , \tag{4.3}$$

where q_{Po} is the pump effective flow rate.

The system rated pressure and flow rate are key parameters when designing the hydrostatic transmission. Pressure was already written in terms of wind and rotor parameters in Section 3.4.2.1 Equation (3.8). However, the equation is written again,

$$p_{Po,ideal} = \frac{\rho A_R \, r^3 c_{p,ideal} {\omega_R}^2}{2\lambda_{ideal}} \frac{\eta_{Pm}\eta_{GBm}\eta_{Rm}}{i_{GB}D_P} + p_{pi}. \tag{4.4}$$

Figure 4.3 presents the plot of the pump outlet ideal pressure for a given set of parameters.

Figure 4.3 - Pump outlet ideal pressure as function of wind speed.

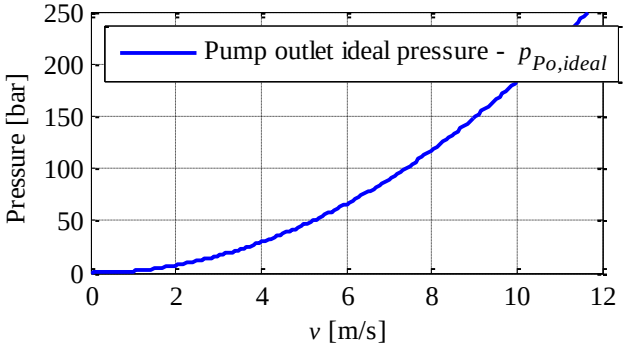

Source: Author.

It is possible to evaluate the pump pressure when operating outside the ideal conditions, which is where it will operate most of the time due to varying wind conditions. This is done by applying, in Equation (4.4), the steady state conditions for a given wind and rotor speed range, and not just the ideal operation parameters. By doing so, a pump outlet pressure surface is obtained as shown in Figure 4.4.

Figure 4.4 - Pump outlet pressure surface.

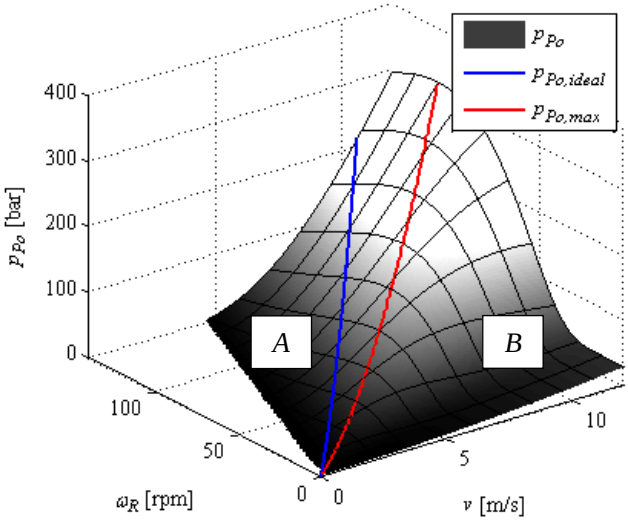

Source: Author.

In Figure 4.4, both the ideal (blue) and maximum (red) pressures are highlighted. It is remarked that the shape of the surface is also determined by the power coefficient that is varying for the different pairs of (ω_R, v), which is described in the sequence.

In order to visualize the rotor steady state operation points, two more surfaces are generated. The rotor power coefficient surface is presented in Figure 4.5 and the tip speed ratio is presented in Figure 4.6. In figures 4.4Figure 4.4 to 4.6 the blue lines represent the ideal operational condition.

In Figure 2.1 the power coefficient was shown as a function of the tip speed ratio and blade pitch angle. In Figure 4.5 it is shown as a function of the wind speed and rotor speed for zero blade pitch angle.

Figure 4.5 - Rotor power coefficient surface.

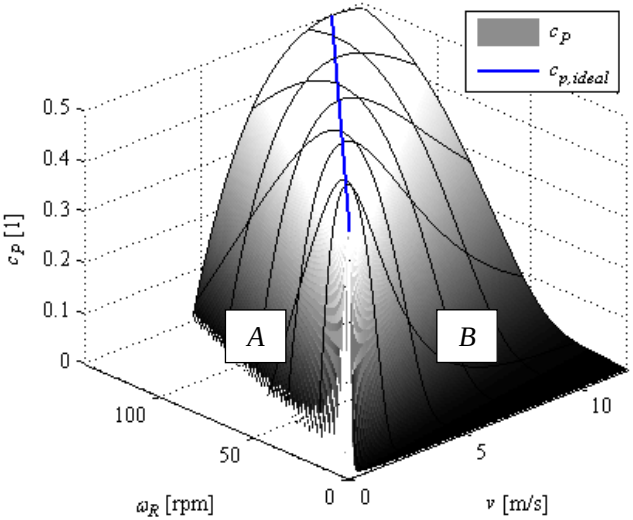

Source: Author.

Figure 4.6 - Tip speed ratio surface.

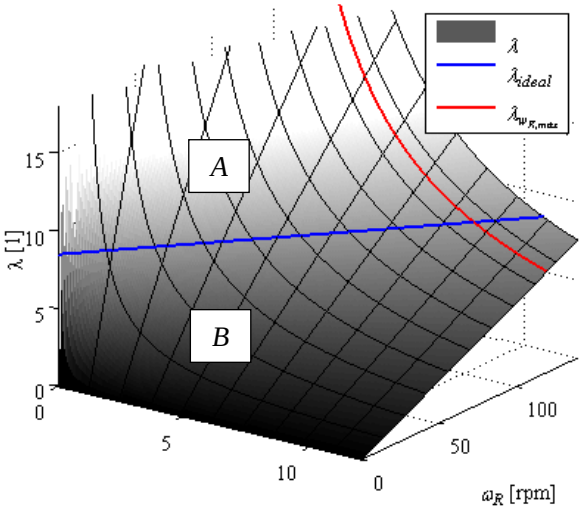

Source: Author.

The discontinuities seen in Figure 4.5 and Figure 4.6 appear because in those points, the values for the power coefficient are smaller than zero and the values for the tip speed ratio tend to infinite. Due to the grid size used to generate the surface the discontinuities are seen.

In figures 4.4 to 4.6, any operation point outside the ideal line (blue), regions *A* and *B*, results in a worst power coefficient. When looking to Figure 4.6 it is seen that in region *A* the TSR is above the ideal while for region *B*, the TSR is below the ideal. Rewriting Equation (2.2) in terms of rotor speed leads to

$$\omega_R = \frac{\lambda v}{r}. \tag{4.5}$$

By analysing Equation (4.5), for a fixed wind speed, if the TSR (λ) is above the ideal, region *A*, the rotor speed will also be above the ideal, so the rotor should decelerate. On the opposite case, if the TSR is below the ideal TSR, region *B*, the rotor speed will also be below the ideal, so the rotor should accelerate.

The actions of accelerating and decelerating the rotor are not that straight forward when the system is controlled by the hydrostatic transmission. The rotor acceleration or deceleration, for a given wind speed, depends on the system pressure, which results in a hydraulic torque that opposes the wind torque. To achieve the ideal rotor speed, if the system is operating in region *A*, pressure should be increased and the rotor will consequently decelerate. If the system is operating in region *B*, pressure should be decreased and the rotor will consequently accelerate.

In Figure 4.6, it is also shown the limit of TSR for the maximum rotor speed (red line). This limit is set due to the operation at constant speed of the rotor when it reaches its maximum.

Using equations (2.13), (4.3) and (4.4), considering zero pump inlet pressure ($p_{Pi} = 0$) the effective pump flow rate when in ideal operation ($q_{Po,ideal}$) can be expressed in terms of wind and rotor characteristics and pump power.

$$q_{Po,ideal} = \frac{P_P}{\frac{\rho A\, r^3 c_{p,ideal}(\omega_R)^2}{2\lambda_{ideal}^3}\frac{\eta_{Pm}\eta_{GBm}\eta_{Rm}}{i_{GB}D_P}} \tag{4.6}$$

The theoretical pump flow rate is defined by,

$$q_{Pt} = D_P \omega_P. \tag{4.7}$$

4.3 MOTOR SPEED, DISPLACEMENT AND TRANSMISSION RATIO

The considerations regarding the transmission ratio and motor speed are made assuming a mechanically and volumetrically loss-less transmission.

If Equation (2.9) is plotted for a certain pump and motor displacement range, it is possible to evaluate what is the hydrostatic transmission ratio between pump speed and motor speed.

Figure 4.7 – Hydrostatic transmission ratio surface.

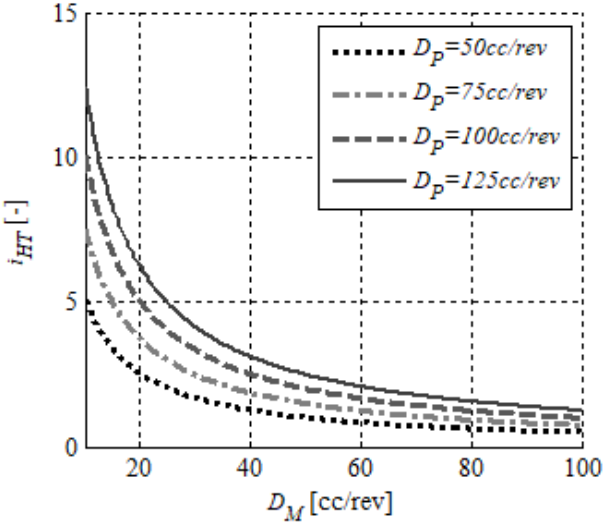

Source: Author.

As described in previous sections, the developed hydrostatic transmission concept is built with a fixed displacement pump and a variable displacement motor. In this case, the transmission ratio range is known and applying a given pump speed range as input, the motor speed can be calculated. The distribution of motor speed as a function of the pump speed and transmission ratio is shown in Figure 4.8.

Figure 4.8 - Motor speed and generator nominal speed.

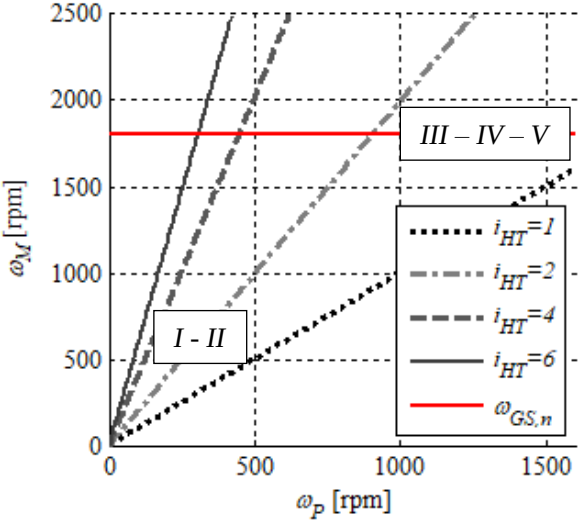

Source: Author.

Five wind turbine operation regions can be seen in Figure 4.8 as well. During the turbine operation regions *I* and *II* (Figure 2.7) the system tries to achieve the synchronization point. During those phases the motor speed varies according to the pump speed and transmission ratio. This is the surface area below the red line. During turbine operation regions *III*, *IV* and *V*, when the generator is coupled to the grid, the motor speed is kept constant and equal to the generator nominal speed. Therefore, the red line represents the system operating at these three regions while synchronized or synchronizing to the grid.

4.4 SYSTEM AND COMPONENTS EFFICIENCIES

In the previous analysis carried in this chapter, the components efficiencies were considered to be constant. However, as it is broadly known, they vary along a system/component operation.

For hydraulic components, the efficiency varies with pressure, speed, displacement, temperature and so on. For the studies carried out here, efficiency models for the pump and motor were introduced by Rapp and Turesson (2015). The models describe the volumetric and mechanical efficiencies as functions of pressure, displacement and rotational speed.

4.4.1 Hydraulic pump and motor efficiencies

Here, the efficiency surfaces for the pump are presented as function of pressure and speed. The pump displacement is fixed. Figure 4.9 presents the pump mechanical efficiency.

Figure 4.9 - Pump mechanical efficiency.

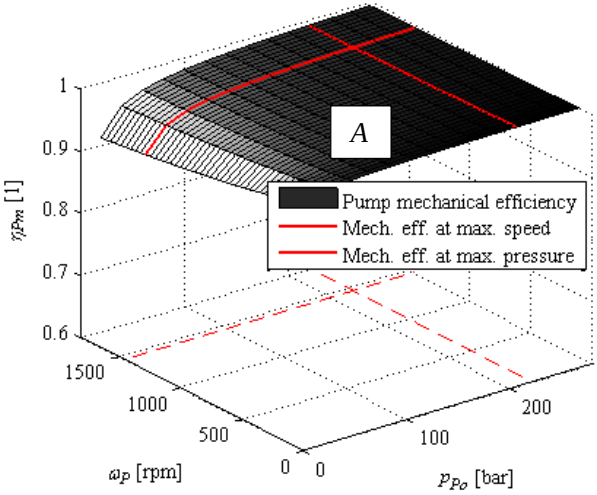

Source: Author.

For Figures Figure 4.9 to Figure 4.11 the region indicated with *A* is the expected pump operation region in the hydrostatic transmission. It is possible to see in Figure 4.9 the lower mechanical efficiency when in low pressure operation.

Figure 4.10 shows the pump volumetric efficiency. It is observed the lower volumetric efficiency when operating at low speeds.

Figure 4.11 is the pump overall efficiency, which is the multiplication of the pump mechanical and volumetric efficiencies. It can be noticed in the pump overall efficiency the influence of the low speed and low pressure due to low mechanical and low volumetric losses respectively.

For the variable displacement hydraulic motor, the efficiencies vary with the displacement setting as well. The smaller the displacement the worst the efficiency.

Figure 4.10 - Pump volumetric efficiency.

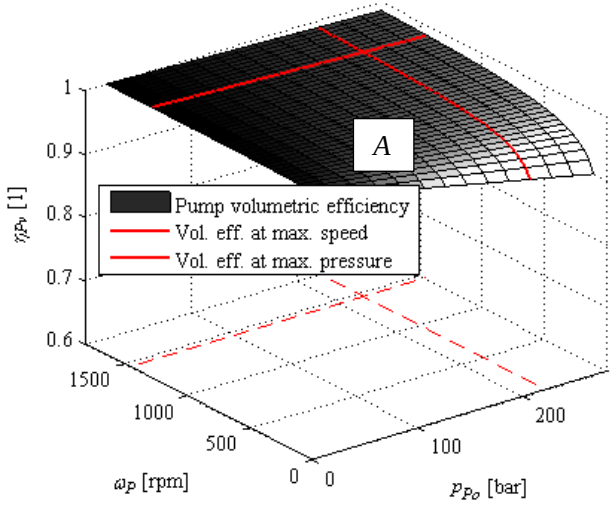

Source: Author.

Figure 4.11 - Pump overall efficiency.

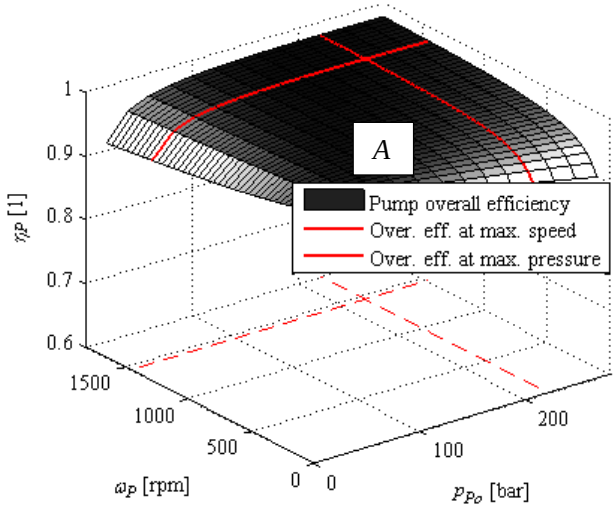

Source: Author.

When the generator is connected to the grid its speed is fixed, therefore the hydraulic motor also operates at constant speed. The hydraulic motor efficiencies plotted in figures 4.12 to 4.15 are for 1800 rpm

(synchronous speed) considering the complete range of displacement setting and pressures.

Figure 4.12 - Hydraulic motor mechanical efficiency at 1800 rpm.

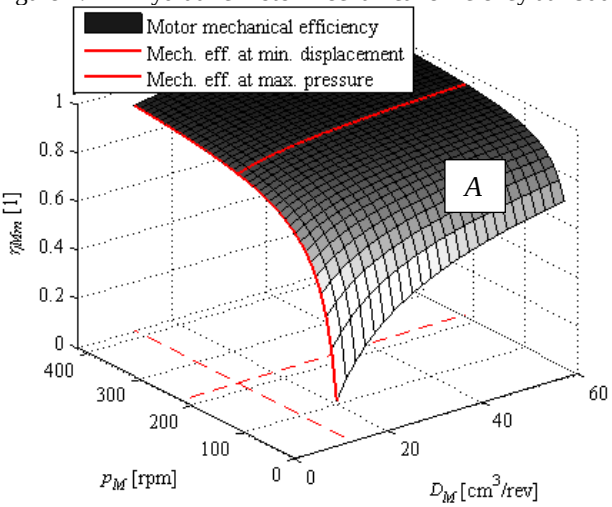

Source: Author.

Figure 4.13 - Hydraulic motor volumetric efficiency at 1800 rpm.

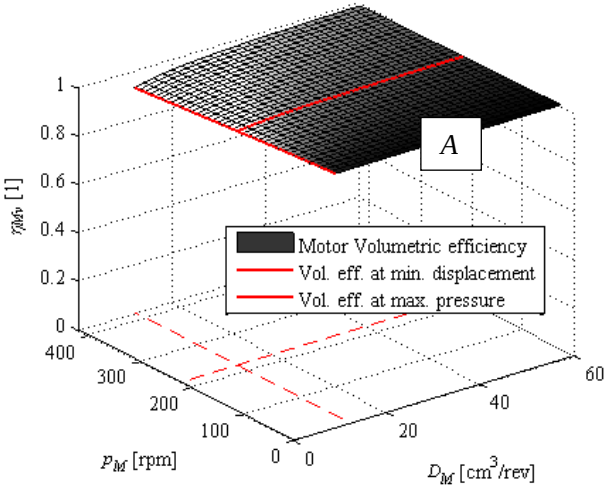

Source: Author.

Figure 4.14 - Hydraulic motor overall efficiency at 1800 rpm.

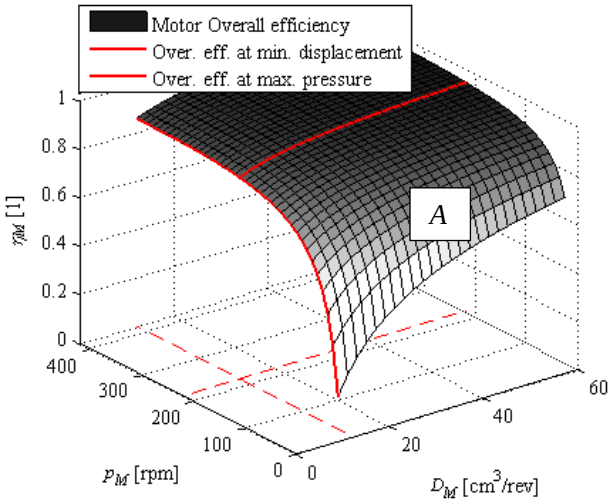

Source: Author.

With the pump and motor efficiencies characterized, it is possible to determine the hydrostatic transmission efficiency. The following equations and descriptions result in a more accurate way of determining the system efficiency. However, they require a whole set of system parameters.

4.4.2 Power input efficiency

The efficiency of the power input (η_i) is related to losses by friction on the gearbox, rotor and the extraction of power from the wind. Therefore, this efficiency can be calculated by

$$\eta_i = \frac{P_{Pi}}{P_{Rw}} = \eta_{Rm}\eta_{GB}c_{p,ideal}, \tag{4.8}$$

where, P_{Pi} is the pump input power, η_{Rm} the rotor mechanical efficiency, η_{GB} the gearbox mechanical efficiency.

Extracted wind power (P_{Rw}) is given by Equation (2.1) and the pump input power is calculate from the rotational speed (ω_P) and input torque product (T_{Pi}),

$$P_{Pi} = T_{Pi}\omega_P. \tag{4.9}$$

4.4.3 Hydrostatic transmission efficiency

The hydrostatic transmission efficiency (η_{HT}) is calculated as,

$$\eta_{HT} = \frac{P_{GSi} - P_{CCi} - P_{HEi}}{P_{Pi}}, \tag{4.10}$$

where, P_{GSi} is the generator power input, P_{CCi} the charging and motor control circuit power input and P_{HEi} is the heat exchanger power input.

The generator power input is the power provided by the hydraulic motor and is given by Equation (4.11), that is the product of hydraulic motor output torque (T_{Mo}) and generator rotational speed (ω_{GS}),

$$P_{GSi} = T_{Mo}\omega_{GS} = p_{Po,ideal} D_M \alpha_M \omega_{GS,n} \eta_{Mm} \eta_{Mv}, \tag{4.11}$$

where it is considered to not have pressure losses on the hydraulic lines.

The hydraulic motor displacement setting is calculated as,

$$D_M \alpha_M = D_P \omega_P \eta_{Pv} \eta_{Mv} / \omega_{GS,n}. \tag{4.12}$$

Charging circuit and motor displacement control power input is calculated as the power required by the electric motor that drives the pumps. At the test bench there is no measurement of torque of the electric motor that drives the pumps 0P2 and 0P3. However, the information of pressure on the pumps outlets, displacement and speed are available. Therefore, neglecting the pump inlet pressure, the power consumed by the charging and motor displacement control systems can be written as,

$$P_{CCi} = \frac{(p_{0P2o} D_{0P2} \eta_{0P3} + p_{0P3o} D_{0P3} \eta_{0P2}) \omega_{CC}}{\eta_{CC} \eta_{0P2} \eta_{0P3}}, \tag{4.13}$$

where, p_{0P2o} is the 0P2 pump outlet pressure, p_{0P3o} the 0P3 pump outlet pressure, D_{0P2} the 0P2 volumetric displacement, D_{0P3} the 0P3 volumetric displacement, η_{CC} the charging circuit motor efficiency, η_{0P2} the 0P2 overall efficiency and η_{0P3} the 0P3 overall efficiency.

The motor that drives the pumps is an induction motor and it is considered to run at constant speed ($\omega_{CC} = 1130\, rpm$) through the whole operation. The charging circuit motor efficiency (η_{CC}) is 66.0 % according to the manufacturer.

The p_{0P2o} pressure is regulated by a relief valve and is considered to be constant and equal to 8.0 bar.

The p_{0P3o} is the hydraulic motor displacement control pilot pressure (p_{Mp}) as explained in Section 3.1.3. In the hydraulic motor control it can be assumed that there is, in steady state, no fluid flow to the motor

and only the pressure actuates on the internal control system. All flow rate provided by 0P3 is directed to the reservoir. Therefore, all the fluid power is dissipated in the proportional pressure relief valve (1V11). Knowing the motor displacement, the displacement control pilot pressure is calculated with Equation (3.2).

There is no information available from the manufacturer about the overall efficiency of the 0P2 and 0P3 pumps. These efficiencies were considered to be 90.0 %.

The heat exchanger has an intermittent operation. However, the worst-case scenario is used in this analysis and it is considered to be running at maximum power the whole time. The heat exchanger used in the test bench has a maximum power consumption of 264.0 W according to its manufacturer.

4.4.4 Power generation and delivery efficiency

Inefficiencies on the power generation and delivery system are summarized as losses at the generator. The generator efficiency is,

$$\eta_{GS} = \frac{P_{GSo}}{P_{GSi}}, \tag{4.14}$$

where, P_{GSo} is the generator power output. η_{GS} is considered constant and equal to 95.0 %. The generator power output is calculated as the product of electric torque (T_{GSe}) and rotational speed,

$$P_{GSo} = T_{GSe}\omega_{GS} \tag{4.15}$$

4.4.5 System global efficiency

The global system efficiency (η_G) is assessed through a set of equations that model the efficiencies on each part and it is calculated as,

$$\eta_G = \eta_i \eta_{HT} \eta_{GS}. \tag{4.16}$$

The system overall efficiency (η_G), when operating in the ideal conditions, is a function of wind speed and its components parameters. To calculate this efficiency, it is necessary to use equations (4.8) to (4.14) together with the maps of motor and pump efficiencies. When implementing a routine to calculate them a loop is formed because the system pressure is dependent on the efficiencies which are dependent on pressure. A simple iterative loop was created to solve it. Figure 4.15 presents the

overall and transmission efficiencies as functions of wind speed. The parameters used are the ones of Table 4.1.

Figure 4.15 - Overall, System and transmission efficiencies as functions of wind speed.

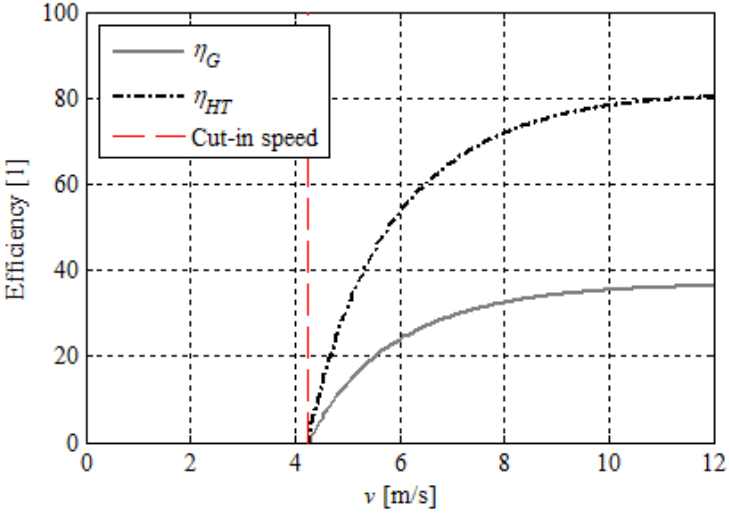

Source Author.

As it is noticeable, no net power is generated below the turbine cut-in speed, which, in this case, is around 4.25 m/s. The cut-in speed is relatively high for such a small rated output power turbine (28.5 kW). However, it is representative since that is within the range of cut-in speeds for wind turbines. It is necessary to remember that the efficiencies presented in Figure 4.15, account the charging circuit and heat exchanger power, which are supplied by external power and not from the wind. Therefore, the actual cut in speed is slightly lower than the one shown.

A figure similar to Figure 4.15 is presented by Laguna and Diepeveen (2011). It can be seen that the system efficiency for low wind speeds is dominated by the pump and motor overall efficiencies. At the same time, at low wind speed the power is very small as well, so at the end there is not much wasted power.

4.5 SYSTEM POWER

With the equations, descriptions and assumptions made through this chapter it is possible to evaluate what would be the system steady state output power (P_{GSo}) when operating in the ideal conditions with

respect to the extraction of power from the wind, which means with maximum rotor aerodynamic performance.

Figure 4.16 shows the variation of the available, extracted and generated powers according to the wind speed.

Figure 4.16 - System power for the ideal operation.

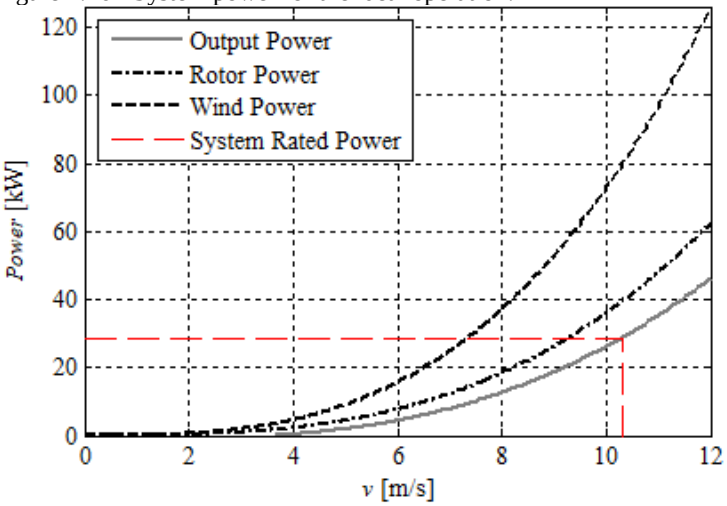

Source: Author.

For the system configuration used in this thesis, the output power should be achieved for a wind speed below 11.0 m/s.

For such systems, the design engineer is not only required to look into the steady state system behaviour, but to look into a few system dynamic behaviour parameters can provide a deeper insight on the whole system.

4.6 SYSTEM NATURAL FREQUENCY

One issue of wind turbines is that the tower shadow effect, explained in Section 2.1, is a form of excitation to the system. The excitation frequency might be equal to the natural frequency of the system comprising the rotor and the hydrostatic transmission. If they are equal this would result in resonance, which is not desired.

Knowing the natural frequency value, allows to define system control parameters and strategies, or even to change the system design, to avoid or overcome the resonant frequency.

Vatheuer *et al*. (2011) states that the rotor excites the system with the frequency of the rotor speed and the frequency of the blades passing the tower. For a three-blade rotor the excitation frequency (f_{exc}) is,

$$f_{exc} = 3\omega_R. \tag{4.17}$$

Here, a more general analysis is carried, where the natural frequency of the rotor/pump plus hydraulic lines is analysed according to the turbine rated output power. Since the turbine operation parameters vary with the different classes of turbine rated power it is interesting to check if for a given operational point the systems are excited with their natural frequency.

The rotor plus hydraulic lines natural frequency is evaluated by "removing" the hydraulic motor and closing the end port of the high pressure line and the inlet port of the low pressure line. In this analysis the gearbox is also removed from the equations.

The continuity equation for both lines and Newton's second law of motion for the pump plus rotor rotational inertia are shown in the following equations.

$$q_{Po} - q_{Mi} = \frac{dV_H}{dt} + \frac{V_{HP}}{\beta_e}\left(\frac{dp_H}{dt}\right), \tag{4.18}$$

$$q_{Mo} - q_{Pi} = \frac{dV_L}{dt} + \frac{V_{LP}}{\beta_e}\left(\frac{dp_L}{dt}\right), \tag{4.19}$$

$$T_{Rw} - D_P(p_H - p_L) - T_{Rloss} = \frac{J_R d\omega_R}{dt}, \tag{4.20}$$

where the term $D_P(p_H - p_L)$ is the theoretical hydraulic torque upon the pump.

Considering that there is no fluid flow at the motor ports ($q_{Mi} = q_{Mo} = 0$), that the rotor torque (T_{Rw}) and losses (T_{Rloss}) are constant, that the hydraulic line volumes are rigid ($dV/dt = 0$) and deriving Equation (4.20) with respect to time yields to,

$$-D_P\left(\frac{dp_H}{dt} - \frac{dp_L}{dt}\right) = \frac{J_R d^2\omega_R}{dt^2}. \tag{4.21}$$

To simplify the analysis, the input torques were considered constant.

Considering that the hydraulic lines volumes are rigid ($dV/dt = 0$) Solving Equations (4.18) and (4.19) with respect to the pressure derivatives and applying them into equation (4.21), leads to,

$$-D_P\left(\frac{\beta_e}{V_H}(q_{Po})+\frac{\beta_e}{V_L}(q_{Pi})\right)=\frac{J_R d^2\omega_R}{dt^2}. \tag{4.22}$$

The input (q_{Pi}) and output (q_{Po}) pump flow rates are written as,

$$q_{Pi}=D_P\omega_R, \tag{4.23}$$

$$q_{Po}=D_P\omega_R\eta_{Pv}, \tag{4.24}$$

where η_{Pv} is the pump volumetric efficiency, considered to be internal losses only.

Applying equations (4.23) and (4.24) and the ratio of the hydraulic line volumes $r_V=V_L/V_H$ into equation (4.22) results in the following equation,

$$-\frac{D_P^2\beta_e}{V_H}\left(\frac{r_V\eta_{Pv}+1}{k_V}\right)\omega_R=\frac{J_R d^2\omega_R}{dt^2}. \tag{4.25}$$

Solving for ω_R results in,

$$\frac{J_R V_H k_V}{D_P^2\beta_e(k_V\eta_{Pv}+1)}\frac{d^2\omega_R}{dt^2}+\omega_R=0 \tag{4.26}$$

The system natural frequency is found to be,

$$\omega_{nf}=\sqrt{\frac{D_P^2\beta_e}{J_R V_H}\left(\frac{k_V\eta_{Pv}+1}{k_V}\right)}. \tag{4.27}$$

The system natural frequency is dependent on three key turbine design parameters: the pump displacement, the line volumes and the rotor mass moment of inertia. The pump volumetric efficiency and the fluid bulk modulus are not considered design parameters in this analysis.

These three design parameters can be related to the desired turbine rated output power, which defines the turbine size. In the following procedure, these three parameters are correlated to the turbine rated output power. This is done to evaluate the natural frequency of turbines with different rated output powers using equation (4.27).

For a given rated output power, the rotor nominal power can be calculated as,

$$P_{Rw,n}=P_{GSo,n}/(\eta_{HT}\eta_{GS}). \tag{4.28}$$

For a given output power, using equations (2.1) and (4.8), the rotor area can be calculated using the nominal wind speed (v_n) and rotor ideal power coefficient ($c_{p,ideal}$).

Burton *et al.* (2011) states that turbine manufacturers limit the maximum blade tip linear speed ($v_{tip,max}$) around 65.00 m/s to comply with noise restrictions. Therefore, the rotor rated rotational speed (ω_{Rn}) can be determined by

$$\omega_{Rn} = \frac{v_{tip,max}}{r}. \tag{4.29}$$

The rotor torque at the nominal speed is then calculated as

$$T_{Rw,n} = \frac{P_{Rw,n}}{\omega_{R,n}}. \tag{4.30}$$

The pump volumetric displacement is calculated as

$$D_P = \frac{T_{Rw,n}}{\Delta p_{P,max}} \eta_{Pm}, \tag{4.31}$$

where, $\Delta p_{P,max}$ is the maximum pressure difference upon the pump, and η_{Pm} is the pump mechanical efficiency.

The lines volumes are calculated as,

$$V = \frac{\pi d^2}{4} h\,. \tag{4.32}$$

where, d is the hydraulic line diameter and h is the tower height. For the hydrostatic transmission concept studied in this thesis, the hydraulic lines length can be approximated as the tower height.

The line diameters are set, as recommended by Mannesmann (1988) to result in a determined fluid speed that, as consequence, produces a lower pressure drop along the lines. In this way the diameters for the high and low pressure lines are calculated with the following equations,

$$d_L = \sqrt{\frac{4\pi D_P \omega_R}{v_{fluid,L}}}, \tag{4.33}$$

and

$$d_H = \sqrt{\frac{4\pi D_P \omega_R \eta_{Pv}}{v_{fluid,H}}}, \tag{4.34}$$

where $v_{fluid,H}$ and $v_{fluid,L}$ are the average fluid speed in the high and low pressure lines respectively. According to Vianna Jr. (2013), to determine the diameter of hydraulic lines taking into account not only the pressure drop but also the costs of installation and purchase of the lines, leads to a more competitive and economically attractive product. The author mentions that the best solution is a balance between energy efficiency and installation costs. Since this thesis is not about product development but about a prove of concept the approach suggested by Mannesmann (1988) is used.

Hassan, G. (2009) in 'Wind Energy – The Facts' correlated the tower height to the rotor radius for a number of different turbines with different sizes. The correlation is,

$$l = h = 2.7936(2r)^{0.7663}. \tag{4.35}$$

These authors presented also two correlations to determine the rotor mass (m_R) and the rotor mass moment of inertia (J_R). They are,

$$m_R = 2.95r^{2.13}, \tag{4.36}$$

and

$$J_R = 0.636 m_R r^2. \tag{4.37}$$

In this way, for a given range of turbines with different rated output power ($P_{GSo,n}$) the natural frequency can be calculated using the equations given from (4.27) to (4.37). This analysis is performed and the natural frequency is compared to the excitation frequency calculated with Equation (4.17). The parameters used for the calculations are shown in Table 4.3.

Table 4.3 - Parameters used for the natural frequency analysis.

Parameter	Adopted value
$v_{fluid,L}$	1.5 m/s
$v_{fluid,H}$	6.0 m/s
η_{Pv}	0.95
η_{Pm}	0.095
Δp_{max}	200.0 bar
$v_{tip,max}$	65 m/s

β_e	1500 MPa
v_n	12m/s
$c_{p,ideal}$	0.496

Source: Author.

The excitation frequency, Equation (4.17) is calculated for two different operation points. One for the point of synchronization to the grid and one for the maximum rotor speed operation point. Figure 4.17 presents two excitation frequencies and natural frequency for a range of wind turbine output nominal powers.

Figure 4.17 - System natural frequency and excitation frequencies.

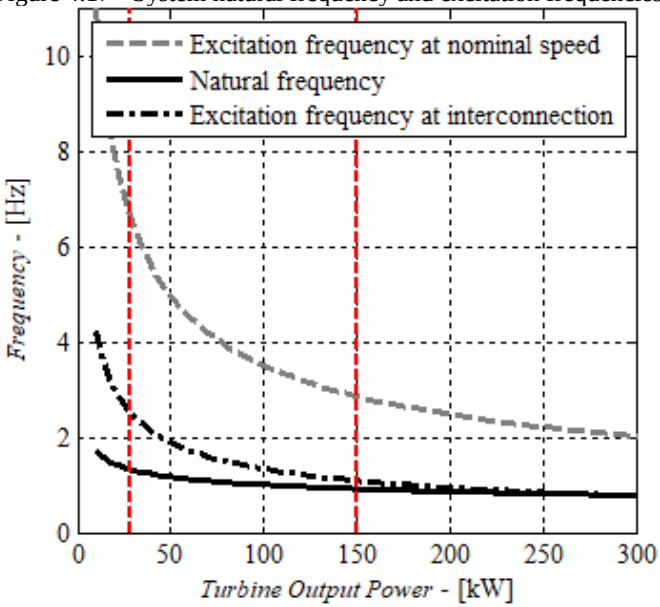

Source: Author.

The system natural frequency, for the all the range of turbine nominal output powers of Figure 4.17, is below the maximum rotor excitation frequency, which occurs at nominal rotor speed. That means that at a certain operation point the rotor speed will produce and excitation equal to the system natural frequency, which is not desired.

Another possible conclusion is that, as higher the power the more the natural frequency becomes closer to the rotor excitation frequency when synchronized to the grid.

It is important to estimate at which operation point the natural frequency will be achieved. If this happens when the system is not delivering power to the grid the effects due to resonance could be small. Before the synchronization point the system net power delivery is still zero and the wind power is only sufficient to overcome the system losses. All the power entering the system is being dissipated. The borderline is at the synchronization point. The following analysis aims to identify what is the rotor speed, and consequently excitation frequency, when the system is at the synchronization point.

Before the synchronization point the generator operates like a free wheel and only the friction losses are present. Therefore, at the synchronization point the power supplied to the generator is

$$P_{GS,sync} = c_{GS}\omega_{GS,n}, \tag{4.38}$$

where c_{GS} is the generator viscous friction coefficient and $\omega_{GS,n}$ is the generator nominal rotational speed. c_{GS} is calculated according to the turbine power size. The coefficient was calculated to have a generator power dissipation of 1.5 % of the rated output power when operating at the generator nominal speed.

The power supplied by the wind is then calculated as

$$P_{Rw,sync} = \frac{P_{GS,sync}}{\eta_{HT}}, \tag{4.39}$$

where η_{GS} is the generator efficiency that must be discounted from the overall efficiency.

Using Equation (2.1), the wind speed can be calculated and with Equation (2.2), at the ideal operation point (λ_{ideal}), the rotor speed when synchronizing $\omega_{R,sync}$ is determined. This speed results in the rotor excitation frequency when synchronizing to the grid. It is the dot-dashed curve in Figure 4.17. It is, for this turbine output power range, above the natural frequency. This means that the rotor will operate with the natural frequency when increasing speed trying to achieve the synchronization point. At that point it has no net output power so the issues related to resonance should not be so significant.

On the other hand, if this analysis is extended for turbines with higher output power that might not be the case. The higher the power, the closer the rotor excitation frequency at the synchronization point becomes to the natural frequency. Eventually the rotor excitation frequency when synchronizing will coincide with the natural frequency, and the resonance issues can be significant.

For a detailed hydrostatic transmission model, Vatheuer *et al.* (2011) showed that the leakages and losses throughout the system resulted in high damping characteristic. Therefore, concluding that the hydrostatic drivetrain would decrease the resonant behaviour.

A similar analysis can be carried aiming to evaluate the system open-loop stability while the generator is connected to the grid. In Section 4.7 this open-loop stability analysis is carried for a wind turbine with a hydrostatic transmission and with a nominal output power equal to the test bench nominal output power.

4.7 SYSTEM OPEN-LOOP STABILITY

In this section a brief analysis is carried out to evaluate the system open-loop stability. A linearized model in the state space form was built for the system when delivering power to the grid and at the optimal rotor speed, which means operating in region *III*. The model describes the rotor interaction with the wind, the pressure behaviour in the lines and the interaction of this system with the grid. The detailed development of the linearized model is described in Appendix A. The author recommends a brief reading of that development to understand the following analysis.

Diepeveen *et al.* (2011) and Schmitz *et al.* (2013) proposed similar models to perform the closed and open-loop analysis of other hydrostatic transmissions for wind turbines. In their models they considered the hydraulic motor speed being constant. Here, the same procedure as the mentioned authors took is done. However, a model for the dynamic coupling between the generator and grid is implemented.

The model has four state variables, rotor speed, pressure difference between lines, hydraulic motor speed and electric torque angle. It also has two inputs, the wind speed and the hydraulic motor displacement setting.

The system was linearized for an operational point. The values for the state variables are calculated with the wind speed at the operational point using the equations previously described in the thesis.

Three wind speeds were chosen to evaluate the stability. One at the beginning of the operation region *III*, one in the middle and one at the end. Since the system is linearized with respect to the operational point the stability is only valid closer to that point.

Only one turbine size was chosen to evaluate the stability and it is the one used in the project, with parameters shown in Table 4.1. However, there is no gearbox, thus the pump displacement is actually 12 times greater than the value shown in Table 4.1.

To analyse the open-loop stability it is necessary to evaluate the poles of the matrix A that multiplies the system states in the state space form representation. The poles are the matrix eigenvalues (λ_A), which were calculated using MATLAB.

Table 4.4 shows the matrix eigenvalues for the three chosen wind speeds.

Table 4.4 - System open-loop stability analysis – Eigenvalues.

Wind Speed [m/s]	λ_A
4.0	$\begin{bmatrix} -0.0813 & +0.6857i \\ -0.0813 & -0.6857i \\ -2.6504 & +8.0691i \\ -2.6504 & -8.0691i \end{bmatrix}$
6.5	$\begin{bmatrix} -0.0862 & +0.6751i \\ -0.0862 & -0.6751i \\ -2.6521 & +8.2165i \\ -2.6521 & -8.2165i \end{bmatrix}$
9.0	$\begin{bmatrix} -0.0904 & +0.6602i \\ -0.0904 & -0.6602i \\ -2.6545 & +8.4267i \\ -2.6545 & -8.4267i \end{bmatrix}$

Source: Author.

For the three wind speeds evaluated, all the real parts of the eigenvalues are negative, So they lay in the left half complex plane, which, according to the Routh-Hurwitz stability criterion, means that the system is stable for those points.

The results achieved in this brief analysis showed, differently than what was presented by Schmitz *et al.* (2013), the system is actually stable when it is coupled to the grid. The inclusion of the generator's synchronization and damping torques resulted in a stable system, which makes perfectly sense. The system is connected to an infinity busbar. If the rated power is small it can't take the grid out of its equilibrium point, so the grid keeps the turbine stable. That is valid for small rated powers. For other rated power this assumption might lose validity.

The analysis carried in this chapter can give a certain insight of what to expect from the system. It was also used to explain a few of the assumptions and technical decisions taken when developing the test bench and its mathematical model for numerical simulation.

5. MATHEMATICAL MODEL FOR NUMERICAL SIMULATION

"Models are always wrong, they are always approximations! What you have to ask is if a model tells you more information that otherwise you would have. If it does, it is skilful!" (Gavin Schmidt – TED talk – The emergent patterns of climate change)

"A model is a simplified representation of a system, intended to enhance our ability to understand, predict and possibly control the behaviour of the system." (Neelamkavil, 1987)

In this section the main features of the system mathematical model for simulation are described. The model is built and simulated in in LMS AMESIM software. Most of the model is built using already validated component sub-models available in the software. Other unavailable, but necessary, sub-models were built using the signal/control library.

The model and its parameters are, later on, adjusted, updated and validated according to measurements obtained from the test bench.

Once the model is validated, it can be used to evaluate similar transmission concepts and/or other rated powers, to develop new control solutions and to evaluate the system overall efficiency, for example.

The model used here is based on the previous models developed by Flesch (2012), Raduenz (2015) and Rapp and Turesson (2015). Here, the intention is not to describe again the whole model but to attain to the main changes and features added to it, for example, the hydraulic motor displacement control model.

In terms of controlling the system in the simulation, a similar control structure as used in the test bench, described in Section 3.4.2, is used. The only difference is that the mathematical model covers the system operation only in regions *III* and *IV*.

The main objective of the mathematical model is to make the validation in the system level and not specifically in the components or sub-model level. The quantity of sensors available and used and their disposal along the system does not allow the experimental validation in component level. As said, what is utilized is the already validated components sub-models available in the software to create a system model capable of describing the static and dynamic behaviour.

Two models are created. The only difference between them is in the power input. One model is for the system validation, where the objective is to represent the test bench. Therefore, the model has no turbine

rotor dynamics, where in its place, it is included the models for the gearbox and the electric motor torque application dynamics. The second model purpose is to represent the real wind turbine, there is no gearbox or electric motor. In their place, the rotor dynamics is added. The only difference in the hydraulic systems model is the size of the pump due to the difference in speeds.

At first place the system power input models are described in Section 5.1, followed by the hydraulic system model in Section 5.2 and the power output model in Section 5.3. The modelling and treatment of sensors signals is described in Section 5.4.

5.1 INPUT POWER MODEL

On the input power side, which resumes to the extraction of power from the wind, the main changes are the modelling of the gearbox between the pump and rotor, and the dynamic behaviour of the electric motor.

5.1.1 Input power model - test bench representation

For the test bench representation, the model has no rotor dynamics but it has the virtual gearbox and the dynamics of the frequency converter and electric motor.

The gearbox is modelled as ideal, where there is no friction or elasticity between the gears. It is represented by Equation (4.1). A similar relation is used to determine the torques relation.

While performing experimental tests, it was observed that the frequency converter and electric motor applied torque (T_{0ME1}) have a first-order behaviour with a time delay with respect to the reference torque ($T_{0ME1,\mathrm{ref}}$) sent to the frequency converter by the controller,

$$T_{0ME1}(s) = \frac{\eta_{0ME1m} e^{-s\tau_{0ME1,d}}}{1 + \tau_{0ME1} s} T_{0ME1,ref}(s). \tag{5.1}$$

In the model, Equation (5.1) is added between the gearbox output torque and the pump input torque to represent this dynamic effect. The behaviour of the frequency converter and electric motor torque is validated in Section 6.1. It is demonstrated that the time delay ($\tau_{0ME1,d}$) is around 0.05 seconds and the time constant (τ_{0ME1}) around 0.55 seconds.

According to the information provided by the electric motor manufacturer, its efficiency (η_{0ME1m}) should be considered constant along the

operation. This efficiency is 96.5 % and is implemented as a gain factor in the first order model behaviour.

The implemented power input model for the test bench representation is shown in Figure 5.1.

Figure 5.1 - Power input model diagram.

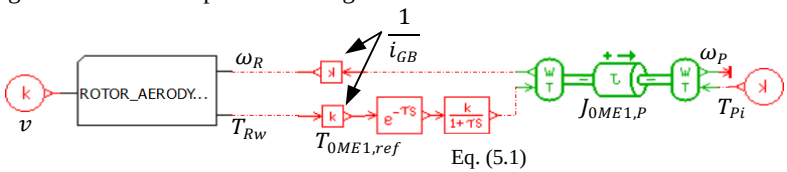

Source: Author.

It is clearly depicted in Figure 5.1 that the applied torque dynamic effect is not substituting the dynamic effect of the electric motor and pump combined mass moment of inertia ($J_{0ME1,P}$). This rotary inertia is modelled without friction since the electric motor losses are accounted in T_{0ME1} and the pump mechanical losses on T_{Pi} which will be described in Section 5.2.3.

The rotor aerodynamics block shown in Figure 5.1 has inside it the same blocks and functions as shown in Figure 3.16.

5.1.2 Input power model - wind turbine representation

Figure 5.2 shows the input power in the simulation model for the wind turbine representation. As it is seen, the gearbox is not present neither the dynamics of the frequency converter. The rotor mechanical losses are as described in Equation (3.6). Due to a much larger rotor mass moment of inertia, the pump mass moment of inertia is neglected.

Figure 5.2 - Wind turbine power input model.

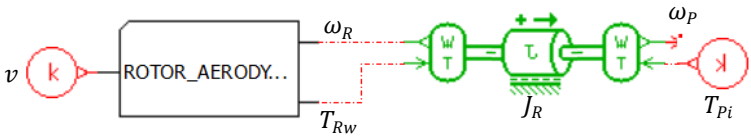

Source: Author.

5.2 HYDRAULIC CIRCUIT AND COMPONENTS MODEL

The main changes in the hydraulic circuit and components model with respect to previous works are the length and model of hydraulic lines

and hoses, position of sensors, pre-charge pressure of accumulators, modelling of the motor displacement control system and localized pressure drops due to filters, for example.

The description of this changes starts with the description of the hydraulic motor displacement control model.

5.2.1 Hydraulic motor control system model

It was explained in Section 4.1.3 that the hydraulic motor displacement setting at the test bench is controlled through a pilot pressure using a pressure relief valve.

The hydraulic motor control circuit, as mentioned in Section 3.1.3, consists of a pump (0P3) a proportional pressure relief valve (1V11), a hydraulic line and the motor displacement control unit, Figure 3.6 and Figure 3.8.

According to Watton (2007), it becomes obvious that much experimental testing of the relief valve is needed to obtain sufficiently accurate data to allow the resulting model to be used in a system simulation. The author presents two equations to describe the dynamics of the relief valve. One is the flow continuity equation and the other is the force balance over the valve spool. However, in the test bench, the fluid flow through the vale (1V11) is nearly zero due to the small movements of the motor displacement control unit valves and internal leakage. The model presented by Watton (2007) also takes into account the solenoid forces against spring and flow forces. Due to the lack of information about spring and valve solenoid forces, and that the only possessed variables are the valve control signal and the measured motor displacement control pressure (p_{MP}), a simpler model is used and the choice for that is also based on the experimental data taken from tests with the valve.

The valve response to the input control signal is assumed, at first hand, to be a second-order equation. This first assumption is made since Watton (2007) mentions that the transient part might be adequately represented by a second-order dynamic characteristic. Also a delay is expected to exist and it is considered as well.

It must be remarked that the behaviour of the regulated pressure is not only a consequence of the valve dynamics but also of the whole motor control actuation system (Figure 4.4) and the volume of fluid in the hose between the valve and motor. Therefore, the observed steady state and dynamic behaviour is from the command signal in volts to the motor pilot port pressure.

In the model, the dynamic behaviour is summarized as a pressure dynamic behaviour. Therefore, the voltage reference is converted into a pressure signal and then the dynamics is applied to it. The relation between the reference pressure ($p_{1V11,\mathrm{ref}}$) and the actual pressure (p_{1V11} or p_{Mp}) is described, as

$$p_{Mp}(s) = \frac{e^{-s\tau_{1V11}}}{1 + \frac{2\zeta_{1V11}}{\omega_{n,1V11}}s + \frac{s^2}{\omega_{n,1V11}^2}} p_{1V11,ref}(s). \tag{5.2}$$

The valve relation between the solenoid voltage reference ($V_{1V11,\mathrm{ref}}$) and the reference pressure was experimentally extracted since the data available at the valve datasheet was observed to be inaccurate. Damping ratio (ζ_{1V11}), natural frequency ($\omega_{n,1V11}$) and time delay (τ_{1V11}) used in the model, were extracted and validated through experimental analysis. Model parameters and valve behaviour validation are shown in Section 6.2.

The motor displacement control model block diagram is shown in Section 6.2 after presenting other necessary equations and experimental data.

5.2.2 Hydraulic lines model

The model used to determine the fluid flow and pressure behaviour inside the main hydraulic lines is the one called *Distributive Lumped element*, where resistive, capacitive and inertial effects are accounted.

A basic analysis was carried to determine the number of line elements that are necessary to obtain a model with reasonable accuracy but not excessive computational cost.

The pressure drop between the pump and motor and motor and pump in the lines was adjusted according to the pressure measurements in the test bench. The adjustment was carried by slightly modifying each pipes/hoses length and diameter. The smaller losses due to curves and connections were not considered. There are not sufficient pressure sensors in each section of lines to build a pressure drop profile along the line that would be capable of validating the model.

5.2.3 Pump and motor volumetric and mechanical efficiencies

The pump and motor volumetric and mechanical efficiencies are calculated as described by Rapp and Turesson (2015). The efficiencies

are functions of pressure difference, displacement and rotational speed. The intention here is not to reproduce the equations or the results obtained by the authors, but to show how they are implemented in the simulation model since the authors did not demonstrated that.

The AMESim provide models for pumps and motor with variable volumetric and mechanical efficiencies. However, the models does not account external volumetric losses. The models does not remove any fluid from the main circuit, which is a phenomenon that occur in real systems. Therefore, the components volumetric and mechanical losses were included (modelled) apart from the component.

Figure 5.3 shows the AMESim model of the pump together with its losses.

Figure 5.3 - Pump mechanical and volumetric efficiencies model.

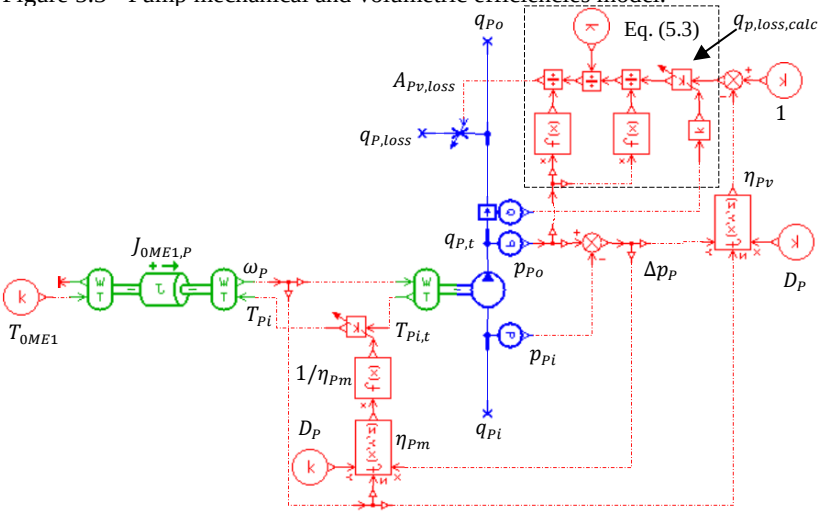

Source: Author.

The pump volumetric losses are actually removed from the transmission main hydraulic circuit for the model to be representative. To perform tha,t it is used a variable hydraulic orifice. The flow rate through the orifice is calculated with the pressure drop over the orifice and the orifice area, which in this case is the variable parameter.

The orifice area is varied according to the pump volumetric efficiency. For a given pump volumetric efficiency (η_{Pv}), the expected flow losses ($q_{P,loss,calc}$) are calculated. Using Equation (5.3), the required orifice area ($A_{Pv,loss}$) is calculated and delivered to the variable orifice.

$$A_{Pv,loss} = \frac{(1-\eta_{Pv})q_{p,t}\sqrt{\frac{2p_{Po}1e5}{\rho_f}}}{A_{Pv,loss,max}(236p_{Po}-240)} \tag{5.3}$$

A better description of this approach can be found in Rapp and Turesson (2015).

As depicted in Figure 5.3, the electric motor and pump combined mass moment of inertia ($J_{0ME1,P}$) are placed together and not directly connected to the pump model to allow the implementation of the pump mechanical efficiency (η_{Pm}) in between.

The torque provided by the pump component is the theoretical torque ($T_{Pi,t}$). The actual pump input shaft torque (T_{Pi}) is bigger than the theoretical torque due to the pump mechanical inefficiency. That is why the theoretical torque is divided by the pump mechanical efficiency (η_{Pm}) and then delivered to the rotary inertia.

At the rotary inertia, the pump speed is a consequence of the balance of the electric motor torque (T_{0ME1}), the pump input torque (T_{Pi}), the Coulomb friction and viscous friction.

Similar efficiency models are implemented in the same way for the hydraulic motor, but are not detailed here.

5.2.4 Filters, heat exchanger, valve pressure drop

The filters, heat exchangers and valves were modelled using standard AMESIM components from the hydraulics library, as presented in the sequence. The data used to adjust the components parameters is extracted from the manufacturers catalogues. Figure 5.4 shows the simplified diagram of the implemented hydraulic circuit model.

Figure 5.4 - Hydraulic circuit model diagram.

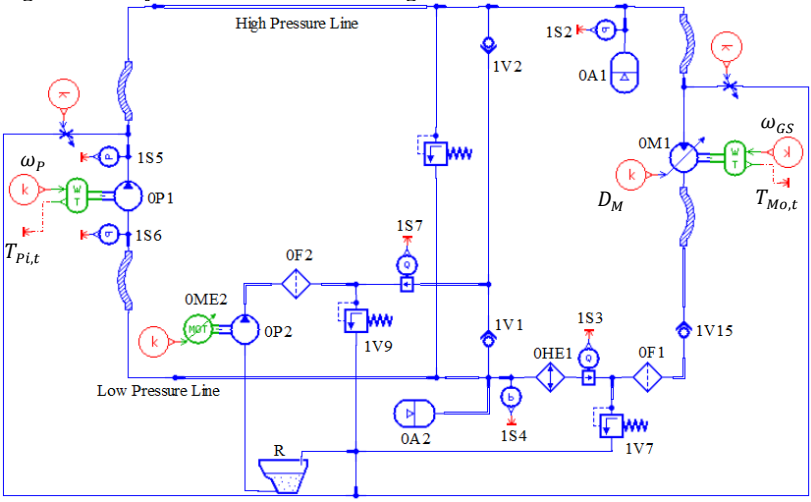

Source: Author.

The check valves 1V1 and 1V2 are modelled as having a linear characteristic of pressure drop to flow rate relation. The cracking pressure is set to be 0.30 bar and the flow rate to pressure gradient is 20.63 L/min/bar.

The check valve 1V15 is also modelled as having a linear characteristic. The cracking pressure is 0.40 bar and the flow rate to pressure gradient is 59.14 L/min/bar.

Both filters pressure drops are modelled as the sum of pressure drop at the filtration element and the pressure drop at the housing. Filter 0F1 has a pressure drop of 0.69 bar at 108.00 L/min and filter 0F2 has a pressure drop of 0.15 bar at 8.00 L/min.

The heat exchanger 0HE1 has a pressure drop of 0.96 bar at 113.60 L/min. The charging circuit relief valve, 1V9, has a linear relation of pressure to flow rate of 1.2 L/min/bar. The adjusted cracking pressure is 5.6 bar. The main circuit pressure relief valve, 1V7, pressure to flow relation is also linear, 2.17 L/min/bar. The adjusted cracking pressure is 5.3 bar.

5.3 OUTPUT POWER MODEL

The output power model describes the interaction between the generator and the grid. The modelling of this generator interaction with the grid during the synchronization phase involves the modelling of electromagnetic forces while the generator is being excited, the model of the grid phase and voltage. Despite being important for whole understanding of

the system, this is out of the scope of the thesis. The modelling of the synchronization action is not performed and is the main reason for the system model be developed only for the turbine operation regions *III* and *IV*, while connected to the grid.

The model of the generator connection to the grid is the same as presented by Flesch (2012). However, the synchronization torque (K_S) and damping torque (K_A) coefficients were calculated for the current system.

The interaction of the synchronous generator with the grid is modelled as an oscillator with second-order differential equation. Equation (5.4) is the transfer function for the equation of motion for the motor and generator.

$$\Delta\overline{\omega_{GS}}(s) = \frac{1}{2Hs}(\Delta\overline{T_{MGSm}}(s) - \Delta\overline{T_{GSe}}(s)), \tag{5.4}$$

where, $\Delta\overline{\omega_{GS}}$ is the normalized generator speed deviation, H is the generator inertia constant ($H = 0.3529 = J_{MGS}\omega_{GS}/P_{GSo,n}$), $\Delta\overline{T_{MGSm}}$ is the normalized mechanical torque deviation and s the Laplace operator. The normalized electrical torque deviation ($\Delta\overline{T_{GSe}}$) is

$$\Delta\overline{\mathrm{T_{GSe}}} = \left(\frac{\mathrm{K_s}}{\mathrm{s}} + \mathrm{K_A}\right)\Delta\overline{\omega_{\mathrm{GS}}}(s), \tag{5.5}$$

where, K_s is the synchronization torque coefficient and K_A the damping torque coefficient. In the simulation a K_s equal to 20.0 and a K_A equal to 1.5 were used.

A detailed block diagram for the implementation of the generators connection to the grid model can be found in Flesch (2012) and in Appendix B.

5.4 SENSORS

In the test bench all signals from sensors pass through first-order low pass filters to reduce the influence of noise in the readings. These filters were also included in the model since they influence the simulation results as well, specially the signals used by the controllers. Table 5.1 shows the time constants used for the sensor signals. Only the most relevant are shown.

Table 5.1 - Filters time constants for signals from sensors.

Sensor	Signal	Time Constant [s]
1S1	*U11* (p_{Mp})	0.05
1S2	*U1* (p_{Mi})	0.05

1S3	q_{1S3}	0.10
1S4	p_{1S4} (p_{Mo})	0.05
1S5	*U3* (p_{Pi})	2.00
1S6	*U12* (p_{Po})	2.00
1S7	q_{1S7}	0.10
1S15	*U2* (ω_R)	0.60
1S17	*U8* (ω_{GS})	0.10
T_{0ME1}	*U7* (T_{0ME1})	0.05
$\omega_{R,ideal}$	$\omega_{R,ideal}$	0.10

Source: Author.

It is noticed in Table 5.1 that some of the time constants are significant. Those signals are used by the system controllers. It was observed during the tests that the system moves towards instability if smaller values for the time constants are used. The values shown were found to be sufficiently small to not observe instabilities in the system.

6. RESULTS

"Simulation is the execution of a mathematical model in order to predict the properties of a design proposal." (Unknown Author)

"Although nature commences with reason and ends in experience, it is necessary for us to do the opposite, that is to commence with experience and from this to proceed to investigate the reason." (Da Vinci)

This section is devoted to present the thesis results. They are results for the test bench characterisation, experimental tests, simulations used to validated the mathematical model and simulations that represent the wind turbine. Results are presented in terms of:

- hydraulic motor displacement control;
- system pressure control;
- generated power frequency;
- wind turbine power coefficient;
- output power;
- system efficiency.

During all the experimental tests, fluid temperature was controlled between 41.5 to 42.5 °C.

In all the following figures the abbreviations *Meas* is used for data measured at the test bench and *Mod* is used for data from the simulation models.

Before presenting the model validation and system results, the first sections describe three system characteristics that were observed during the experimental tests.

6.1 FREQUENCY CONVERTER AND MOTOR TORQUE TIME RESPONSE

The objective of this section is to show the frequency converter and electric motor (0ME1) torque time response and steady state error. Since they should represent the wind power input to the system according to the real-time simulation, ideally they should have a zero time response, or in other words, no dynamic behaviour. What is observed is that it has a fairly significant dynamic behaviour which must be taken into account when developing the simulation model of the system and also when adjusting control parameters.

As explained in Section 3.4.1, the motor is controlled via a torque reference signal determined via the wind and rotor interaction that is the result of a real-time simulation.

There is no sensor to measure the torque being applied by the electric motor to the 0P1 pump shaft. The measurement of the torque applied by the motor, used in the test bench supervisory system, is calculated by the frequency converter using its current and voltage internal measurements.

The frequency converter manufacturer states that in the torque control mode the precision is ±5.0 % of the motor nominal torque. It also mentions that the most accurate control operation range is between 5.0 to 90.0 % of the motor nominal torque. The motor nominal torque is 290.0 Nm and there is a ±14.5 Nm expected torque error in the range between 14.5 to 161.0 Nm.

Figure 6.1 shows the time response of the frequency converter and electric motor. A step torque reference signal is sent to the frequency converter and the frequency converter torque measurement is recorded. Together with the measured signal the simulation model output signal is plotted according to Equation (5.1) with adjusted parameters according to Table 6.1.

Figure 6.1 - Frequency converter and 0ME1 Electric motor time response.

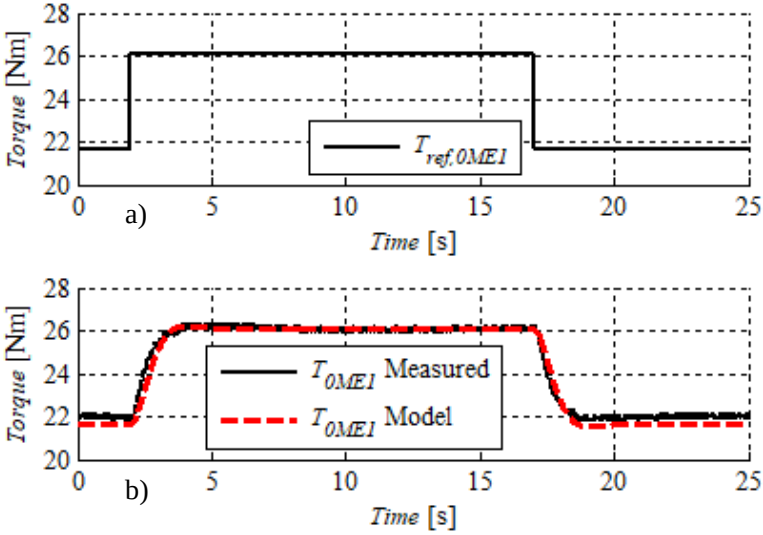

Source: Author.

Table 6.1 - Frequency converter and electric motor simulation model parameters.

Description	Symbol	Value
Time constant	τ_{0ME1}	0.55 s
Time Delay	$\tau_{0ME1,d}$	0.14 s

Source: Author

It can be seen that the frequency converter and electric motor has a time response of around 2.5 seconds and, consequently, it is not possible to be neglected in the model neither in the determination of controllers gains.

During the model validation it was seen that the simulated pump outlet pressure was not matching the measured steady state pressure. The measured pressure was always laying above the modelled, despite the simulated and measured electric motor torques being the same. The first possible reason was thought to be the pump and motor mechanical efficiency. From Equation (3.11) it is seen that a lower mechanical efficiency leads to lower reference pressure for the same rotor speed. Therefore, probably the modelled mechanical efficiency was lower than the actual mechanical efficiency. These first observations are shown in Figure 6.2.

The procedure adopted to verify the possible usage of a wrong efficiency in the model was to change the parameters in the model that affect the pump and motor mechanical efficiency to see if by doing so the pressures would match. Even doing so the pressures were not equal.

Figure 6.2 - 0ME1 torque deviation. a) Torque references; b) Applied torques; c) Pump outlet pressures.

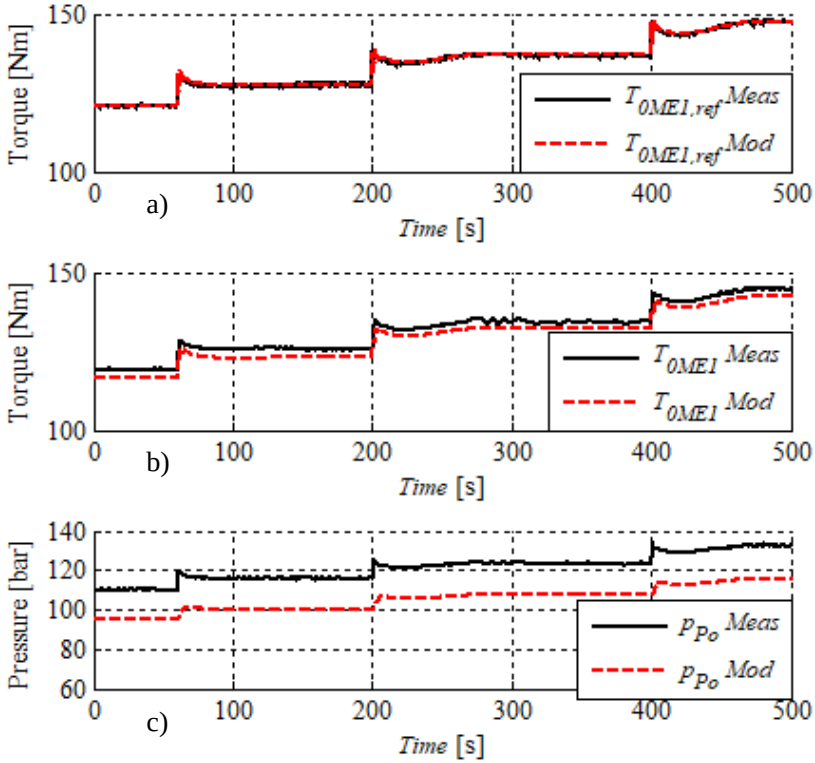

Source: Author.

An ideal system was simulated and compared to the measured values. The ideal simulated system considered a 100.0 % mechanical efficiency both in the electric motor and pump. That should result in the highest controlled system pressure in order to achieve the ideal rotor speed. The results for this comparison are plotted in Figure 6.3.

In Figure 6.3, it is seen that the simulated pressure still became lower than the measured pressure for higher wind speeds. That occurs even for a simulated torque higher than the measured torque. The higher torque at the simulation model is a consequence of the 100.0 % efficiency.

Since the torque references were the same in Figure 6.2, and based on the observed in Figure 6.3, it can be concluded that in the test bench, the electric motor is applying a torque higher than the measured torque it is giving as measurement.

Figure 6.3 - 0ME1 torque deviation. a) Applied torque; b) Pump outlet pressure.

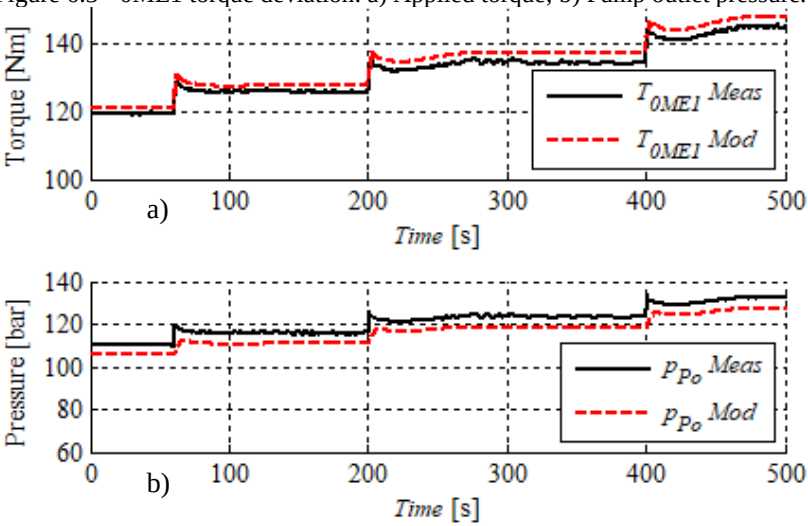

Source: Author.

To overcome this pressure deviation and for them to be the same, a correction factor was implemented in the simulation model torque in order for the steady state pressure to match the measured one. The correction factor is a linear equation having the reference torque as independent variable and the adjusted torque as dependent variable. The equation is,

$$T_{0ME1} = 1.21T_{0ME1,ref} - 6.76. \quad (6.1)$$

Figure 6.4 presents the test bench measured torque, the simulated torque with the correction and the measured torque with the correction factor (*Adjusted* torque in Figure 6.4). This is for the case with the original pump and motor efficiency parameters in the model.

It is seen that the pressures are now matching. From now on, all the model results presented in the model validation contain this torque correction factor.

Figure 6.4 - 0ME1 torque analysis. a) Applied torque; b) Pump outlet pressure.

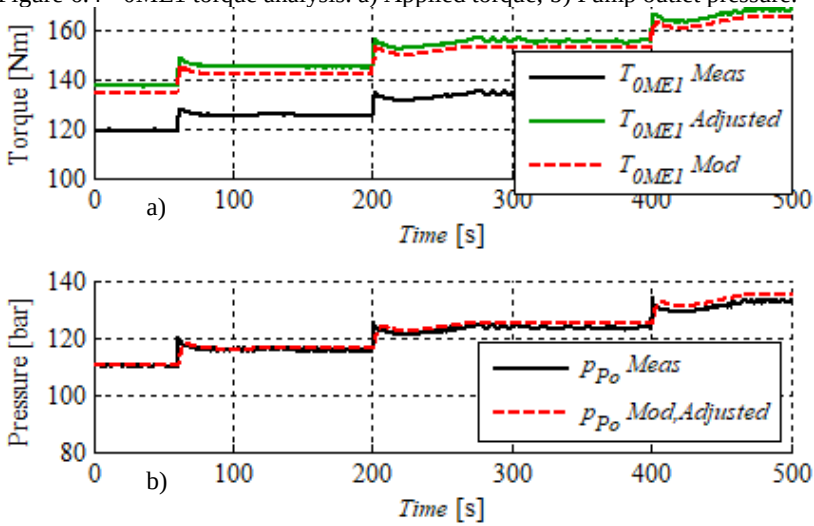

Source: Author.

6.2 HYDRAULIC MOTOR CONTROL PRESSURE BEHAVIOUR

Here it is validated the dynamic behaviour model of the hydraulic motor displacement control pressure. The purpose is to determine if the second-order dynamic behaviour model, described in Section 5.2.1, describes the valve.

The valve is controlled via a PWM signal that is generated by an electronic control module (PCD). The PCD receives a 0.0 to 10.0 V control signal, transforms it into a PWM signal with duty cycle between 0.0 and 100.0 % and delivers that signal to the valve, which results in the regulated pressure. The pressure is measured at the hydraulic motor control port. The motor control pressure range is 10.0 to 35.0 bar.

An open-loop test was performed to validate the pressure dynamic behaviour model. There is no controller operating, only a direct voltage is applied as reference signal.

When performing such test, it was observed that the voltage to pressure relation, given at the valve datasheet (Figure 3.10), was not representing the valve open-loop steady state behaviour. For the same voltage a different pressure was obtained each time. Therefore, using such curve in the simulation model would lead to a much different open-loop steady state response, which is not desired.

In the valve datasheet it is written that it has a maximum hysteresis of 5.25 bar for the pressure range between 0.0 and 350.0 bar. It also says that the repeatability is less than ±1.0 % and linearity of 2.8 %. Knowing that valve hysteresis could lead to a considerable steady state deviation, a test was made to assess the pressure hysteresis with respect to the voltage reference signal. If there is a considerable hysteresis, the observed steady state pressure deviations are explained.

For the hysteresis assessment, the applied control signal is a ramp-like signal from 2.0 to 5.0 V and back to 2.0 V, with a 10 minutes duration. A low frequency ramp signal is applied to avoid the influence of the valve dynamic behaviour in the hysteresis assessment.

A new valve voltage to pressure curve was extracted. The average value between the upper and lower parts of the hysteresis curve was taken and a fifth order polynomial regression was applied to obtain the mean voltage to pressure response. Figure 6.5 presents the obtained results.

Figure 6.5 - 1V11 control signal versus regulated pressure.

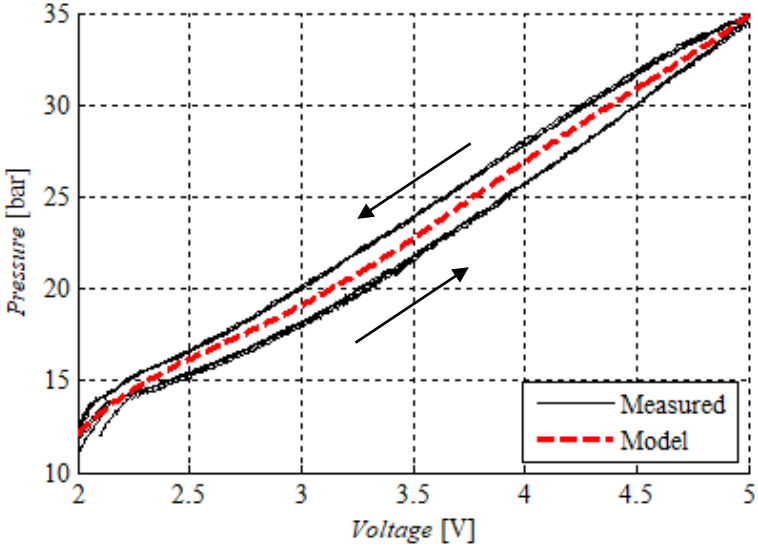

Source: Author.

As seen, the valve hysteresis is significant, being higher than 2.0 bar at 3.5 V, for example. The significant valve hysteresis could be the reason for the open-loop steady state deviations. Equation (6.2) is the valve steady state voltage to pressure curve and is used in the model.

$$p_{1V11,ref}(V_{1V11,ref}) = 0.41756V_{1V11,ref}^{5} - 7.67555V_{1V11,ref}^{4} + 55.14302V_{1V11,ref}^{3} - 192.71990V_{1V11,ref}^{2} + 333.680574V_{1V11,ref} - 216.10966. \quad (6.2)$$

It is seen in Figure 6.5 that the model steady state response, using Equation (6.2), will hardly match the actual valve steady state response.

If comparing Figure 6.5 and Figure 3.10, considering the PWM signal and the reference voltage to be equivalent, it is seen that the data provided by the manufacturer differs from the experimental test. This demonstrate the necessity of extra tests to gather better data to describe the equipment being used.

The next analysis verifies the expected second-order behaviour of the valve and adjust the model parameters. However, a steady state deviation is observed, as expected. Figure 6.6 shows the valve dynamic response for a given step control signal. The adjusted model response for the same control signal is also shown.

Figure 6.6 - Motor control pressure dynamic behaviour. a) Valve reference voltage; b) Valve regulated pressure.

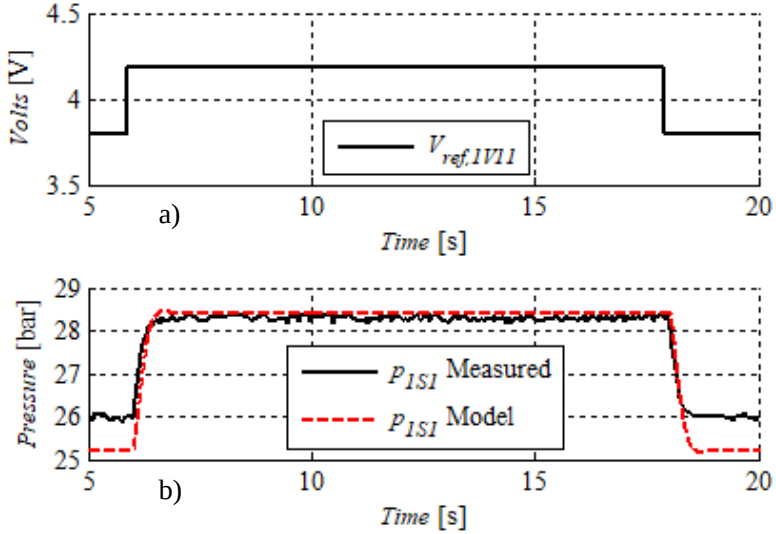

Source: Author.

It is seen in Figure 6.6 that the pressure at motor control port has a second-order behaviour. It was observed from the measured data that it has also a delay.

The observed steady state deviation between the model and the measured data fall within the range of the expected hysteresis. The test shown was made with the generator disconnected from the grid. The same test was performed with the generator connected to the grid. Both tests gave a similar second-order response in the motor control pressure behaviour.

The adjusted parameters for the second-order equation used in the model are summarized in Table 6.2.

Table 6.2 - 1V11 model parameters, Equation (5.2).

Description	Symbol	Value
Natural Frequency	$\omega_{n,1V11}$	1.20 Hz
Damping Ratio	ζ_{1V11}	0.80
Time Delay	τ_{1V11}	0.14 s

Source: Author.

It must be remembered that the dynamic behaviour is not only of the valve itself, but of the set of valve, hose, pipe and equilibrium of forces of the motor control actuation system (Figure 3.6 and Figure 3.8).

When in closed-loop control, the steady state deviations are overcome by the controller and the correct motor displacement is obtained.

It is necessary to have an equation that determines the pressure to voltage relation on the valve. This equation is used both in the model and in the test bench. In the control structure, it is used after the motor displacement control pressure PI controller (Figure 3.20). The controller outputs a signal that is the motor control pressure reference, Equation (6.3) is used to convert it to the reference voltage for the PCD module.

$$\begin{aligned} V_{1V11,ref}(p_{1V11,ref}) &= -0.000002p_{1V11,ref}^5 \\ &+ 0.000309p_{1V11,ref}^4 \\ -0.014759p_{1V11,ref}^3 &+ 0.339377p_{1V11,ref}^2 \\ -3.605395p_{1V11,ref} &+ 16.095342. \end{aligned} \tag{6.3}$$

Equation (6.3) is also a fifth order polynomial regression, however it has the pressure (Figure 6.5) as input variable and the voltage as output variable.

Figure 6.7 presents a block diagram of the motor displacement control simulation model.

Figure 6.7 - Motor displacement control model block diagram.

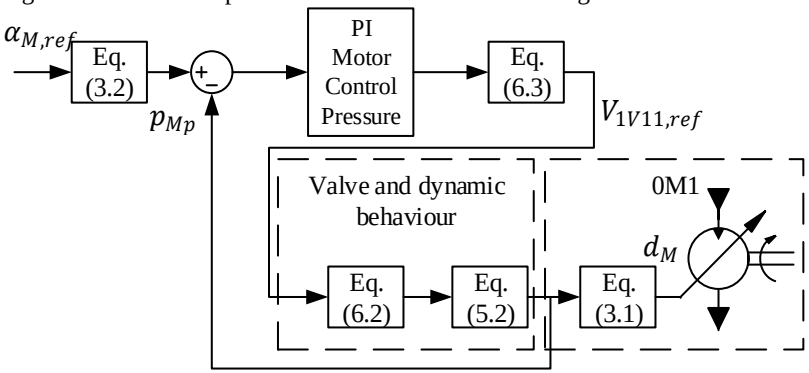

Source: Author.

6.3 SPEED COMPENSATION CONTROLLER

As explained in Section 3.4.2.1, it is necessary to have the speed compensation controller in order to reduce the deviation in the rotor speed from the ideal operation point. Another thought benefit of using it is the faster rotor speed time response. However, the wind behaviour is always changing in intensity and direction. Therefore, it is necessary to analyse the effectiveness of the speed compensation controller.

Using the test bench with the generator connected to the grid, a constant wind speed is set as reference and the speed compensation is turned on and off. When it is on, it means that the reference pressure for the system is calculated with Equation (3.11). When it is off it means that the reference pressure for the system is calculated with Equation (3.8). Figure 6.8 demonstrates the operation of the speed compensation controller in terms of compensation signal ($f_{\omega_R,comp}$), system reference pressure ($p_{Po,ideal}$), rotor ideal speed ($\omega_{R,ideal}$) and measured speed (ω_R).

At the beginning of the time Figure 6.8, the compensation signal is off, so the system is not operating at the ideal conditions. In Figure 6.8c) it is seen that the rotor is not operating at the ideal speed. The speed compensation signal is 1 (Figure 6.8d)).

Around 10 seconds the speed compensation controller is turned on and starts to operate, adjusting the compensation signal to a value that changes the reference pressure (Figure 6.8b), making the rotor to achieve the ideal rotor speed at around 100 seconds (Figure 6.8c). When the speed compensation controller is turned off, around 120 seconds, the system returns to a non-optimal operation point.

Figure 6.8 - Speed compensation action. a) Speed compensation operation; b) Pump pressure; c) Rotor speed; d) Compensation signal.

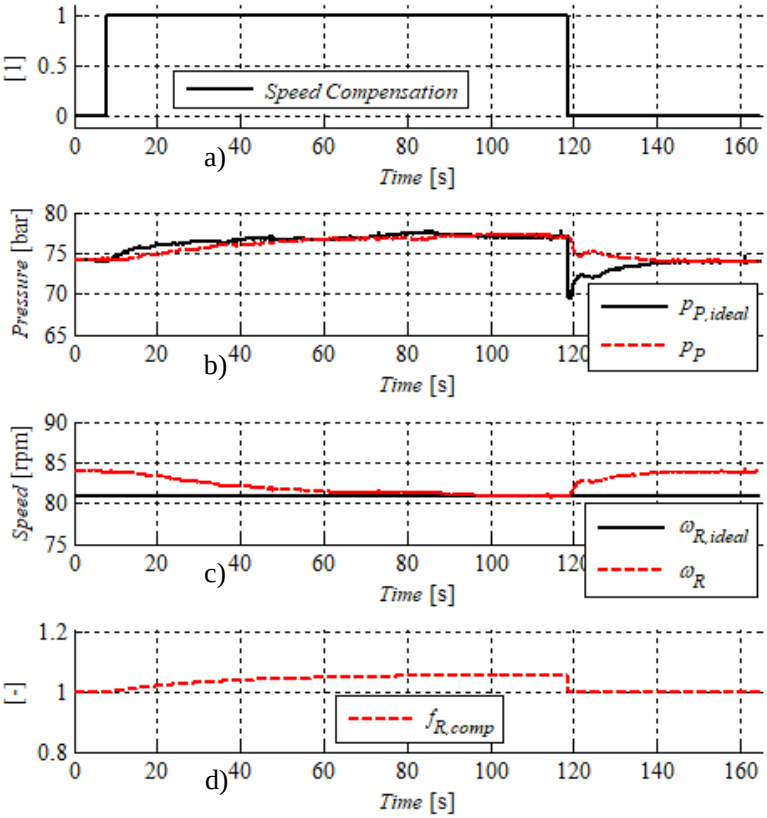

Source: Author.

The system performance is evaluated henceforth with the speed compensation controller.

A paper was published regarding the action and capacities of this speed compensation controller, the reader is invited to read it. The paper is *"Speed Compensation in Hydraulic Wind Turbine Control"*, accepted to be published in the 2018 Global Fluid Power Society conference.

6.4 SYSTEM MODEL VALIDATION

In this section the simulation model described in Section 5 is validated with the experimental data from the test bench. Also in Section 5, it was described that the test bench system model does not take into

account the rotor inertia, but only the dynamics of the electric motor and frequency converter. Therefore, the validation carried out here is for the test bench operating according to a wind input however without the rotor dynamics.

The controller gains used in the tests are the same as present in Section 3.4.5. They are the same at the test bench and at the simulation model.

Two cases are shown to demonstrate the model validity. One is in operation region *III* for a wind speed from 6.0 m/s to 6.2 m/s, when the system is operating with maximum power tracking . The second is in operation region *IV* for a wind speed from 7.4 m/s to 8.0 m/s, when the system is operating with the rotor nominal speed.

It is remarked that the system parameters might have changed during the simulation model validation process with respect to the parameters used in the thesis until here. The changes are made to validate the model. They are, for example, the cracking pressure setting of relief valves, the pressure drop across components, length of hydraulic lines and so on. The changes were not significant up to a point of system de-characterization. A resume of the system model main parameters is shown in Appendix C.

6.4.1 System model validation – Case 1

Case 1 is for the wind speed from 6.0 to 6.2 m/s and the system operating according to the maximum power tracking strategy. The wind speed for the first case is shown in Figure 6.9 together with the rotor torque and applied motor torque.

Figure 6.9 - Model Validation - input references. a) Wind Speed; b) Rotor torque; c) Electric motor torque.

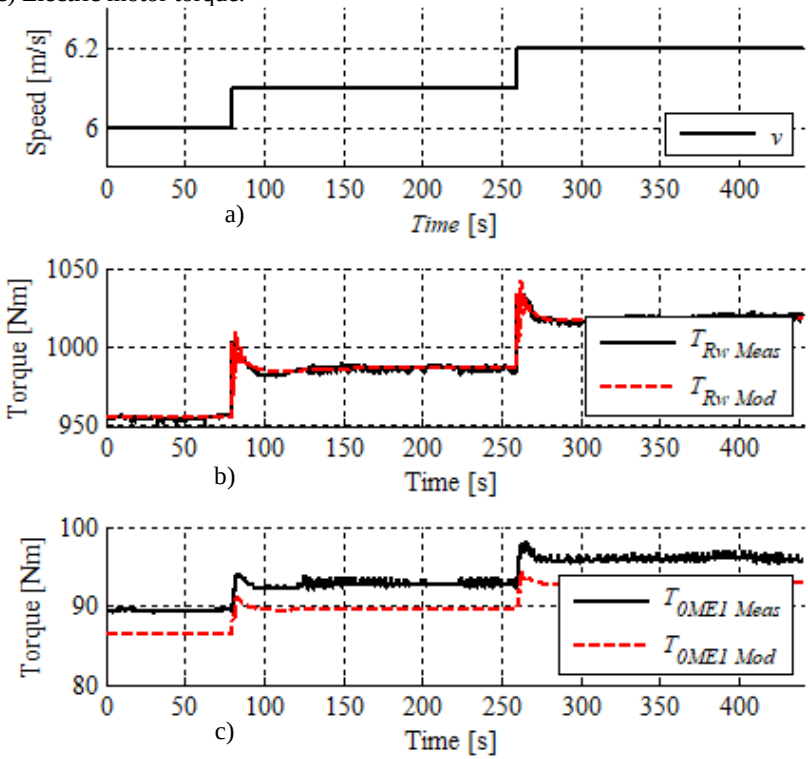

Source: Author.

From Figure 6.9 it is seen that, in terms of torque input, the model can represent correctly the test bench behaviour. It must be remembered that the measured electric motor torque was multiplied by the correction factor.

In Figure 6.10 it is shown the power input to the system and the rotor speed which is the controlled variable.

Figure 6.10 - Model Validation - power input. a) Rotor extracted power; b) Rotor speed.

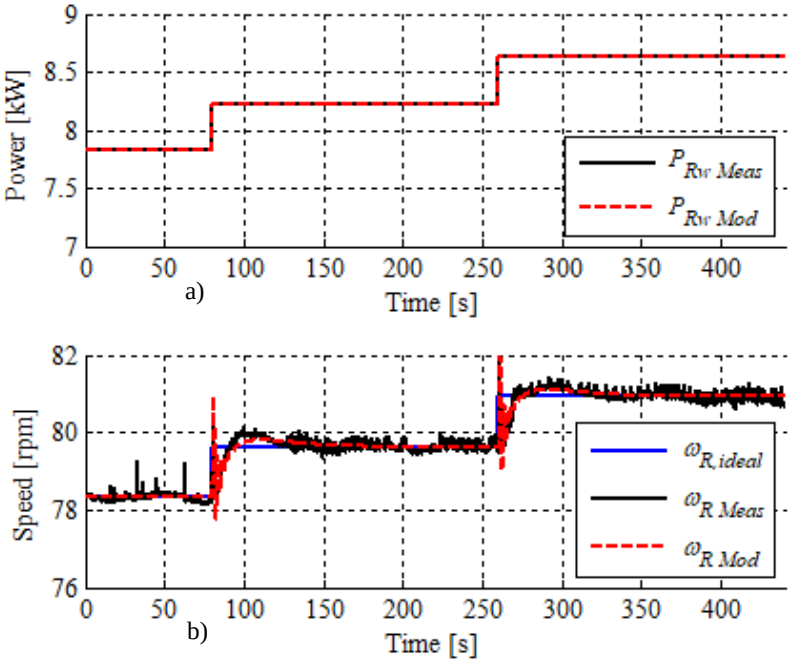

Source: Author.

The power input shown in Figure 6.10a is the torque multiplied by the rotor speed, calculated in the real-time simulation. In Figure 6.10b it is seen that in terms of rotor speed control the experimental and model systems could control the rotor speed to its ideal point. At the same time, the dynamic behaviour of both systems are similar, which is an indicative of the model capacity to represent the real system.

In Figure 6.11 it is shown the validation of the hydraulic motor control pressure and displacement.

A small deviation is observed between the modelled and measured reference pressures (Figure 6.11a), however it is smaller than 0.5 bar. Despite the steady state deviation, the dynamics of this pressure are quite the same Figure 6.11b, which again demonstrates the model validity. In Figure 6.11c it is shown that the test bench can regulated the reference pressure with a considerable accuracy at the motor displacement control port. That demonstrates the capacity of the implemented motor displacement pressure controller.

Figure 6.11 - Model Validation - hydraulic motor control - a) Reference control pressure; b) Measured pressure; c) Control capacity; d) Displacement.

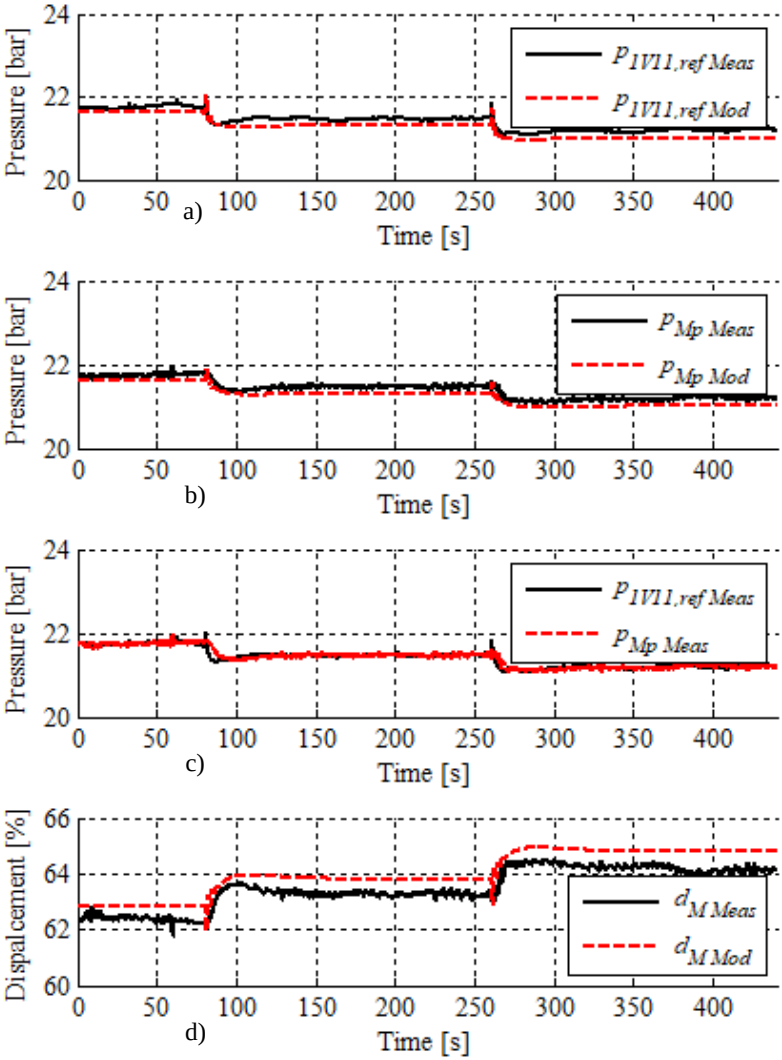

Source: Author.

In Figure 6.12 is shown the high pressure line pressure behaviour.

Figure 6.12 - Model Validation - high pressure line. a) Ideal pressure; b) Pump outlet pressure; c) Motor inlet pressure; d) Control action; e) Line pressure drop.

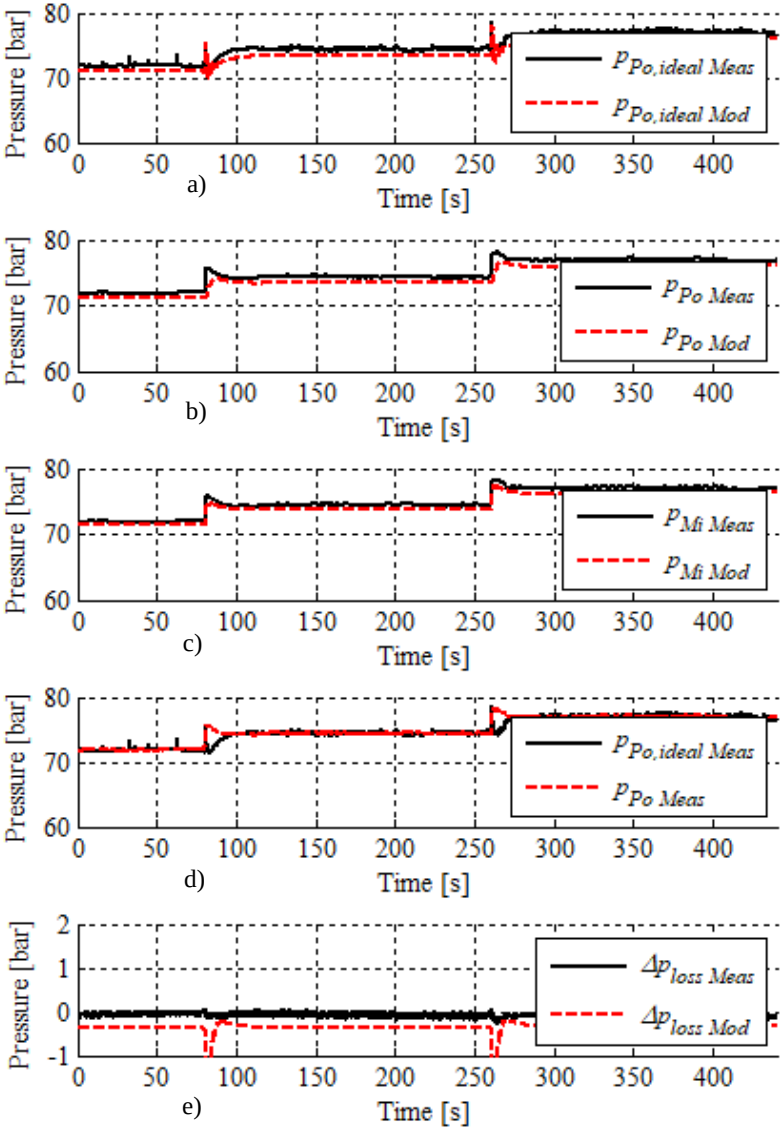

Source: Author.

It is shown in Figure 6.12c the controller capacity to regulate the reference pressure in the system. It is also seen that the dynamics of the

pressures, measured at the pump outlet (1S6) and motor inlet (1S2), are well described by the model.

In Figure 6.13, the behaviour of the low pressure line, is shown. As explained in Section 3.1.2, the low pressure line has its pressure regulated by the charging circuit and relief valves. That is observed by the small deviation in pressure for the different wind speeds.

Figure 6.13 - Model Validation - low pressure line. a) Motor outlet pressure; b) Pump inlet pressure; c) Pressure drop.

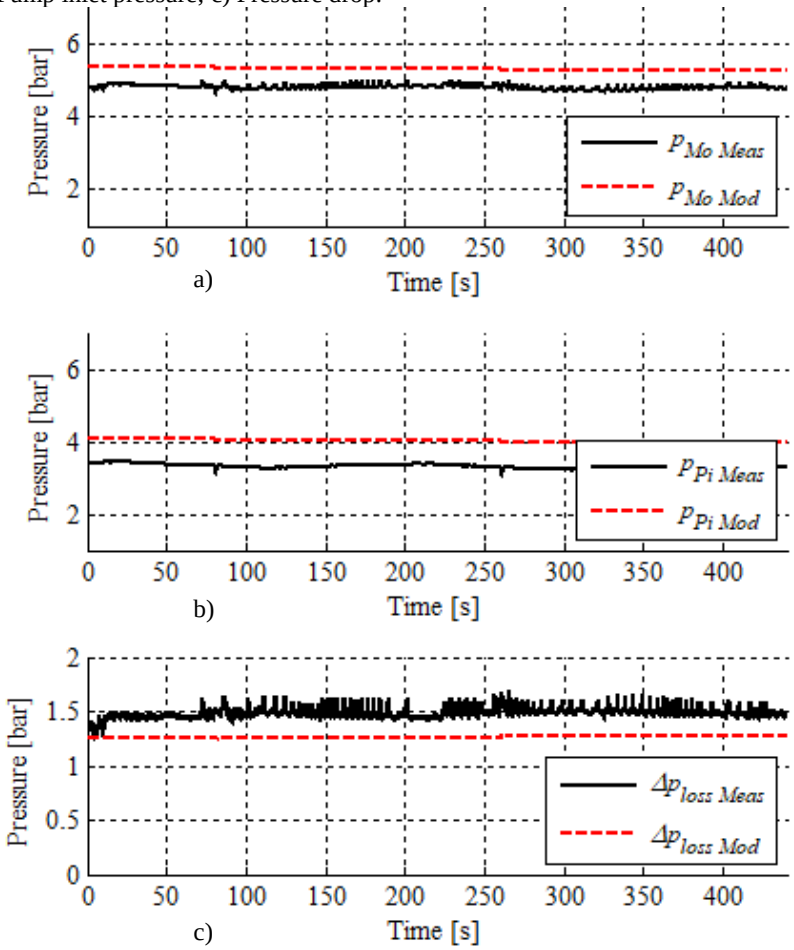

Source: Author.

Figure 6.14 shows the flow rate behaviour.

The flow rate sensors are not capable to measure the high frequency dynamic behaviour. Therefore, the only conclusion from Figure 6.14 is that the model can predict the system steady state flow rate and the dynamic behaviour to some extent.

Figure 6.14 - Model validation - flow rate. a) Main circuit flow rate; b) Charging circuit flow rate.

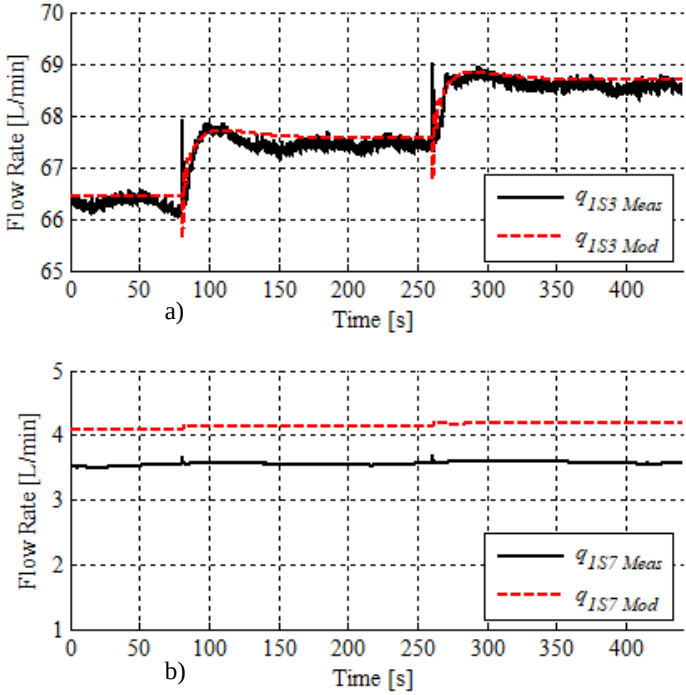

Source: Author.

When connected to the grid the generator operates with the principle of infinite busbar, where the frequency and voltage are kept constant and equal to the grid. In Figure 6.15, this principle is senn with measurements of the grid frequency and voltage. The voltage is not modelled, only the measured voltage is shown.

The measured grid frequency is slightly aboce 60.00 Hz. The same happens for the voltage, instead of 380.00 V it is around 381.05 V.

Figure 6.15 - Model validation - Generator. a) Frequency; b) Voltage.

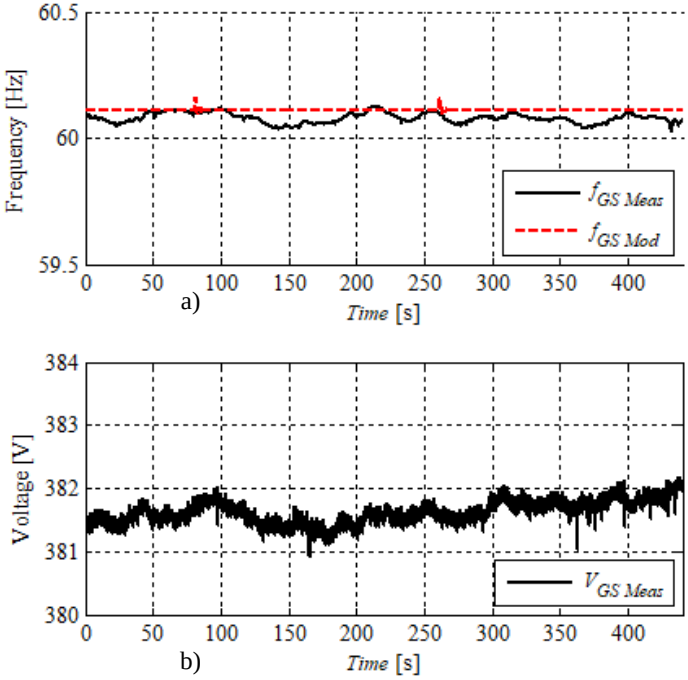

Source: Author.

It is necessary to mention that both frequency and voltage have oscillations and suffer small variations along the tests. The dynamic behaviour is also modelled, that is the reason for observing small frequency deviations in the simulation (Figure 6.15a).

From Figure 6.9 to Figure 6.15 it was the good correspondence of the model to the real system in terms of torque and power input, rotor speed control, pressure control and flow rate. In the following figures the model is validated in terms of the aerodynamic performance indexes and grid frequency.

Figure 6.16 shows the tip speed ratio and the rotor power coefficient. As seen, the model could predict with a high accuracy the behaviour of the rotor performance parameters.

Figure 6.16 - Model Validation - Rotor performance. a) Rotor Speed; b) Power Coefficient; c) Tip Speed Ratio.

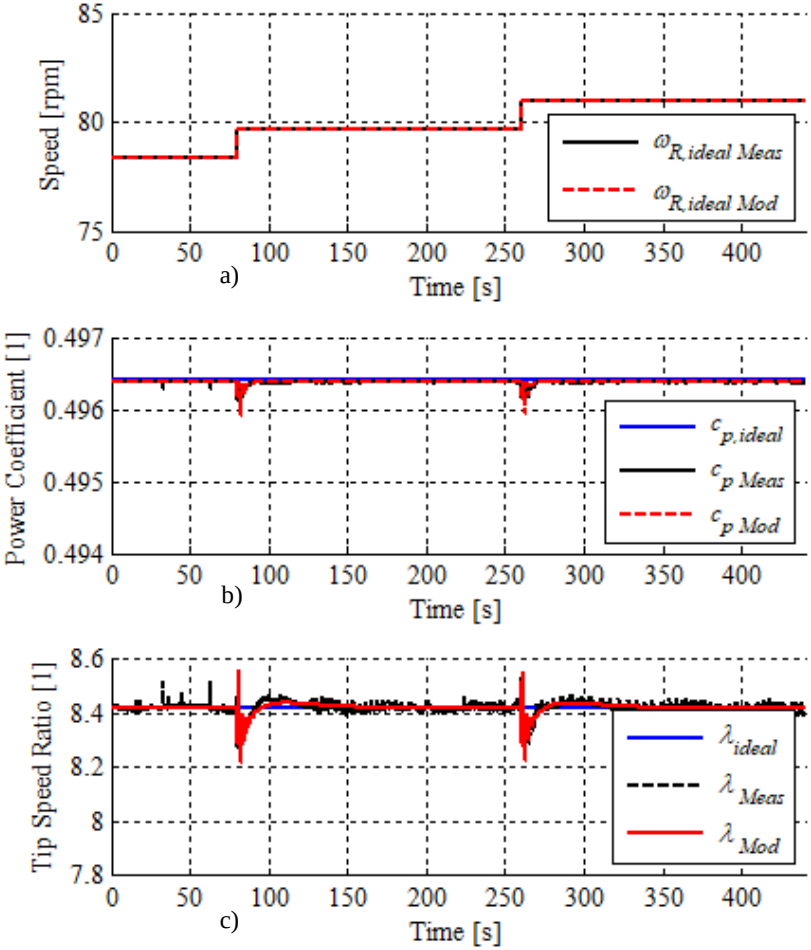

Source: Author.

Figure 6.17 shows the system power. The simulated electric motor power and generated power are shown. The motor power is calculated with the torque reference send to it times its shaft speed. For the generator is the input shaft torque times its shaft speed.

Figure 6.17 - Model validation - system power – electric motor and generated power.

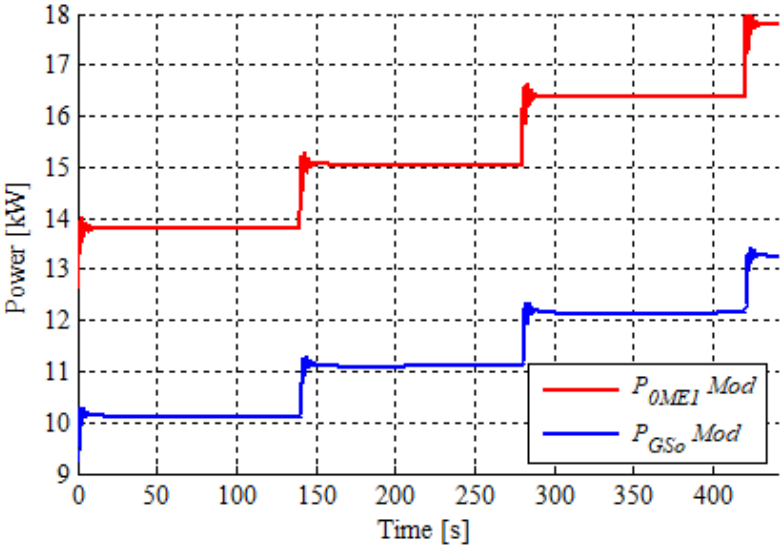

Source: Author.

6.4.2 System model validation – Case 2

Here results are shown regarding the system operation in region *IV*. Only results of input rotor speed and high pressure line pressure are shown. The other variables presented in Section 6.4.1 are not shown since their behaviour was similar and the model predicted with good accuracy the experimental results.

The wind speed input is shown in Figure 6.18a. Figure 6.18b shows the ideal rotor speed in blue and the rotor speed control reference in green. The simulated and measured speeds are also shown.

Figure 6.18 - Rotor maximum speed control validation; a) Wind speed reference; b) Rotor ideal speed, control reference speed, measured and simulated speed.

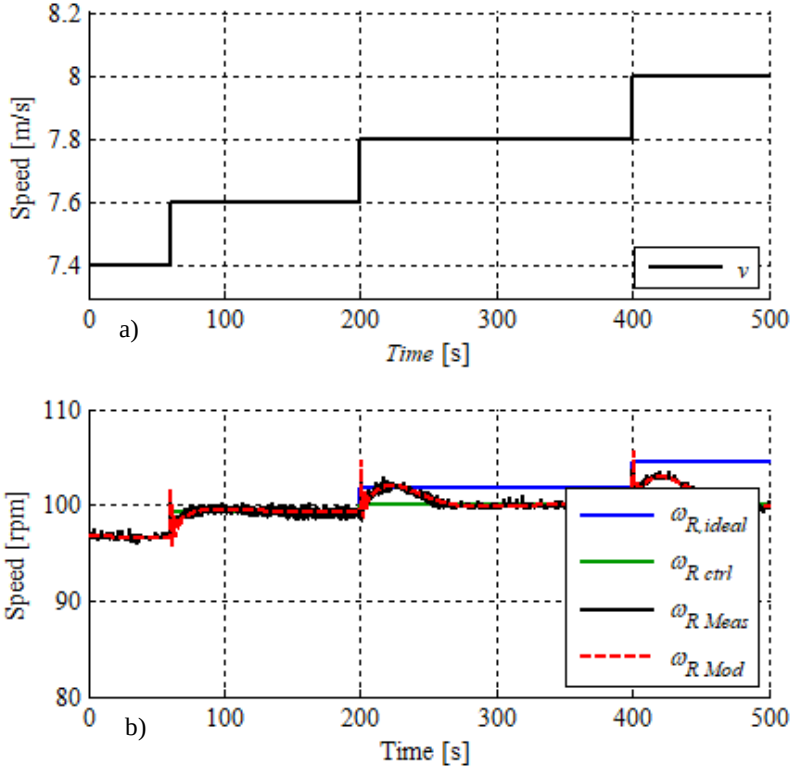

Source: Author.

For a wind speed of 7.6 m/s the rotor speed, control reference and ideal speed, are just below the 100.0 rpm limit. When the wind speed changes to 7.8 m/s the ideal speed (in blue) becomes higher than 100.0 rpm but the control rotor speed reference (in green) is limited to 100.0 rpm. The measured rotor speed is than controlled to remain at 100.0 rpm.

For this case, the model also showed to be very representative. The proposed controller using just a saturation element also proved its effectiveness.

Figure 6.19 shows the high pressure line pressure behaviour.

Figure 6.19 - Rotor maximum speed control - pressure behaviour. a) Ideal pressure. b) Pump outlet pressure. c) Ideal and measured pump outlet pressures.

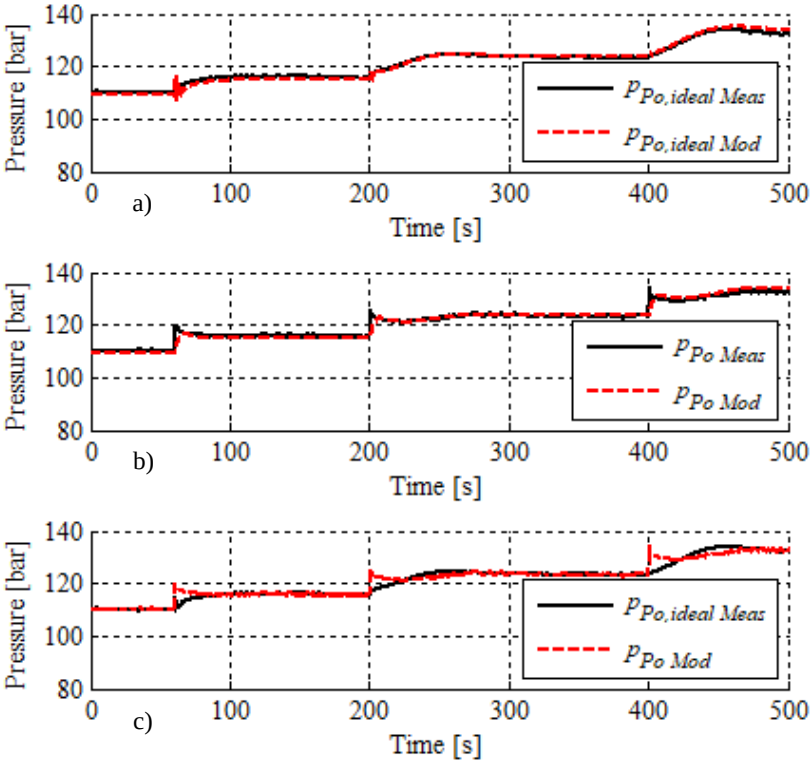

Source: Author.

As seen in Figure 6.19, the model and test bench had approximately the same behaviour. It is also seen the effectiveness of the pressure controller in the operation region *IV*.

Figure 6.18 and Figure 6.19 demonstrate the controllers capacity, in the experiment and model, to limit the rotor speed to 100.0 rpm.

6.4.3 System model validation – steady state power and system efficiency

This section is intended to present the steady state results for the system power and energy efficiency. All results are plotted with respect to the wind speed.

Figure 6.20 shows the electric motor and generator steady state power.

Figure 6.20 – System steady state power.

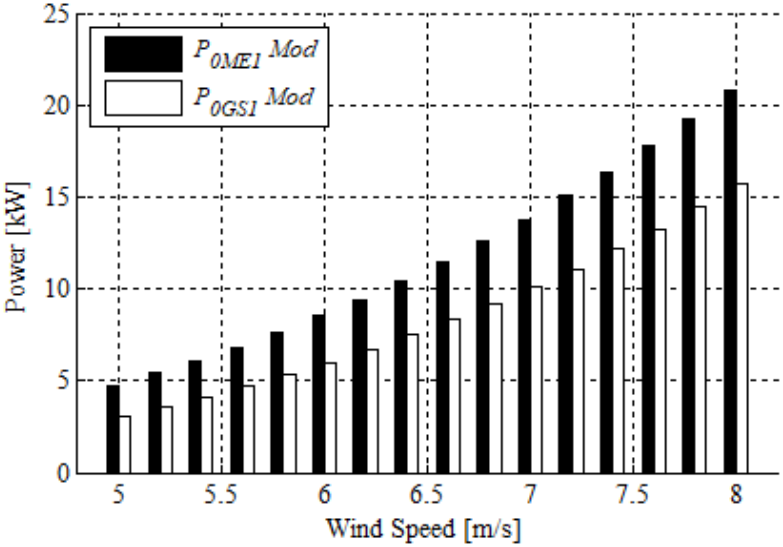

Source: Author.

Due to the system losses it is able to start to deliver power to grid only at around 4.5 m/s and reaches the maximum power generation at 10.2 m/s. This is roughly what was estimated in the analytical analysis in Section 4.5.

Figure 6.21 shows the pump and motor steady state efficiencies.

It is seen that the system efficiency increases with the wind speed as predicted in the analytical analysis. Lower efficiency occur at lower wind speeds.

Sections 6.4.1, 6.4.2 and 6.4.3 demonstrated that the developed system mathematical model predicted the experimental data with accuracy both in terms of steady state behaviour and dynamic behaviour. This validation allows a further and better analysis of the wind turbine operation with the hydraulic transmission through simulation.

The next step is to evaluate the wind turbine operation with the mathematical model by removing the dynamics of the electric motor and gearbox and implementing a bigger volumetric displacement pump.

Figure 6.21 - System steady state efficiency. a) Pump and motor. b) Hydrostatic transmission and overall.

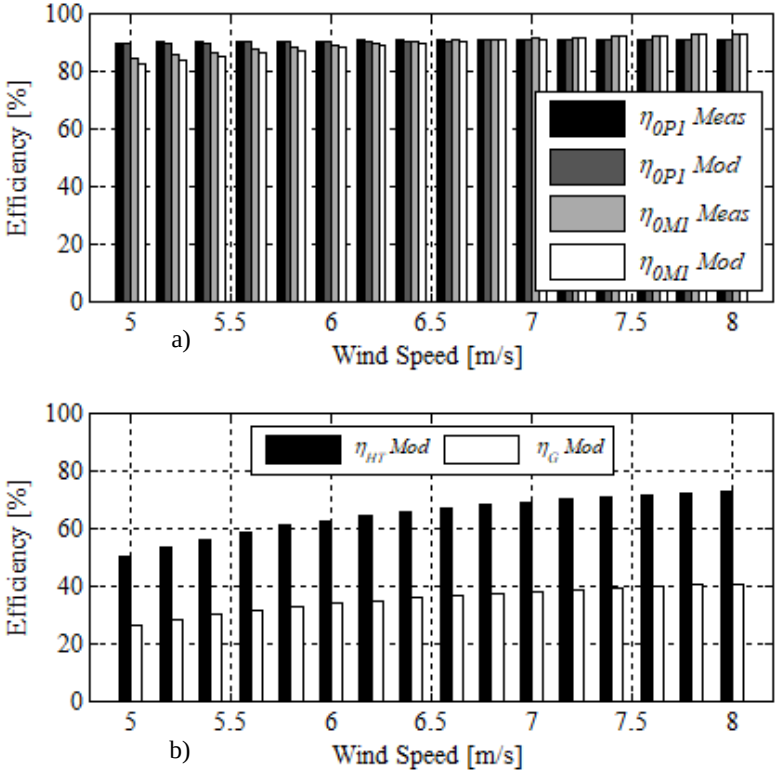

Source: Author.

6.5 WIND TURBINE SIMULATION

In this section the model validated in Section 6.4 is used to simulate a wind turbine operation. The dynamics of the frequency converter and electric motor, included in the model and described in Section 6.1, is substituted by the rotor dynamics that was described in Section 3.4.1. The objective is, by having a model that represents the behaviour of the hydraulic system and grid connection, to evaluate the system performance when the turbine rotor is driving it. The rotor inertia is included in the form of a rotary mass with mass moment of inertia of 3650.0 kgm². The viscous and Coulomb friction coefficients for the rotor shaft are set to 0.025 N/rpm and 1.0 Nm, respectively.

Another modification is the pump size and gearbox. A considerably bigger pump is used and the gearbox is removed. The gearbox removal requires the use of a pump with bigger volumetric displacement. The pump is directly driven by the rotor shaft, which runs at low speed. Therefore, a bigger pump is used in order to match the flow rate requirement for the turbine to achieve is nominal generated power. The pump size is 860.0 cm^3/rev.

In terms of control, the gains were changed since the dynamics of the system are much different now due to the large rotor mass moment of inertia. Figure 6.22 presents the new controller gains used for the wind turbine simulation.

Figure 6.22 - Wind turbine simulation model gains. a) MPT controller; b) Speed Compensation controller; c) 1V11 valve controller.

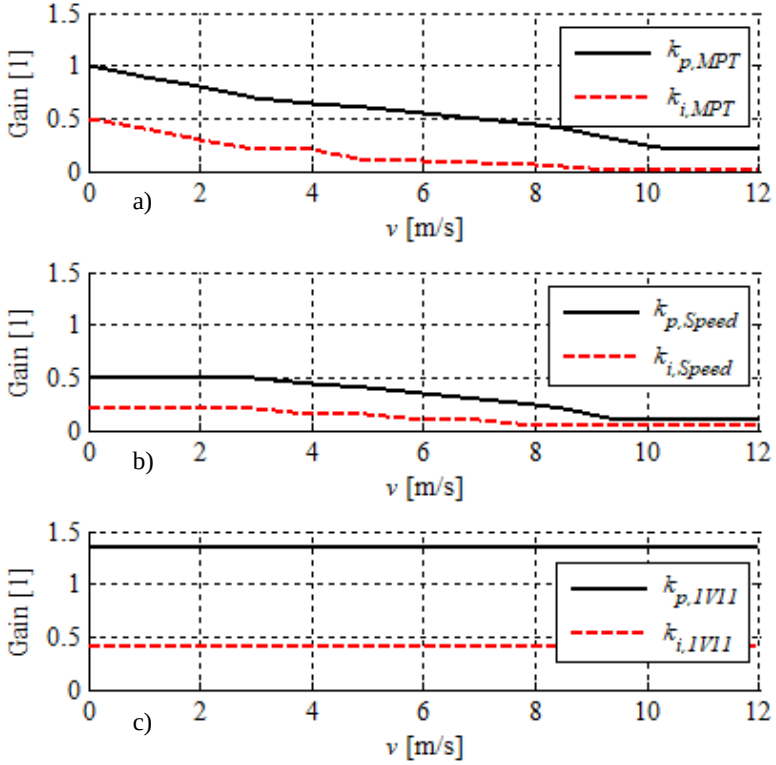

Source: Author.

In comparison to the test bench controller gain scheduling shown in Figure 3.23, the turbine controllers gains were increased.

6.5.1 Wind turbine simulation – step/ramp-like wind profile

This section is used to demonstrate the wind turbine behaviour through the simulation model using a step/ramp-like wind profile. Figure 6.23 shows the rotor speed behaviour for a step/ramp-like wind speed input.

Figure 6.23 - Wind Turbine simulation – step/ramp wind speed. a) Wind speed; b) Rotor speed; c) Pump outlet pressure.

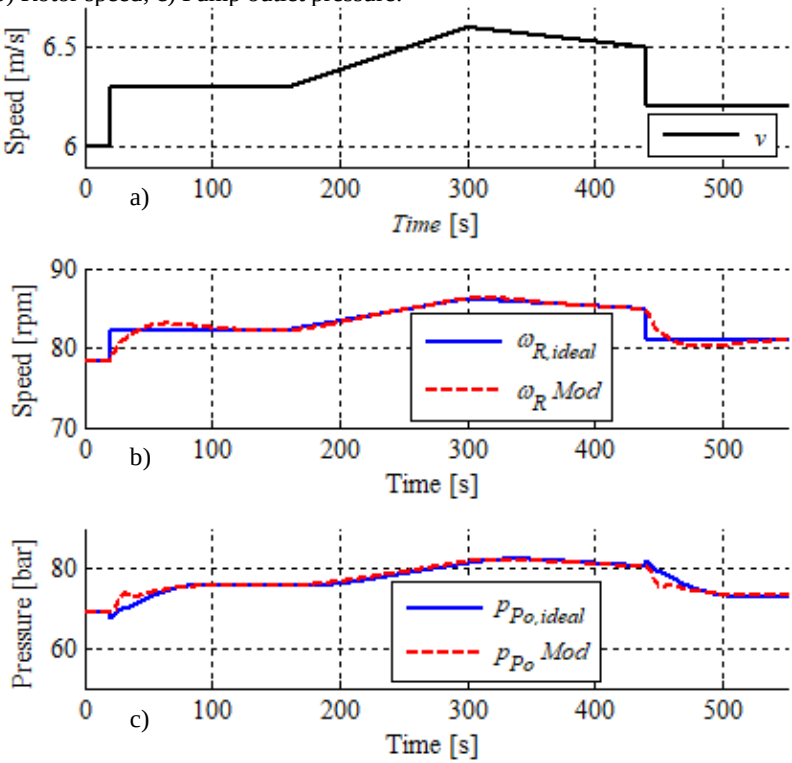

Source: Author.

In Figure 6.23c it is observed that the system is able to regulate the ideal pressure, which results in a good tracking of the ideal rotor speed.

It is very clear to see the action of the speed compensation controller during wind speed steps. When the wind speed steps up, the pressure controller reference is decreased and the increased afterwards. That allows a faster acceleration of the rotor, which tends to result in a faster

response. For the wind speed step down case, the opposite occur. The reference pressure increases and then decreases. That results in a faster rotor deceleration, which also tends to result in a faster response.

In the sequence, Figure 6.24 shows the wind turbine rotor aerodynamic performance.

Figure 6.24 - Wind Turbine simulation – step/ramp wind speed. a) Power coefficient; b) Tip Speed Ratio.

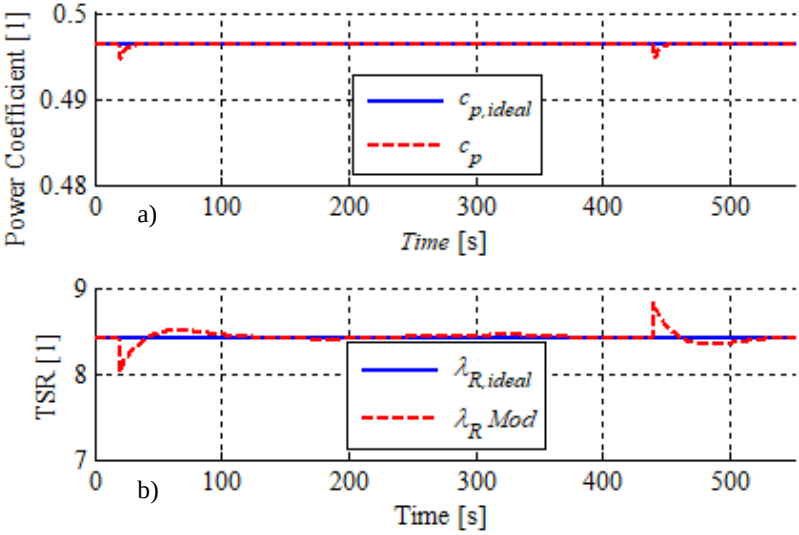

Source: Author.

In both figures 6.24a and Figure 6.24b, after the steps the power coefficient and the tip speed ratio have a significant deviation. During the constant speed or ramp phases the deviation is considerably smaller. The proposed control system is able track and maintain a high rotor aerodynamic performance.

The behaviour of the hydraulic motor in terms of displacement setting and control pressure is shown in Figure 6.25.

The hydraulic motor control pressure (Figure 6.25a) is directly related to the displacement setting (Figure 6.25a). It is observed that the tracking of the reference control pressure occurs.

Figure 6.25 - Wind Turbine simulation – step/ramp wind speed. a) Control pressure; b) Displacement setting.

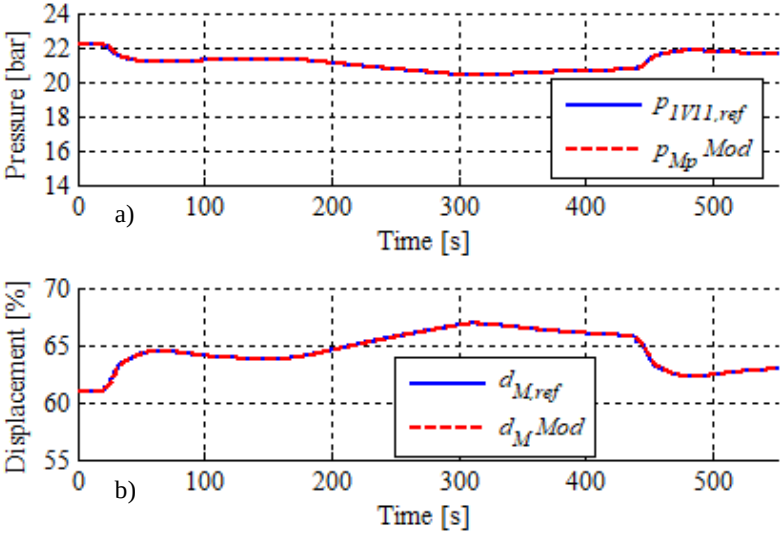

Source: Author.

6.5.2 Wind turbine simulation – realistic wind profile

This section is used to demonstrate the wind turbine behaviour through the simulation model using a realistic wind profile. Figure 6.26 shows the wind profile, rotor speed and pump outlet pressure.

The wind speed input, Figure 6.26a has a considerable higher variation in comparison to the wind profile used in Section 6.5.1. Despite the varying wind profile, the system is able to track the reference pressure, Figure 6.26c, which results in the tracking of the ideal rotor speed.

Due to the good rotor speed tracking the system operates with a relatively high aerodynamic efficiency, which is shown in Figure 6.27 in terms of power coefficient and tip speed ratio.

Figure 6.26 – Wind turbine simulation - real wind speed. a) Wind speed; b) Rotor speed; c) Pump outlet pressure.

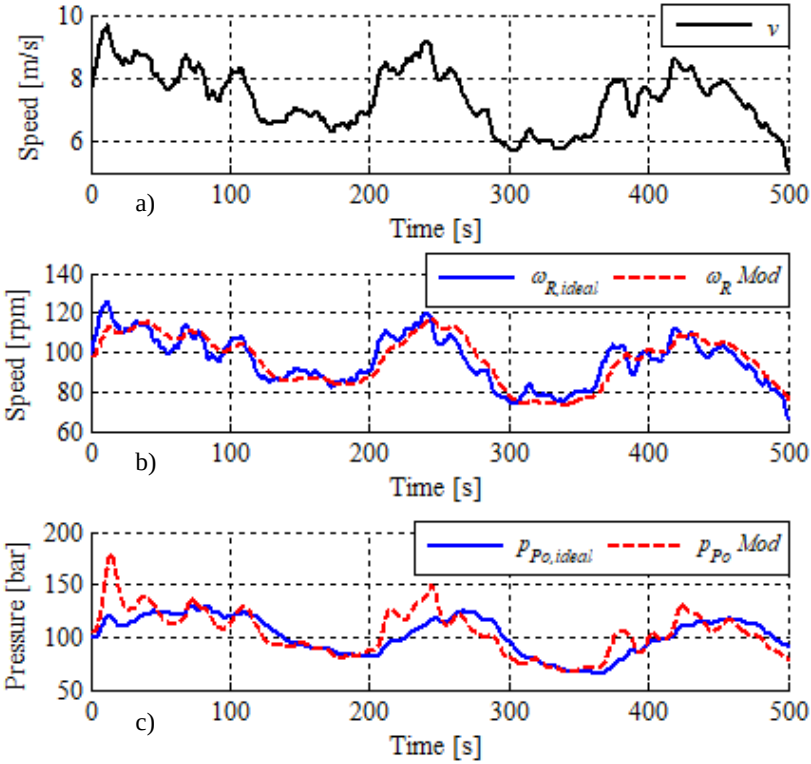

Source: Author.

Despite the faster changing wind the controller brings the rotor to the ideal tip speed ratio (Figure 6.27b) which results in a high power coefficient, Figure 6.27a.

Figure 6.27 - Wind turbine simulation - Real wind speed. a) Power Coefficient; b) Tip speed ratio.

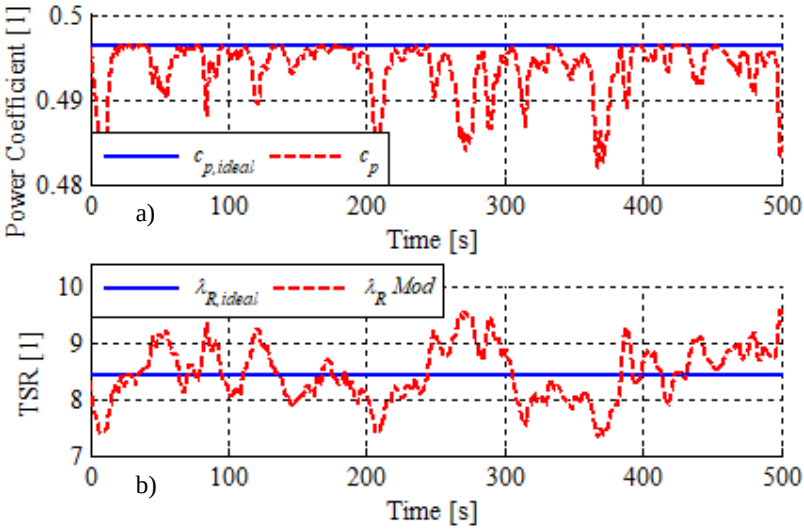

Source: Author.

Figure 6.28 shows the hydraulic motor displacement setting control behaviour.

The system is able to keep a good tracking of the hydraulic motor control pressure reference. That is also one reason of why the system can have a good control of the rotor speed.

Figure 6.28 - Wind turbine simulation - Real wind speed. a) Hydraulic motor control pressure; b) Hydraulic motor displacement.

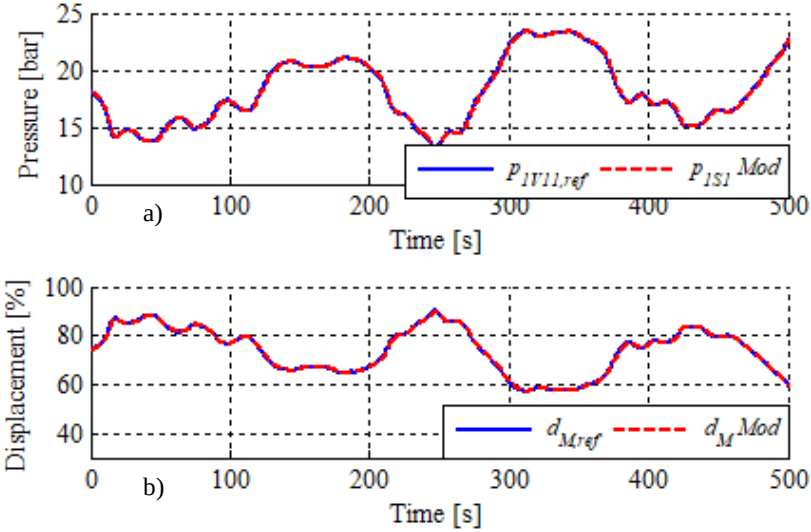

Source: Author.

In this chapter it was demonstrated through experiments and mathematical model simulations the actual system main characteristics and capabilities. These results can know be linked to, and discussed with respect to the theory, modelling and teste bench development explained in previous sections.

7. DISCUSSIONS

7.1 ANALYTICAL MODEL AND ANALYSIS

The system mathematical model, developed in Section 4, linked the rotor aerodynamics field with the system concept and with the hydraulics field. Looking from the perspective of system design, the formulation proposed in that section serves as a basic tool for the system designer. It allows her/him to have early conclusions about what it can be expected from a system in terms of components size, operation range, natural frequency and system open-loop stability. The analysis and mathematical model described in that section can be done in the very beginning of the project development or feasibility assessment.

One of the main achievements with that analysis is the assurance that the proposed system concept has a rated power upper limit. The bigger the rated power bigger are the components size, pipes length and diameter, necessary fluid volume, lower efficiency, the system operates closer to its natural frequency and the closed-loop stability gets worst. Since hydrostatic transmissions commonly operate with 400 bar, to handle the transmitted power, the flow rate is considerably big. With this, the pipes diameters become large in order to keep a low pressure drop along them.

7.2 MATHEMATICAL MODEL FOR NUMERICAL SIMULATION

In Section 5 the system mathematical model for simulation was developed. Based on that and on the test bench, two mathematical models for system simulation were presented.

The main purpose of these models were to describe the system with a certain accuracy such that it would be possible to extract more information from them than what the test bench can provide. Other possible use of the models are to test different control structures, system concepts and other add-on features.

The test bench simulation model showed to be representative after being validated and compared with the experimental data. By analysing the results it was observed that in steady state and dynamic behaviour the model could represent with accuracy the system real behaviour.

One behaviour that was observed at the test bench and not in the simulations is a low frequency oscillation in almost all the measured variables. For example, in the flow rate (Figure 6.14), low pressure line

pressures (Figure 6.13) and rotor speed (Figure 6.10). Two possible sources of such oscillations were observed. The first one is the input torque applied by the electric motor. Oscillations in the measured torque are seen in Figure 6.9c. This would result in a power input that oscillates and therefore all the system variables would have a certain influence from that. Another possible reason, are the grid frequency oscillations. A low frequency oscillation is observed in Figure 6.15a. Despite not being of high amplitude, they result on a generator speed oscillation. These frequency oscillations could be transmitted to the whole system.

It is believed that the model has a few weak points that could be improved. The main weaknesses are the pumps and motor efficiency models. Despite the approach used be sufficient to validate the system and conclude the prove of concept, there is a significant uncertainty in them. If it is possible to have that information, the use of real pumps and motor efficiency maps would increase significantly the model accuracy.

7.3 CONTROL METHOD

Regarding the system control and supervisory controller, it could be seen, through the comparison with a real wind turbine control sequence that the developed system for the bench is close to what a real wind turbine requires. With small modifications in the control structure, the addition of pitch control and clearly the changes in sensors signals, the developed supervisory controller can be applied to a real wind turbine with a hydrostatic transmission to operate automatically according to the wind and the wind farm operator commands.

7.3.1 General comments from observations at the test bench

One issue is how to determine the motor required hydraulic torque to overcome the motor and generator losses in order to maintain the system operating at the synchronous speed while synchronizing it to the grid.

When speed and voltage of the generator are increased, the losses are increased. They must be overcome through an increase in the power extracted from the wind. For that, there are two options, either to wait for an increase in the wind speed, or to increase the power coefficient.

The wind speed is not possible to be controlled. Therefore, the only option is increase the power coefficient if below optimal or to maintain it at a high value if already there. For that, the solution is to operate inside MPT controller while exciting the generator. That would result in having the correct voltage before having the correct speed.

At the same time, there is a strong link between the generator speed and excitation. Two conditions were observed at the test bench: If the power coefficient is low, with the TSR above the ideal, and the generator is excited, it will reduce the rotor speed, since the generator load is increased. To reduce the rotor speed reduces the TSR therefore, increasing the power coefficient, which will increase the power fed into the system. That might over-speed the generator or to work fine and keep everything stable.

If the power coefficient is low with the TSR below the ideal and the generator is excited, it will reduce the rotor speed, since the generator load is increased. To reduce the rotor speed reduces the TSR further, therefore reducing even more the power coefficient, which will reduce the power fed into the system. That will reduce the generator speed. The power coefficient can only be increase back again if the wind speed is reduced or if the generator excitation is removed, which will probably result in a generator over-speed afterwards.

Considering the first condition, once the synchronization process happens, and the circuit breaker is closed, the TSR is above the ideal, the controller is switched back to MPT, this will make it chase the high power coefficient again, increasing the system pressure, this will feed the generator with more power. The grid will hold the generator at the synchronous speed.

Considering that the synchronization occurs, and the TSR is below the ideal, the controller is switched back to MPT, will make it chase the high power coefficient again, decreasing the system pressure, to increase the rotor speed. The decrease of pressure makes the generator to be driven by the grid, on the other hand, the power fed into the system will be increased. The grid will hold the generator at the synchronous speed.

When not synchronized and the generator not excited, the load upon the generator is small, such that small changes in the wind speed result in high changes in generator speed, which makes the system controllability to be a difficult task.

As turbine diameters increase in relation to the lateral and vertical length scales of turbulence, it becomes more difficult to achieve the ideal power coefficient anyway because the non-uniformity of the wind speed over the rotor swept area. Thus, if one part of the blade is at its optimum angle of attack, other parts won't be (BURTON *et al.* (2011)).

The inclusion of a few sensors in the system would give a better understanding of the system. One of them is on measuring the leakage flow rate from the pump and motor. Another one is to measure the pressure at the charging circuit pump outlet.

7.4 SYSTEM CONCEPT

The gearbox is a drawback in the project since one of the objectives of a hydrostatic transmission is to remove it as it is one of the major causes of downtime in wind turbines. On the other hand, it was needed to use the already available PARKER pump.

The power produced by the motor is directly proportional to the pressure drop on it. The higher pressure in the low pressure line decreases the pressure drop over the hydraulic motor resulting in a smaller power generation. This pressure level is maintained by the charging circuit.

The charging system is necessary for the system to run but it works against the system global efficiency since it requires an extra source of power to drive it. The flow that is not supplied to the main circuit pressure is throttled through the valve 1V9, Figure 3.4.

From the natural frequency analysis carried in Section 4 it was observed that the use of the hydrostatic transmission with the generator at the ground is not practical above a certain system nominal output power. For high nominal output powers the rotor excitation frequency becomes closer to the system natural frequency at the synchronization point which is an issue that must be solved. For smaller nominal output powers the fluid volume in the hydrostatic transmissions is smaller and the natural frequency higher (Equation (4.27) and Figure 4.17). The excitation frequency at the synchronization point also becomes higher and more apart from the natural frequency. Therefore, smaller wind turbines with hydrostatic transmission should not have resonance issues at the point of synchronization.

Regarding the hydraulic motor control unit, one possibility is to use a solenoid and hydraulic driven displacement control unit instead of the current hydraulic driven displacement control unit. As a matter of comparison, the rated power consumed by the solution with solenoid, according to the manufacturer, is 130 W while the rated power consumed by the hydraulic solution is 260 W. The usage of half the power makes a difference in the long term cost effectiveness of the turbine. It must be said that the use of a linear variable differential transformer (LVDT) sensor to measure the hydraulic motor displacement setting would make the system control more accurate and less complex.

Regarding the system efficiency, it was noticed that it is smaller for small wind speeds and it is mainly driven by the hydraulic system efficiency. The maximum efficiency achieved was 70.0 % to 80.0 %. This is considerably below the efficiency of mechanical gearboxes or direct coupling. One important thing that must be taken into account is that this

system has no frequency converter between the generator and its connection to the grid. The overall system performance should be compared with the one from a wind turbine with frequency convert.

8. CONCLUSIONS AND FUTURE POSSIBILITIES

"I hope I have helped to raise the profile of science and to show that physics is not a mystery but can be understood by ordinary people." (Stephen Hawking)

"For the first time in history, around 1400, world maps were drawn with blank areas, suggesting that the people from that time were motivated with the question: What lies there, beyond that point, beyond what we know so far? That sort of question pushed the society in to the ages of gran discoveries and later on into science and technology development." (Harari, 2014)

A few objectives were determined for this thesis. The main one was to make a prove of concept of the wind turbine hydrostatic transmission with a direct connection to the grid. Another one was to develop a mathematical model and validate it through experiment, this would serve for future system analysis. A third one was to suggest few changes that could improve the system.

Regarding the main objective, it can be concluded that the system is proved to work. With the test bench it was shown that it is possible to use a hydrostatic transmission to transfer the power from the top of the nacelle to drive a generator at the ground and directly connected to the grid. This process can be achieved while controlling the rotor with the respective turbine operation region objective, that are maximum aerodynamic performance or to limit the rotor speed. It is also concluded that it is possible to use off-the-shelve components, avoiding the development of specific components.

It was necessary to build a state machine to control the test bench in all operation regions. This state machine was built from a state machine of a hydroelectric power plant. After the modifications it showed to be effective and can be seen as a first step into building a state machine for a real wind turbine with a hydrostatic transmission.

Regarding the system control, the proposed strategy included a gain scheduling approach, a rotor speed compensation controller and the use of saturation elements to avoid the use of another controller. The proposed controller is able to control the system. However, other more advanced control techniques could bring a significant increase in the system control performance.

A mathematical system was improved and validated with the test bench measurements. It is believed that this model will serve for future

analysis of this system while operating with other control structures, or the same system structure, but for a different rated power or even to explore different hydraulic system configurations.

Regarding the analytical model, it is seen that with a few basic equations it is straight forward to predict the system behaviour with a certain accuracy. It is also possible to use this analysis to determine the system stability and to explore what are the practical limits of this technology.

At the end, but not least, it is concluded that the proposed wind turbine hydrostatic transmission with direct connection to the grid has limitations with respect to maximum turbine size. The system control is considerably complex. However, there is a significant amount of fields to explore within and around it and this makes room for a huge amount of improvements.

This thesis opened a few possibilities for further research and now serves as a first step to each of these different paths.

As it was shown previously, the system has a low time response and to operate it according to the wind that is passing or passed through the blade looks to be inefficient. With short term wind speed forecast it might be possible to anticipate the turbine control action and to increase power generation. The rotor can speed up or slow down before the coming wind such that in the average a higher power production is achieved. This can be done by feeding the controller with the short term wind forecast and to anticipate the control action on the system pressure (WANG *et al.* (2013)).

Hydraulic systems are known for their power storage capacity. They have high power density while electric systems have a high energy density. The nature of electric power generation is more related to energy density since it has a long time nature. Therefore, an electric energy storage should be more effective to store the surplus electric power production for long term usage. However, for a certain wind turbulence amplitude with the average wind speed at the maximum power limit, the hydraulic system could be effective. If the winds vary around the rated wind speed, it is possible to store and deliver the surplus power several times. Therefore, for those wind conditions it seems to be more effective to recover and deliver the power right away than to aim for long term storage. It also has the capacity to smooth the turbines power output. Those short term cycles of surplus power recover and deliver can be effectively performed with hydraulic accumulators. Such systems are already well studied and applied for hybridization of vehicles. In the wind power field, Dutta *et. al.* (2012) studied such system and found that that can have a gain in total yearly energy production. However, it is not clear in their

study how they accounted the inefficiencies of the recover and storage hydraulic system. At the same time it is believed there are different hydraulic systems that might be more effective. A study in this topic might further increase the potential usage hydraulic drivetrains in wind turbines.

In this thesis a brief introduction was made into the analysis of the system stability through linear state equations. A simplified model for the rotor, transmission and connection to the grid was developed. Its open-loop stability was analysed for specific wind speeds inside the operation region *III*. However, the analysis carried was brief. It remains the task to make an open-loop stability analysis for the whole operation range and for different wind turbine sizes. The linearized model is already developed. The focus of continuing studies could go straight into the analysis. To extend the open-loop analysis by including the controller and its feedback loop, looking into the system closed-loop stability, can bring a significant amount of information to the understanding of such system behaviour and control quality.

As it was mentioned in the discussions chapter, the controllers behaviour are strongly dependent on the system state such that there is the possibility to tune them not for one specific operation point, but optimize them according to the current state of operation, this would result in the best performance throughout the whole wind turbine operation range. This optimization could be applied to define controller gains or to build up an adaptive controller. This can be carried together with the closed-loop stability analysis.

A future work can also be done towards extending the system model for other turbine operation regions. The synchronization is an action performed by both exciting and controlling the speed of the generator. These two actions are not simple to be modelled since they involve the generator excitation and the influence of that in terms of opposing torque over the hydraulic motor. One future study might be the implementation of this phase modelling on the already validated model. This would lead to a model that covers all the operation regions presented in Figure 3.21. The model can be validated using the test bench. Such complete model should be accompanied by a controller that covers the whole turbine operation as well. This controller can be based on the state-machine already developed.

There are two main points that are claimed as advantages of the proposed system with respect to conventional wind turbines.

The first point is the efficiency on power generation with the system directly coupled to the grid. The hydrostatic transmission has a smaller efficiency than the gearboxes or direct coupling shafts. On the

other hand, the hydrostatic transmission solution does not require frequency converter. A study could be carried to compare the efficiencies of the turbine with hydrostatic transmission and no frequency converter, with the turbine with gearbox or direct shaft and frequency converter. The main objective would be to determine if the efficiencies are comparable or how smaller the hydrostatic transmission solution is compared to the conventional solution.

The second point claimed is in the area of maintenance and reliability. It is pointed that the solution using the hydraulic transmission and placing the generator at the ground level brings an operation cost reduction. Mainly because most of the maintenance procedures will occur in ground level and because hydraulic systems tend to be more reliable requiring less maintenance. These statements were not proven yet. A study aiming to compare the maintainability and reliability of the proposed hydrostatic transmission system with a conventional solution could promote the technology even further if those claims are proved.

Another possible future study is to take the validated model, and explore which parts are not contributing for a high system efficiency. That can bring a new perspective of which parts of the system must be improved to become more competitive with respect to the conventional wind turbines.

In Section 4, a theoretical analysis showed that there might be some technical and practical limitations on the maximum rated power that the proposed solution could achieve, for example due to resonant frequencies, range of speeds, size of components, and so on. The volume of fluid, size of hydraulic components, system natural frequency, controllability, overall efficiency and pressure level cannot be changed spontaneously to meet the output power demand. Therefore, a study to identify such limitations could result in a practical maximum rated power that this systems can achieve. To know these practical limits can improve the design process of such systems.

Thinking in the same way as Lord Kelvin did… In future, with the research and inventions to come, this technology can conquer its place in the wind power world.

"The important thing is not to stop questioning. Curiosity has its own reason for existing." (Albert Einstein)

REFERENCES

ALI, M. H. Wind Energy Systems – Solutions for Power Quality and Stabilization. CRC Press. Florida, USA. 2012.

BURTON, T., JENKINS, N., SHARPE, D., BOSSANYI, E. Wind Energy Handbook. 2nd Ed. John Wiley and Sons, Ltd. Chichester, UK. 2011.

CAMBRIDGE DICTIONARY. On-line access. http://dictionary.cambridge.org/dictionary/english/theory. Accessed in: 23rd October 2017.

COSTA K. G., SEPEHRI, N. Hydrostatic Transmissions and Actuators – Operation, Modelling and Applications. 1st Ed. John Wiley & Sons, Ltd. Chichester, UK. 2015.

DIEPEVEEN, N. F. B., LAGUNA, A. J. Dynamic Modelling of Fluid Power Transmissions for Wind Turbines. EWEA OFFSHORE 2011, Part I: Journal of Systems and Control Engineering, v. 224, n. 6; p. 619-621. 2011.

DIEPEVEEN, N., LAGUNA, A. J. Preliminary Design of the Hydraulic Drive Train for a 500kW Prototype Offshore Wind Turbine. Proceedings of the 9th International Fluid Power Conference, Volume 3. IFK2014. Aachen, Germany. 2014.

DIEPVEEN, N. F. B. On the Application of Fluid Power Transmission in Offshore Wind Turbines. PhD Thesis. Delft University of Delft. Delft, Netherlands, 2013.

DOLAN, D. S. L., LEHN, P. W. Simulation Model of Wind Turbine 3p Torque Oscillations due to Wind Shear and Tower Shadow. IEEE Transactions on Energy Conversion, Vol. 21 No. 3, September 2006.

DOLAN, B., ASCHEMANN, H. Control of a Wind Turbine with a Hydrostatic Transmission – an Extended Linearisation Approach. 17th International Conference on Methods and Models in Automation and Robotics. Poland, 2012.

DUTTA, R., WANG, F., BOHLMANN, B., STELSON, K. Analysis of Short-Term Energy Storage for Mind-Size Hydrostatic Wind Turbine.

FLESCH, E. A. Projeto de Transmissão Hidrostática para Aerogeradores de Eixo Horizontal. Master Thesis. Mechanical Engineering Department, Federal University of Santa Catarina. Florianópolis, Brazil, 2012.

GONZALEZ, F. E. Estudo de Forças Atuantes em Mecanismos de Regulação de ângulo de Passo e Desenvolvimento de um Sistema Emulador de Cargas. Master Thesis. Mechanical Engineering Department, Federal University of Santa Catarina. Florianópolis, Brazil, 2012.

HARARI, Y. N., Sapiens – A Brief History of Humankind. Vintage Books. London, 2014. ISBN 9780099590088.

HAU, E. Wind Turbines – Fundamentals, Technologies, Application, Economics. 2nd Edition. Springer-Verlag. Germay. 2006.

KUNDUR, P. Power System Stability and Control. McGraw-Hill, Inc. New York. 1994.

LAGUNA, A. J., DIEPEVEEN, N. F. B. Dynamic Analysis of Fluid Power Drive-trains for Variable Speed Wind Turbines: a Parameter Study. EWEA OFFSHORE 2011, Part I: Journal of Systems and Control Engineering, v. 224, n. 6; p. 619-621. 2011.

LAGUNA, A. J., DIEPEVEEN, N. F. B., VAN WINGERDEN, J. W. Analysis of Dynamics of Fluid Power Drive-trains for Variable Speed Wind Turbines: a Parameter Study, IET Renewable Power Generation, Vol. 8, Issue: 4, pp. 398-410, May 2014.

LAGUNA, J. PhD. Centralized electricity generation in offshore wind farms using hydraulic networks.

LIN, Y., TU, L., LIU, H., LI, WEI. Hybrid Power Transmission Technology in a Wind Turbine Generation System. IEE/ASME Transactions on Mechatronics. 2014.

MANNESMANN Rexroth . Proyecto y construcción de equipos hidráulicos: training hidráulico, compendio 3. São Paulo: Mannesmann Rexroth GmbH. 1988.

MASASHI, S., ATSUSHI, Y., TOSHIKAZU, H., HIROSHI, N., MICHIYA, U., TOSHIHIDE, N. Large Capacity Hydrostatic Transmission With Variable Displacement. The 9th International Fluid Power Conference, 9, IFK. Aachen, Germany. 2014.

MUYEEN, S. M., AL-DURRA, A., HASANIEN, H. M. Modeling and Control Aspects of Wind Power Systems. InTech. Croatia. 2013.

NEELAMKAVIL, F. Computer Simulation and Modelling. John Willey & Sons. New York. 1987.

PEDERSEN, N. H., JOHANSEN, P., ANDERSEN, T. O. LQR Feedback Control Development for Wind Turbines Featuring a Digital Fluid Power

Transmission System. Proceedings of the 9th Ph.D. Symposium on Fluid Power, FPNI2016, Florianópolis Brazil, October 26-28, 2016.

RADUENZ, H. Desenvolvimento de Protótipo de Transmissão Hidrostática para Aerogeradores. Course Woke. Mechanical Engineering Department, Federal University of Santa Catarina, Florianópolis, Brazil. 2015.

RAJABHANDHARAKS, D. Control of Hydrostatic Transmission Wind Turbine. Master's Theses, Department of Electrical Engineering, San Jose State University, San Jose, USA, December 2014.

RAMPEN, W. Gearless Transmission for Large Wind Turbines – The History and Future of Hydraulic Drives. Artemis IP Ltd. Scotland, 2006.

RAPP, J., TURESSON, J. Hydrostatic Transmission in Wind Turbines: Development of Test Platform. Master Thesis. Department of Management and Engineering. Linkoping University. 2015.

SCHMITZ, J., VATHEUER, N., MURRENHOFF, H. Development of a Hydrostatic Transmission for Wind Turbines, 7th International Fluid Power Conference, Aachen, Germany, 2010.

SCHMITZ, J., VATHEUER, N., MURRENHOFF, H. Dynamic Analysis and Measurement of a Hydrostatic Transmission for Wind Turbines, 8th International Fluid Power Conference, Dresden, Germany, 2012.

SCHMITZ, J., VUKOVIC, N., MURRENHOFF, H. Hydrostatic Transmission for Wind Turbines – an Old Concept, New Dynamics, Proceedings of the ASME/BATH 2013 Symposium on Fluid Power & Motion Control, FPMC2013. Sarasota, USA, October 2013.

SCHULTE, H., GEORG, S. Nonlinear Control of Wind Turbines with Hydrostatic Transmission Based on Takagi-Sugeno Model. Journal of Physics: Conference Series, Vol. 524, June 2014.

SHEPHERD, W., Zhang, Li. Electricity Generation Using Wind Power. World Scientific Publishing Co. Pte. Ltd. Singapore, 2011.

THUL, B., DUTTA, R., STELSON. K. A. Hydrostatic Transmission for Mid-Size Wind Turbines. 52nd National Conference on Fluid Power, Las Vegas, USA, 2011.

VATHEUER, N., SCHMITZ, J., MURRENHOFF, H. Efficient Hydrostatic Heavy-Duty Drive Train in Renewable Energy Branch, Proceedings of the Twelfth Scandinavian International Conference on Fluid Power: SICFP11, Tampere, Finland, May 2011.

VARPE, S. A. Control system on a wind turbine, 2008.

VIANNA JR, W. Velocidades Ideais de Escoamento de Fluido Hidráulico em Tubulações e Dutos de Manifolds. Presentation held at the FORUM MDA – Motion, Drive & Automation. March 2013.

WATTON, J. Modelling, Monitoring and Diagnostic Techniques for Fluid Power Systems, Springer-Verlag, London, 2007.

WANG, F., STELSON, K. A., Model Predictive Control for Power Optimization in a Hydrostatic Wind Turbine, The 13th Scandinavian International Conference on Fluid Power, SICFP2013, Linköping, Sweden, June 2013.

WIND ENERGY – THE FACTS. 2009. <https://www.wind-energy-the-facts.org/hub-height.html>. Accessed in: 16th January 2018.

APPENDIX A – Open-loop system stability – derivation of the state equations and representation in matrix format

"Truth is ever to be found in simplicity, and not in the multiplicity and confusion of things" (Isaac Newton)

This appendix is devoted to presented the derivation of the simplified system state equations to perform the open-loop system stability analysis made in Section 4.7.

The derivation is performed for the system without gearbox. The system being modelled is the one presented in Figure A.1.1.

Figure A.1.1 – System diagram for open-loop stability analysis.

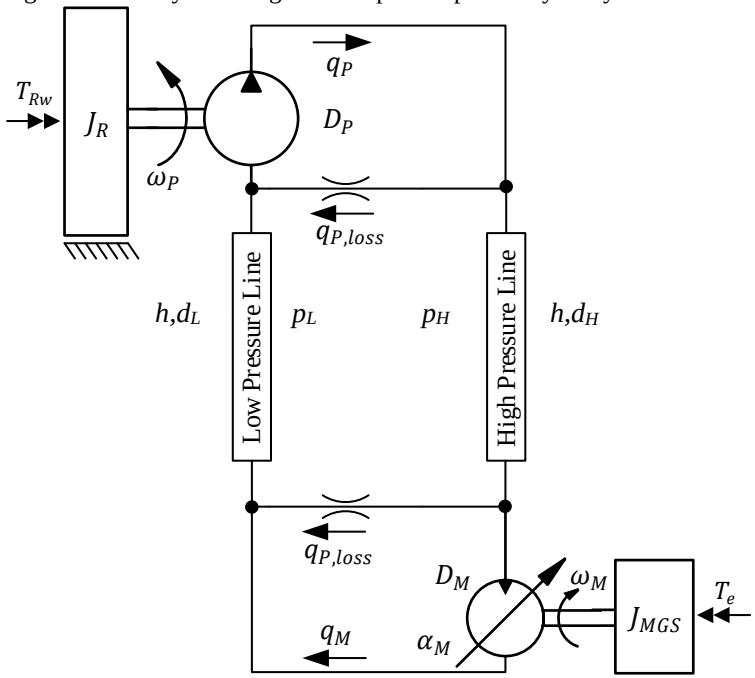

Source: Author.

Looking to the system it is seen that there are four states. They are: rotor/pump speed, pressure in the low pressure line, pressure in the high pressure line and hydraulic motor/generator speed. The state equations that describe them are written in the sequence,

$$q_P - q_M - q_{P,loss} - q_{M,loss} = \frac{dV_H}{dt} + \frac{V_H}{\beta_e}\left(\frac{dp_H}{dt}\right), \quad \text{(A.1)}$$

$$q_M + q_{M,loss} + q_{P,loss} - q_P = \frac{dV_L}{dt} + \frac{V_L}{\beta_e}\left(\frac{dp_L}{dt}\right), \quad \text{(A.2)}$$

$$T_{Rw} - T_{Pt} - T_{RP,loss} = \frac{J_R d\omega_R}{dt}, \quad \text{(A.3)}$$

$$T_M - T_e = J_{MGS}\frac{d\omega_M}{dt}. \quad \text{(A.4)}$$

Equations (A.1) and (A.2) are the hydraulic lines continuity equations and (A.3) and (A.4) the rotor/pump and generator/motor equations of motion.

The first assumption made is that the hydraulic line volumes are rigid. So the derivatives of the volumes with respect to time are zero. Other assumptions on this model are that there is no external leakage, pump and motor internal leakage coefficients are equal, the pump and rotor mechanical losses are summed and the hydraulic motor and generator mechanical losses are summed inside the opposing electric torque T_e.

The following equations are steady state equations that describe a few of the terms of equations (A.1) to (A.4). These equations might have appeared before in the text, but are brought again,

$$q_P = D_P\omega_R, \quad \text{(A.5)}$$

$$q_{P,loss} = q_{M,loss} = c_{vi}(p_H - p_L), \quad \text{(A.6)}$$

$$q_M = D_M\alpha_M\omega_M, \quad \text{(A.7)}$$

$$T_{Rw} = \frac{1}{2}\rho A c_p\left(\frac{v^3}{\omega_R}\right), \quad \text{(A.8)}$$

$$T_{Pt} = D_P(p_H - p_L), \quad \text{(A.9)}$$

$$T_{RP,loss} = c_R\omega_R, \quad \text{(A.10)}$$

$$T_M = D_M\alpha_M(p_H - p_L). \quad \text{(A.11)}$$

Substituting equations (A.5) to (A.11) into equations (A.1) to (A.4) and transforming the states p_H and p_L into one state only $\Delta p = (p_H - p_L)$,

$$\left(\frac{dp_H}{dt} - \frac{dp_L}{dt}\right) = \frac{d\Delta p}{dt} = \beta_e \left(\frac{1}{V_H} + \frac{1}{V_L}\right)(D_P\omega_R - D_M\alpha_M\omega_M - 2c_{vi}\Delta p), \tag{A.12}$$

$$\frac{d\omega_R}{dt} = \frac{\frac{1}{2}\rho A c_p\left(\frac{v^3}{\omega_R}\right) - D_P\Delta p - B_{RP}\omega_R}{J_R}, \tag{A.13}$$

$$\frac{d\omega_M}{dt} = \frac{D_M\alpha_M\Delta p - T_e}{J_{MGS}}. \tag{A.14}$$

Looking to equations (A.12) to (A.14) it is seen that there are three states (Δp, ω_P, ω_M) and three inputs (v, α_M, T_e). At the same time there are three non-linear terms that prevent to make a simple analysis using the state space representation form.

Before applying a linearization technique, it is necessary to return to equations (A.1) to (A.4) and substitute the non-linear terms there by their deviation with respect to an operation point (*op*), resulting in,

$$\left(q_P - q_{P,op}\right) - (q_M - q_{M,op}) - (q_{P,loss} - q_{P,loss,op}) - (q_{M,loss} - q_{M,loss,op}) = \frac{V_H}{\beta_e}\left(\frac{d(p_H - p_{H,op})}{dt}\right), \tag{A.15}$$

$$(q_M - q_{M,op}) + (q_{P,loss} - q_{P,loss,op}) + (q_{M,loss} - q_{M,loss,op}) - \left(q_P - q_{P,op}\right) = \frac{dV_L}{dt} + \frac{V_L}{\beta_e}\left(\frac{d(p_L - p_{L,op}}{dt}\right), \tag{A.16}$$

$$\left(T_{Rw} - T_{Rw,op}\right) - \left(T_{Pt} - T_{Pt,op}\right) - \left(T_{RP,loss} - T_{RP,loss,op}\right) = J_R\frac{d\left(\omega_R - \omega_{R,op}\right)}{dt}, \tag{A.17}$$

$$\left(T_M - T_{M,op}\right) - \left(T_e - T_{e,op}\right) = J_{MGS}\frac{d\left(\omega_M - \omega_{M,op}\right)}{dt}. \tag{A.18}$$

Now adding equations (A.15) and (A.16) as before and also applying equations (A.5) and (A.11) into equations (A.15) to (A.18) results in the state equations with respect to an operation point. Since the

operational point is in equilibrium/steady state, it doesn't add any dynamics or constant value to the state equations.

$$\frac{d(\Delta p - \Delta p_{op})}{dt} = \beta'\big(D_P\big(\omega_R - \omega_{R,op}\big) - (D_M\alpha_M\omega_M - D_M\alpha_{M,op}\omega_{M,op}) - 2c_{vi}(\Delta p - \Delta p_{op}\big) \tag{A.19}$$

$$\frac{d(\omega_R - \omega_{R,op})}{dt} = \frac{1}{J_R}\left(\left(K_R\left(\frac{v^3}{\omega_R}\right) - K_R\left(\frac{v_{op}^3}{\omega_{R,op}}\right)\right) - D_P\big(\Delta p - \Delta p_{op}\big) - B_{RP}\big(\omega_R - \omega_{R,op}\big)\right) \tag{A.20}$$

$$\frac{d(\omega_M - \omega_{M,op})}{dt} = \frac{(D_M\alpha_M\Delta p - D_M\alpha_{M,op}\Delta p_{op}) - (T_e - T_{e,op})}{J_{MGS}} \tag{A.21}$$

$$K_R = \tfrac{1}{2}\rho A_R c_p \qquad \beta' = \beta_e\left(\tfrac{1}{V_H} + \tfrac{1}{V_L}\right) \tag{A.22}$$

In Equation (A.19) the second term of the right side is the hydraulic motor flow rate deviation. In Equation (A.21) the first term on the right side is the rotor torque deviation. In Equation (A.21) the first term on the right side is the hydraulic motor torque deviation. The non-linear terms are still present in equations (A.19) to (A.21).

These non-linear terms are linearized using a Taylor series truncated in the first-order term. The linearized terms are shown in the sequence,

$$D_M\alpha_M\omega_M \cong D_M\alpha_{M,op}\omega_{M,op} + D_M\omega_{M,op}(\alpha_M - \alpha_{M,op}) + D_M\alpha_{M,op}(\omega_M - \omega_{M,op}), \tag{A.23}$$

$$K_R\left(\frac{v^3}{\omega_R}\right) \cong K_R\left(\frac{v_{op}^3}{\omega_{R,op}}\right) + 3K_R\left(\frac{v_{op}^2}{\omega_{R,op}}\right)(v - v_{op}) - K_R\left(\frac{v_{op}^3}{\omega_{R,op}^2}\right)(\omega_R - \omega_{R,op}), \tag{A.24}$$

$$D_M\alpha_M\Delta p \cong D_M\alpha_{M,op}\Delta p_{op} + D_M\alpha_{M,op}(\Delta p - \Delta p_{op}) + D_M\Delta p_{op}(\alpha_M - \alpha_{M,op}). \tag{A.25}$$

Substituting equations (A.23) to (A.25) into equations (A.19) to (A.21) results in,

$$\frac{d(\Delta\Delta p)}{dt} = \beta'\big(D_P(\Delta\omega_R) - 2c_{vi}(\Delta\Delta p) - (D_M\alpha_{M,op}\Delta\omega_M) - (D_M\omega_{M,op}\Delta\alpha_M)\big), \tag{A.26}$$

$$\frac{d(\Delta\omega_R)}{dt} = \frac{1}{J_R}\left(-\left(K_R\left(\frac{v_{op}^3}{\omega_{R,op}^2}\right) + B_{RP}\right)\Delta\omega_R - D_P(\Delta\Delta p) + 3K_R\left(\frac{v_{op}^2}{\omega_{R,op}}\right)(\Delta v)\right), \tag{A.27}$$

$$\frac{d(\Delta\omega_M)}{dt} = \frac{(D_M\alpha_{M,op}\Delta\Delta p + D_M\Delta p_{op}\Delta\alpha_M) - \Delta T_e}{J_{MGS}}, \tag{A.28}$$

where,

$$\Delta\omega_R = \omega_R - \omega_{R,op}, \tag{A.29}$$

$$\Delta\Delta p = \Delta p - \Delta p_{op}, \tag{A.30}$$

$$\Delta\omega_M = \omega_M - \omega_{M,op}, \tag{A.31}$$

$$\Delta T_e = T_e - T_{e,op}, \tag{A.32}$$

$$\Delta v = \Delta v - \Delta v_{op}, \tag{A.33}$$

$$\Delta\alpha_M = \alpha_M - \alpha_{M,op}. \tag{A.34}$$

For a synchronous generator connected to an infinite busbar, Flesch (2012) describes the generator electric torque (T_e) as a function of the generator rotor torque angle (δ). It is the angle between the generator

stator electromagnetic field and the generator's rotor electromagnetic field. Both the fields are rotating with the synchronous speed (ω_{Mn}), but with a phase difference (δ).

If $\delta < 0$ it means that the grid is supplying power/driving the generator. If $\delta > 0$ the generator is supplying power/driving the grid. (HAU, 2006).

However, the grid is considered infinite. Therefore, the generator cannot influence on the grid frequency or voltage. Which means that the in steady state the generator always operates at the synchronous speed. So the generator speed at any operation point is equal to the synchronous speed ($\omega_{Mop} = \omega_{Mn}$). However, during transients the coupling between the grid and generator has a dynamics involved.

Starting from one operation point, when the mechanical torque changes from $T_{M,op}$ to T_M it will make the generator produce and opposing torque change from $T_{e,op}$ to T_e. The change of the electric torque can be described as an oscillator by,

$$T_e - T_{e,op} = K_S(\Delta\delta) + K_A \frac{d(\Delta\delta)}{dt}, \tag{A.35}$$

where, $\Delta\delta = \delta - \delta_{op}$, K_S the synchronization torque coefficient and K_A the damping coefficient.

The interpretation of equation (A.35) is as follows: due to the change in the generator mechanical torque input from $T_{M,op}$ to T_M, there will be a change in the torque angle from δ_o to δ, which causes a change in the electric torque from $T_{e,op}$ to T_e.

The variation of the torque angle, while in the transient after the mechanical torque change, can be described by the change in the generator rotor speed with respect to the operation point value. This is true because δ is rotating at the synchronous speed ($\omega_{M,n}$), with respect to the same fixed referential.

$$\frac{d(\Delta\delta)}{dt} = \frac{d\left(\delta - \delta_{op}\right)}{dt} = \frac{d\delta}{dt} = \omega_M - \omega_{M,n} \tag{A.36}$$

Equation (A.36) is a state equation that describes the variation of the torque angle change with respect to the generator rotor speed.

Equations (A.26) to (A.28) and (A.36) are the linearized system state equations that describes the system behaviour near the operation point. They represent a deviation from the equilibrium point. Their general representation in state space form is given by,

$$\begin{aligned} \Delta\dot{x} &= A\Delta x + B\Delta u, \\ \Delta y &= C\Delta x + D\Delta u. \end{aligned} \tag{A.37}$$

The states, inputs and outputs are shown in the sequence,

$$\begin{aligned} \Delta\dot{x} &= \begin{bmatrix} \Delta\dot{\omega}_R \\ \Delta\dot{\Delta}p \\ \Delta\dot{\omega}_M \\ \Delta\dot{\delta} \end{bmatrix}, \\ \Delta x = \begin{bmatrix} \Delta\omega_P \\ \Delta\Delta p \\ \Delta\omega_M \\ \Delta\delta \end{bmatrix} &= \begin{bmatrix} \omega_P - \omega_{P,op} \\ \Delta p - \Delta p_{op} \\ \omega_M - \omega_{M,op} \\ \delta - \delta_{op} \end{bmatrix}, \\ \Delta u = \begin{bmatrix} \Delta v \\ \Delta\alpha_M \\ 0 \\ 0 \end{bmatrix} &= \begin{bmatrix} v - v_{op} \\ \alpha_M - \alpha_{M,op} \\ 0 \\ 0 \end{bmatrix}, \\ \Delta y &= \Delta x. \end{aligned} \tag{A.38}$$

The matrixes A, B are shown in the sequence.

$$A = \begin{bmatrix} A_{11} & A_{12} & 0 & 0 \\ A_{21} & A_{22} & 0 & 0 \\ 0 & A_{23} & A_{33} & A_{34} \\ 0 & 0 & 1 & 0 \end{bmatrix}, \tag{A.39}$$

$$B = \begin{bmatrix} B_{11} & 0 & 0 & 0 \\ 0 & B_{22} & 0 & 0 \\ 0 & B_{23} & 0 & 0 \\ 0 & 0 & 0 & 0 \end{bmatrix}, \tag{A.40}$$

where the A and B matrixes coefficients are,

$$A_{11} = -\frac{1}{J_R}\left(\frac{1}{2}\rho A_R c_p \left(\frac{v_{op}^3}{\omega_{R,op}}\right) + B_{RP}\right), \quad \text{(A.41)}$$

$$A_{12} = -\frac{D_P}{J_R}, \quad \text{(A.42)}$$

$$A_{21} = D_P\beta(\tfrac{1}{V_H} + \tfrac{1}{V_L}), \quad \text{(A.43)}$$

$$A_{22} = -2c_{vi}\beta\left(\frac{1}{V_H} + \frac{1}{V_L}\right), \quad \text{(A.44)}$$

$$A_{23} = -D_M\alpha_{M,op}\beta\left(\frac{1}{V_H} + \frac{1}{V_L}\right), \quad \text{(A.45)}$$

$$A_{32} = \frac{D_M\alpha_{M,op}}{J_{MGS}}, \quad \text{(A.46)}$$

$$A_{33} = -\frac{K_A}{J_{MGS}}, \quad \text{(A.47)}$$

$$A_{34} = -\frac{K_S}{J_{MGS}}, \quad \text{(A.48)}$$

$$A_{43} = 1 \quad \text{(A.49)}$$

$$B_{11} = \frac{1}{J_R}\left(\frac{3\rho A_R c_P v_{op}^2}{2\omega_{R,op}}\right), \quad \text{(A.50)}$$

$$B_{22} = -D_M\alpha_{M,op}\omega_{M,op}\beta\left(\frac{1}{V_H} + \frac{1}{V_L}\right), \quad \text{(A.51)}$$

$$B_{32} = \frac{D_M\Delta p_{op}}{J_{MGS}}. \quad \text{(A.52)}$$

APPENDIX B – Switching controllers between turbines operation region

In this appendix the rules for witching controllers between operation regions are explained.

B.1. Start-up

The start-up phase comprehends the wind speed range from 0 to *b*. The objective is to extract as much power from the wind as possible to overcome the system losses and bring the generator to near its nominal speed.

In this region the generator is disconnected from the grid and there is no controlled electric torque opposing its rotation. It operates as a flywheel and accelerates accordingly to the torque balance between the applied motor hydraulic torque, friction and induced magnetic torques.

Knowing this, the first switching rule is set.

1st Rule: *If the wind speed is below b and the generator speed is below 98.0 % of its nominal speed, the MPT controller is active.*

The generator must be close to its nominal speed before changing to the synchronization controller. That is the reason to have a rule also based on the generator speed.

The MPT controller will ensure that the rotor is always operating with high aerodynamic efficiency, even for such low wind speeds.

When wind speed *b'* is reached it is possible to start the synchronization of the generator with the grid. The controllers are switched and the system is controlled in order to achieve the synchronization.

The opposite of the first rule is the switch command for the synchronization controller SYNC: *If the wind speed is above b and the generator speed is above 98.0 % of its nominal speed, MPT controller is deactivated and the SYNC controller is activated.*

B.2. Synchronization

When operating at low rotational speeds, is mostly the partial load efficiency of the hydraulic drives which may determine the cut-in wind speed (LAGUNA *et al.*, 2011). The cut-in speed is when it is possible to deliver power to the grid. The cut-in speed was first determined through simulations by estimating system losses.

The wind speed region where the synchronization occurs is for wind speeds higher than *b* and up to *b'*, which is the cut-in speed. When the SYNC controller is operating it controls the generator speed to its nominal value, which is also the nominal frequency.

This process of bringing the generator to its nominal speed can occur at wind speed *b*. However, to achieve the nominal voltage the generator must be excited, and that imposes a higher electrical load on the generator. It is necessary to have more power to enable the generator excitation. More power enters the system with a higher wind speed. The wind speed where the generator can be excited is *b'*, the cut-in speed.

When conditions of frequency, voltage are within the range of 0.5 % of their nominal value, the automatic synchronizer is enabled. It will compare the generated voltage amplitude, frequency and phase with the grid voltage amplitude, frequency and phase. Based on the difference between them it sends control commands to force the generated voltage amplitude, frequency and/or phase to match the grid. Once that happen, it sends the command to close the circuit breaker (52) that connects the generator and the grid. After closed, it remains for 5 seconds in the SYNC controller. Afterwards, it switches back to the MPT controller. The second rule for switching is defined.

2nd Rule: *If the wind speed is above b' and after 5 seconds of the circuit breaker (52) being closed, the MPT controller is activated.*

During the SYNC controller operation the rotor rotational speed is no longer controlled. This is because the motor displacement that was used to control the rotor speed is than being used to control the generator speed. The power coefficient is not at its maximum value.

Once the circuit breaker is closed the system can start to deliver power to the grid.

B.3. Power Delivery

As it was mentioned, during the SYNC the power coefficient is not at its maximum. When the circuit breaker is closed there is no power deliver to the grid, it is a called a zero load point. When the controller is switched back to the MPT controller it will control the rotor speed again in order to achieve the maximum power coefficient. Therefore, even for the same wind speed, *b'*, there will be an increase in the generated power because the power coefficient increases. Since the generator is directly connected to the grid its speed is kept constant.

The maximum power tracking method is used throughout the entire operation region *III*, from wind speed *b'* to *c*, when the rotor nominal speed ($\omega_{R,n}$) is reached. From this wind speed and upwards the speed limitation explained in Section 3.4.2.2 assumes the system control and keeps the rotor speed constant up to wind speed *d*.

B.4. Return to stand-by position

If the wind speed decreases too much or if the user wants to stop the system, the backwards process must be performed.

Considering that the turbine was operating in region *IV*, if the wind speed decreases below *d*, the saturation element will no longer limit the rotor speed compensation such that the MPT controller returns to control the rotor speed at its optimal value.

When the wind speed drops below *b'*, there will be no capacity to deliver power to the grid, the generator will pass the zero load point, and starts to be driven by grid. At the zero load point the circuit breaker (52) must be opened and the controller must be switched back to the SYNC controller. Than, the third control switching rule is written.

3rd Rule: *If the system is connected to the grid (closed 52), the wind speed drops below b' and the system is close to the zero load point, the SYNC controller is activated.*

When the SYNC controller is active the circuit breaker opens and the generator is disconnected from the grid. However, the generator is still excited and running at its nominal value. The process of opening the circuit breaker is called desynchronization.

If the wind speed further decreases, the generator excitation must be removed. This process tends to speed up the generator since the load is removed from it. Hau (2006), says that a sudden load disconnection, for example due to failure of the grid or an electrical fault, is always a critical moment for a wind turbine. The loss of the generator torque requires immediate action from the rotor brakes system in order to avoid the rotor from "running away". In the hydrostatic transmission it resumes to the fast action of the SYNC controller to avoid the generator and rotor "running away".

What would be the fourth rule refers to the switching from the SYNC back to the MPT controller when the wind speed and generator speed drops below b. This is the first rule, but for a decreasing wind speed.

APPENDIX C - Resume of the model main parameters

Figure B.1.1 - Mathematical model overview.

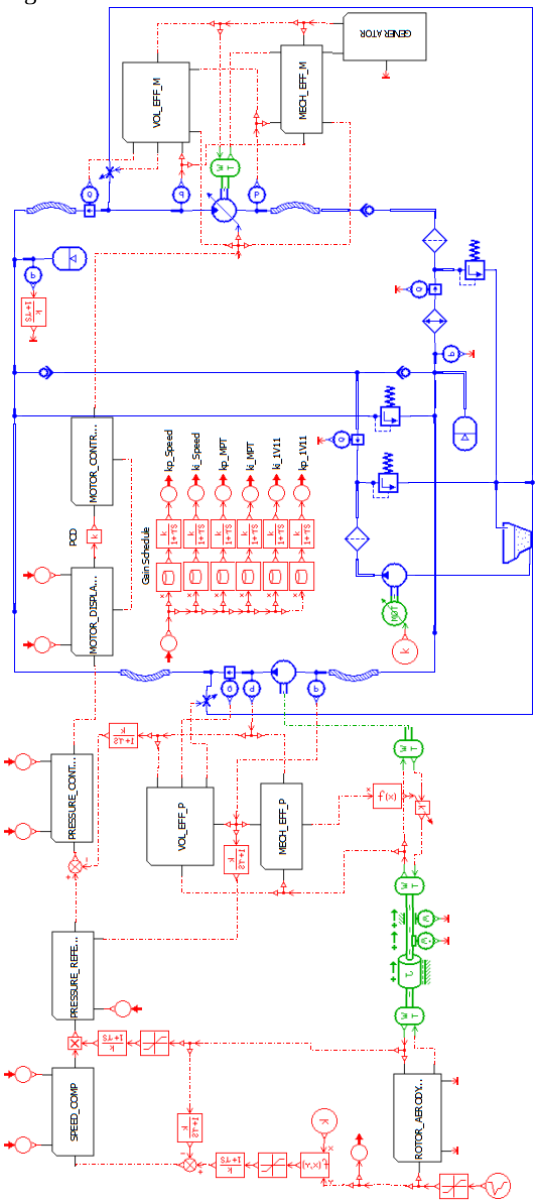

Source: Author.

Figure B.1.2 shows the numerical model block diagram for the generator connection with the grid.

Figure B.1.2 - Generator model block diagram.

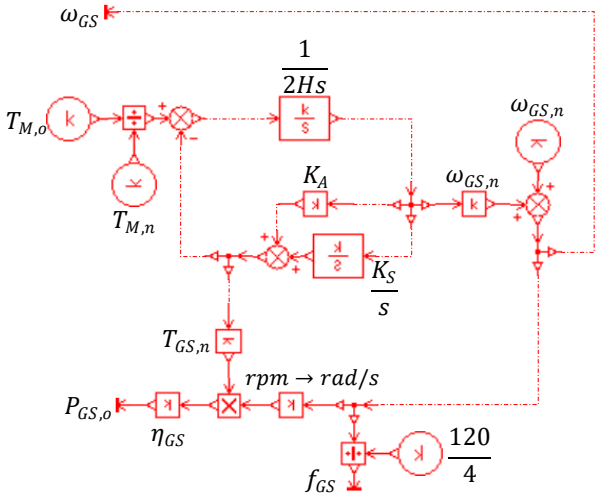

Source: Author.

Table B.1 - Model main parameters

Component	Specification
Rotor mass moment of Inertia	AMESIM submodel code: RL04 Moment of Inertia: 3650 kgm² Coefficient of viscous friction: 0.025 Nm/rpm Coulomb friction torque: 1.0 Nm Stiction torque: 1.5 Nm
High Pressure Line	AMESIM submodel code: HL040 Diameter: 24 mm Length: 8 m Number of internal nodes: 5 Number of states for f.d.f.: 2
Low Pressure Line	AMESIM submodel code: HL042 Diameter: 22.6 mm Length: 8 m Number of internal nodes: 5 Number of states for f.d.f.: 2
Accumulator - 0A2	AMESIM submodel code: HL000 Gas precharge pressure: 3.0 bar

	Accumulator Volume: 9.47 L
Accumulator - 0A1	AMESIM submodel code: HL000 Gas precharge pressure: 30.0 bar Accumulator Volume: 1.9 L
Heat Excahnger	AMESIM submodel code: OR0000 Characteristic flow rate: 113.6 L/min Corresponding pressure drop: 2.5 bar
Low pressure line filter – 0F1	AMESIM submodel code: OR0000 Characteristic flow rate: 108.0 L/min Corresponding pressure drop: 0.69 bar
Charging circuit filter – 0F2	AMESIM submodel code: OR0000 Characteristic flow rate: 8.0 L/min Corresponding pressure drop: 0.15 bar
Check Valve – 1V1, 1V2	AMESIM submodel code: CV000
	Cracking pressure: 0.3 bar
	Flow rate pressure gradient: 20.63 L/min/bar
Check Valve – 1V15	AMESIM submodel code: CV000
	Cracking pressure: 0.4 bar
	Flow rate pressure gradient: 59.14 L/min/bar
Relief Valve – 1V7	AMESIM submodel code: RV000 Cracking pressure: 5.3 bar Flow rate pressure gradient: 2.17 L/min/bar
Relief Valve – 1V9	AMESIM submodel code: RV000
	Cracking pressure: 5.6 bar
	Flow rate pressure gradient: 1.2 L/min/bar
Relief Valve – 1V5	AMESIM submodel code: RV000 Cracking pressure: 220.0 bar Flow rate pressure gradient: 10.0 L/min/bar

APPENDIX D – Hydraulic components list

Table D.1 - Hydraulic components list.

Component	Specification
Fixed displacement Inline piston pump – 0P1	PD075PS02SRU5AL00S0000000 Volumetric displacement: 75 cm³/rev Speed range: 600 – 2500 rpm Maximum pressure: 280 bar
Variable displacement piston motor – 0M1	V12060MUSVS000D0060/012HPS01I010/025 Volumetric displacement: 60 cm³/rev Speed range: 50 - 4100 rpm Maximum pressure: 420 bar
Double fixed gear pump – 0P2 and 0P3	Volumetric displacement: 8 and 4 cm³/rev Speed range: 1130 rpm Maximum pressure: 250bar
Piston accumulator – 0A1	A4N-0116D1K Maximum pressure: 207 bar Pre-charge pressure: 60 bar Volume: 1.9 L
Acc. Safety Block	0A1 - 2V4 - SBAT20M1T-250-TA1
Control Flow Valve	NVH101K Nominal Flow Rate: 60 L/min Maximum inlet pressure: 350bar
Pilot Operated Relief Valve	RAH101K50-6B Nominal Flow Rate: 113 L/min Maximum inlet pressure: 350 bar
Piston accumulator – 0A2	A4K-0578D1K Maximum pressure: 20 bar Pre-charge pressure: 3 bar Volume: 9.47 L
Acc. Safety Block	0A2 - 2V3 - SBAT20M1T-050-TA1
Control Flow Valve	NVH101K Nominal Flow Rate: 60 L/min Maximum inlet pressure: 350bar
Direct Acting Relief Valve	RD102S30 Nominal Flow Rate: 38 l/min Maximum inlet pressure: 250 bar
Pilot Operated Relief Valve - 1V5, 1V6	RAH101K50-12T Maximum pressure: 350 bar Nominal flow rate fully open: 190 L/min

Pilot Operated Relief Valve - 1V7, 1V10	RAH101K10-12T Cracking pressure: 15 bar Nominal flow rate fully open: 190 L/min
Direct Acting Relief valve - 1V8	RD102S30 Maximum inlet pressure: 250 bar Nominal Flow Rate: 38 L/min
Direct Acting Relief valve – 1V9	A02B2FW-N-6B Cracking pressure: 5 bar Nominal flow rate fully open: 30 L/min
Check valve - 1V4, 1V3	CVH103P20-6B Cracking pressure: 1.4 bar Nominal flow rate fully open: 38 L/min
Check valve - 1V1, 1V2	CVH081P-6B Cracking pressure: 0.3 bar Nominal flow rate fully open: 38 L/min
Ball valve	1V12 - KH3/4X
Ball valve	2V1, 2V2 - KH1X
Filter – 0F1	FP40-010FV-10B-LN3 Maximum pressure: 320 bar Maximum flow rate: 120 L/min
Filter - 0F2	FP10-010FV-10B-LV3 Maximum pressure: 320bar Maximum flow rate: 120 L/min
Tank Air Filter - 0F3	FR16010
Heat exchanger – 0HE1	LDC-011-A-000SB (12V) Maximum flow rate: 120 L/min Maximum pressure: 20 bar
Proportional Pressure relief valve - 1V11	RE06M10W2V1XW Maximum pressure 105 bar Rated flow rate 3 L/min
Control flow valve - 1V13	9F1200S rated flow rate: 95 L/min Maximum pressure: 240 bar
Two-way normally open poppet valve - 1V14	DSH161NRE_SPA240C Maximum Pressure: 350 bar Nominal flow rate: 150 L/min
Check valve - 1V15	9C2000S Cracking pressure: 0.4 bar Maximum pressure: 345 bar Rated flow rate: 265 L/min

APPENDIX E – Electric components list

Table E.1 - Electric components list

Component	Specification
Electric motor – 0ME1	Power: 75cv – 55.2kW Rated speed: 1800 rpm Power supply: 380V Rated current: 98A
Frequency converter - 0FE1	WEG - BRCFW110105T4SZ Power: 75cv Power supply: 380V Rated current: 98A
Electric motor - 0ME2	Power: 0.75cv Rated speed: 1130 rpm Power supply: 220/380V Rated current: 3.08A/1.78A
Soft-starter - 0SS1	WEG SSW - 04.30/220-440 Power supply: 220/440V Output voltage: 220/440V Rated output current: 30A Electronics data: 90-250V AC 50-60Hz
Heat exchanger motor - 0ME3	SPAL VA34AP70/LL 36a 12V Power supply: 12V CC Current: 15.6 – 21.4A Rated power(maximum): 264W
Synchronous generator - 0GS1	WEG GTA162AI32 Power: 38kVA – 30.4kW (power factor 0.8) Rated speed: 1800 rpm Poles: 4 Frequency: 60Hz Voltage: 380V
Electronic Module for 1V11 valve	PARKER PCD 00A-400 Supply voltage: 18 - 30V Supply current: 5A Control Signal: 0-10V Enable signal: 9 - 30V
Control, Input and Output Module - MAC01	REIVAX MAC01
Programmable Controller	REIVAX CPX05
Voltage Regulator	REIVAX DRV01
Synchronizer - SNX100	REIVAX SNX100

APPENDIX F– Sensors and data acquisition components list

Table F.1 - Sensors and Data Acquisition Components

Component	Specification
Level and Temp Sensor - 1S13	PARKER SCLTSD3701005 Analog output: 0 -20mA or 4-20mA Supply Voltage: 15 - 30 VDC Temperature Range: -20 - 85°C
Pressure transducer - 1S1	WIKA Supply voltage: 8 - 30 V Read signal: 4 – 20 mA Pressure Range: 0 – 60 bar
Pressure transducer - 1S2	Model/Manufacturer: SERVUS TPE 350 Supply voltage: 10V (excitation) Read signal: 0 a 20 mV Pressure Range: 0 - 350bar
Flow rate transducer - 1S3	WEBTEC/ CT 150-5V-B-B-6 Supply voltage: 12 - 32 V Read signal: 0 - 5V Flow Range: 10 - 150 L/min
Pressure Sensor - 1S4	WIKA Supply voltage: 8 - 30 V Read signal: 4 - 20mA Pressure Range: 0 – 40 bar
Pressure Sensor - 1S5	HMB/ Modelo P8AP Supply voltage: 5V (excitation) Pressure Range: 0 - 10 bar
Pressure Sensor - 1S6	SERVUS/Modelo TPE 350 Supply voltage: 10V Read signal: 0 a 20 mV Pressure Range: 0 - 350bar
Flow rate transducer - 1S7	WEBTEC/ CT 15-5V-B-B-6 Supply voltage: 12 - 32 V Read signal: 0 - 5V Flow Range: 1 – 15 L/min
Thermocouple - 1S9	Temperature Range: -50 - 760 °C
Thermocouple - 1S10	Temperature Range: -50 - 760 °C
Thermocouple - 1S20	Temperature Range: -50 - 760 °C
Pressure Gauge - 1S11	SALCAS
Pressure Gauge - 1S12	SALCAS

Pressure Gauge - 1S16	SALCAS
Pressure Switch - 1S14	Rexroth HED3 0A 33/400 Supply voltage: 12V DC; 1A maximum Command signal: 40V DC; 1A maximum
Contamination indicator - 1S18	PARKER - Visual
Contamination indicator - 1S19	PARKER - Visual
0ME1 Speed Encoder - 1S15	DYNAPAR B58N1024ACDDA0 Supply Voltage: 5 - 26 VCC Read signal: 5 - 26VCC Speed Range: 0 - 6000rpm
0GS1 Pick Up - 1S17	BALLUFF BES 516-325-G-E5-Y-S4 Supply Voltage: 10 - 30 VDC Read signal: MAC 01